University of Insubria

PhD Program in Chemical and Environmental Sciences
(XXX Cycle)

Analysis of the impacts of geomorphological disturbance on alpine and polar vegetation.

PhD Thesis

Supervisor: **Prof. Mauro Guglielmin**
Co-supervisor: **Prof. Nicoletta Cannone**

Candidate: **Stefano Ponti**
N°: **713419**

ABSTRACT

Under a context of climate change, polar and alpine regions have been demonstrated to be highly susceptible to climatic factors in various scientific fields. One aspect of susceptibility is treated in this thesis in terms of biogeomorphology, in particular for those geomorphic processes that couple the surficial displacements with the vegetation distribution. For these reasons, 3 study areas have been selected in polar (Svalbard and Antarctica) and alpine (Central Alps) regions to carry out this project. The methods used are different depending on the scale and the location of the target. On the Alps, at large scale, surface and climatic data have been used to produce thematic maps useful for a surface dynamic prediction model, while at landform scale, various system have been chosen to observe surface displacements (e.g., painted lines, height-o-meter) in relation to the vegetation distribution (vegetational relevé, line intercept). To quantify small-scale processes, a close-range photogrammetric application has been developed to produce detailed digital elevation models (DEMs) at a millimetric resolution. In the Arctic, ground thermistors and a time-lapse camera were set on a circumpolar active layer monitoring (CALM) grid to assess relationships among ground surface temperature (GST), snow distribution and active layer thickness (ALT) at a sub-metric scale. For understanding the effect of thaw depth on the CO2 fluxes on an arctic tundra environment, an infra-red gas analyzer (IRGA) system was coupled with a frost probing survey on different vegetation communities. In Antarctica, ground penetrating radar (GPR) with electrical resistivity tomography (ERT) have been utilized to detect ice content in 2 rock glaciers and an ice-core stratigraphy validated the digital findings.

The results of this project demonstrate that a novel prediction model that take in consideration both surface and climatic data (in particular snow distribution/persistence) to quantify mountainous surface displacement is possible. In addition, the annual surface velocities of 3 alpine rock glaciers were calculated and associated to different geomorphic processes that, in turn, create specific niches for alpine tundra species, able to tolerate specific substrate rates. Further, for small processes like needle ice, new minima of soil water content and cooling rate have been defined to initiate its formation, as well as the importance of minimum air temperature for the length of ice needles. Needle ice dynamic has been quantified and coupled with a high spatial variability as well as the absence of relation between frost heave and frost creep. In the Arctic we have demonstrated how small-scale spatial distribution of snow cover affects GST, leading in turn to a high spatial variability of ALT. This is majorly driven by the microtopography of the surface in terms of slope and convexity. ALT is also the best driver of net ecosystem exchange (NEE) in arctic tundra and, coupled with the importance of soil temperature for ecosystem respiration (ER), it is a novel key of interpretation of the arctic carbon cycle. In Continental Antarctica 2 active rock glaciers have been demonstrated to be ice-cored, differently than thought in the past. This led consequences for their proved glacial origin and also for the type of creep occurring within their bodies.

The strength of this project could be considered as the dependence of geomorphic processes (that induce surface displacements) on climatic factors, thus being able to be extrapolated under the future climate change scenarios. In addition, despite considerable differences in vegetation composition and functioning, the 3 distant study areas account for similar geomorphic processes that could be compared in future research to have a global understanding of surficial dynamics.

INDEX

DISSERTATION STRUCTURE

This dissertation is structured as following:

1. **INTRODUCTION**. Here, after a preface that gives the rationale of the thesis, the aims of the PhD project are presented. Subsequently, the state of the art is treated. The three different but interconnected topics of the project are shown in terms of definitions and explanation of the most recent researches present in literature. This gives a focus on what other authors figured out in researches with similar aims concerning the climate change, the geomorphic processes in cold environments and the interaction between geomorphic processes with vegetation.
2. **STUDY AREA**. It describes in terms of geography, climate, geology, geomorphology, flora and vegetation, the three investigated areas: the Alps, the Svalbard archipelago and the continental Antarctica.
3. **CLIMATIC ANALYSIS**. This section illustrates how the most recent climate is changing at the three investigated sites. It compares the trends of air temperature, total precipitations and snow cover thickness with the trends found by other researchers.
4. **METHODS**. In this section all the materials and methods used for the data acquisition and analysis are listed and grouped in sub-sections inherent to the three different study areas.
5. **RESULTS**. Here the results (published paper, submitted manuscript or non-submitted manuscript) are presented. The sub-sections are the titles of the focuses given to the projects carried out on the Alps, at Svalbard and in continental Antarctica.
6. **CONCLUSION**. This part summarizes and links all the results found in this dissertation, also giving suggestions for future perspectives.
7. **ACKNLOWLEDGMENTS**. Here a series of important people are thanked for their support to the thesis.
8. **REFERENCES**. Here all the references of citations that are not comprehended in the submitted or published papers are listed.

1. INTRODUCTION

1.1 PREFACE

This dissertation takes place in the context of the environmental sciences that concern the landscape in terms of geomorphological reading and ecological functioning of the vegetation in cold environments.

The natural environment that encircles human beings is subjected to continuous changes both due to the human activity and natural alterations/adjustments. In this view, ecosystems are the fundamental key to be understood and maintained in terms of supplies as ecosystem services and principal component of biomes. The different way to react to changes depends on the interactions occurring within and among the ecosystems both at abiotic and biotic level. Since ecosystems are too wide to be fully comprehended in a scientific way, many studies have been focusing on specific relationships or cases that vary from a context to another. In the recent years, climate change has been object of attention by the scientific and ordinary society because of the visibility of its impact on human activities and ecosystems. In other words, the 3 components of the environment: human activity, ecosystems and climate change are interconnected and strictly depend on each other. Beyond the big question about the human responsibility to the recent climate change (RCC), it is important to exclude the direct impact of human activities on the ecosystems to figure out better the “natural” adjustments driven by climatic factors. As a consequence, cold regions have been selected in many studies for this purpose: they are the farthest places connected to the human presence. Indeed, this dissertation treats about 3 different cold regions in order to have different cases of study. Further, due to the impossibility to study cold region ecosystems as a whole object, the focus is given to that stage in which climatic variables affect the landscape modelling (abiotic components) and (in turn) the vegetation (biotic component) as the first level of the trophic chain.

This topic also rises for a lack in the literature of an understanding of surficial dynamics of cold region environments and how this could be treated as abiotic driver on the vegetation ecology.

1.2 AIMS

The aims of the thesis focus on the dynamics of biogeomorphic processes in cold environments in a context of climatic change. Since climate change is displaying its effects more rapidly in polar and alpine regions, the areas of interests were chosen in arctic, Antarctic and alpine regions. In this way, a comparison of the processes involved in different ecosystems will be possible in future perspectives.
The first step for understanding biogeomorphic processes in periglacial areas is to investigate the relationships between climate change factors and the dynamics occurring at the top part of the regolith, deposits or soils. In these terms, environmental variables that act as climatic drivers play a key role in changing the surficial dynamics and therefore the velocity of the surface displacements occurring at different spatial and temporal scales. Therefore, a knowledge and a distinction of processes that may vary under a climate change future scenarios is important to forecast the landscapes changes.
Surficial displacements produce impacts on the ecosystems, especially the most vulnerable that is vegetation. Therefore, the understanding of vegetation changes in terms of floristic composition and coverage can be treated as also a direct consequence of surficial dynamics.
The knowledge on these vegetation changes can be relevant for the change of ecosystem services and also for climate change feedbacks. In fact, only certain adapted species could tolerate specific surficial rates, others prefer to anchor the substrate to auto-build their favorable niche, others succumb. By altering the first step of the trophic chain, the ecosystems may mutate their function and in a long-term produce negative or positive feedbacks. For instance, recently interesting studies focused on the quantification of soil + vegetation ecosystems to uptake or release CO_2 (the most abundant greenhouse gas) (e.g., Hayes et al., 2014; Euskirchen et al., 2012; Koven et al., 2011; Schuur et al., 2009). Changes in these interacting structures can provoke a shift from CO_2 sink to source behavior or vice versa and thus produce an additional contribution to the future climate (Fig. 1.1).

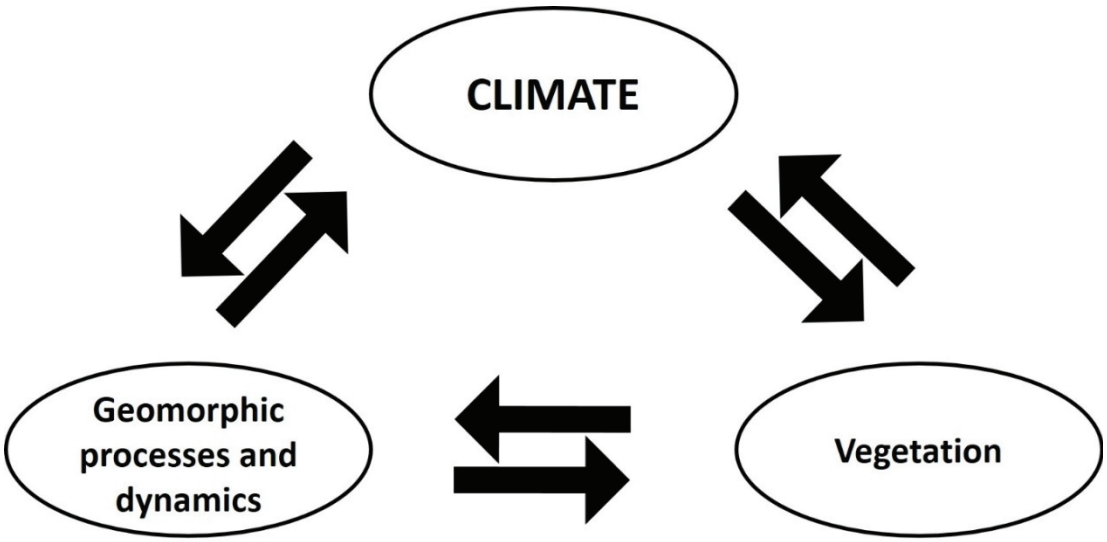

Figure 1.1. A schematic representation of the relationships occurring between climate change, geomorphology and vegetation. Climate is the principal driving force, but it can be changed by feedbacks from vegetation and geomorphology dynamics.

In detail, the objectives of the thesis are:

a) Assess the surficial rate of displacements of 3 alpine rock glaciers both at seasonal and annual scale. Subsequently, to find out the vegetation composition and changes on the rock glaciers in order to identify the relations occurring between alpine tundra species and surface instability.
b) Join the climatic data variables and the topographic characteristics of an alpine area to produce a surficial displacement prediction model.
c) Understand the environmental responsibles of the needle ice formation in central Alps. Assess its spatio-temporal distribution and provide a quantification of its dynamic, in terms of frost heave and needle ice creep with a new close-range photogrammetric application.
d) Focus on a small-scale spatial distribution of snow cover, ground surface temperature and active layer thickness in a high arctic region to understand the relationships among snow and active layer thickness spatial variability with the vegetation pattern.
e) Figure out the dynamics of CO_2 fluxes in a high arctic valley as a result of an interaction of abiotic (thaw depth, soil temperature and moisture, photosynthetically active radiation) with biotic (vegetation community types and vegetation phenology) factors throughout an arctic summer growing season.
f) Understand the internal structure of 2 Antarctic rock glaciers and the identification of the ice type through geophysical surveys and ice-core stratigraphy in order to reconstruct their origin in a glacial evolution context.

1.3 CONTRIBUTIONS TO SCIENTIFIC PAPERS

The present dissertation encompasses 5 manuscripts, aimed to be published in different scientific journals:

1) Ponti, S., Cannone, N. and Guglielmin, M. Surface dynamic in paraglacial and periglacial mountains of the Central Alps: a simple topo-climatic model. Manuscript in preparation.
2) Ponti, S., Cannone, N. and Guglielmin, M., 2018. Needle ice formation, induced frost heave and frost creep: a case study through photogrammetric technique at Stelvio Pass (Italian Central Alps). Catena, 164, 62-70.
3) Guglielmin, M., Ponti, S., Mazzola, M. and Cannone, N. Ecogrid: Integrated abiotic and biotic monitoring at metric scale to understand the interactions between snow cover, vegetation and active layer thickness in a High Arctic site. Manuscript submitted for publication.
4) Cannone, N., Ponti, S., Christiansen, H.H., Christensen, T.R., Pirk, N. and Guglielmin, M. Active layer seasonal dynamics and plant phenology effect on the CO_2 fluxes in the High Arctic. Manuscript submitted for publication.
5) Guglielmin, M., Ponti, S. and Forte, E., 2018. The origins of Antarctic rock glaciers: periglacial or glacial features? Earth Surface Processes and Landforms. http://dx.doi.org/10.1002/esp.4320.

The contribution as co-author to the listed manuscript has been involved in the data collection on the fieldwork and data analyses, text writing, as well as the figures preparation.

1.4 STATE OF THE ART

1.4.1 CLIMATE CHANGE

RCC is known to occur since the 1950s (Trenberth et al., 2007; Mann et al., 2008; IPCC, 2013) and its evidences are significant worldwide with changes such as: ocean acidification, glaciers and sea ice retreats, sea level rise, extreme meteorologic events, etc. However, the more common and measured climatic parameters primary responsible of climate change impacts are surface temperature and precipitation (IPCC, 2013). In fact, it has been demonstrated that air temperature and precipitation have direct secondary effects on the extend of glaciers (e.g., Kaser et al., 2006; Zemp et al., 2007; Diolaiuti et al., 2011; Gardner et al., 2011 Huss and Fischer, 2016), distribution and duration of snow cover (Brown et al., 2010; Callaghan et al., 2011; Bavay et al., 2013), permafrost distribution (Gruber and Haeberli, 2007; Grosse et al., 2011; Stoffel and Huggel, 2012; Schuur et al., 2015).
Among the different areas in which RCC has been studied, the more sensitive because of their higher vulnerability are the high latitude and high altitude regions (Beniston, 1994; Serreze et al., 2000; Theurillat and Guisan, 2001; Root et al., 2003; Chapin et al., 2008; Gobiet et al., 2014).
Effects of climate change are more visible in cold regions because physical and biological processes are very sensitive to temperature increase (e.g., Chapin et al., 2008) and here rate of warming by the end of the 21st century is faster than ever recorded from historical data (Stoffel and Huggel, 2012).
Responses could be abiotic (e.g., ground temperature increase, sea level rise, surface roughness change, permafrost thawing) or biotic (e.g., species competitions, change in population structure) but it is important to keep in mind that abiotic and biotic responses are coupled in the same ecosystem (Hinzman et al., 2005). Therefore, the whole ecosystem response is called feedback to climate change (Lyon et al., 2010) that could be positive or negative (Chapin et al., 2008).
The high topographic variability in mountainous areas affects abiotic factors that change rapidly with the altitude such as air temperature and precipitation (Becker and Bugmann, 1997). In turn, climatic condition changes in mountainous areas may have not only a direct impact on hydrology, vegetation and ecosystems (Whiteman, 2000), but also effects on the population living at the bottom of mountains (Meybeck et al., 2001). Thus, alpine regions offer a high geo and biodiversity that are important to study because of their susceptibility to climate change. In fact, on the Alps, the increase of mean annual air temperature from 1850 is twice the global average (2.0 °C vs. 0.7 °C) (Beniston, 2003; Walther et al., 2002) and a decrease of solid precipitation have been occurring since the XX century (Bianchi Janetti et al., 2008; Gorni et al., 2008). Here, the importance of the alpine cryosphere rises as the environmental component directly affected by climate change and able to affect ecosystems and economy (Haeberli and Beniston, 1998; Beniston, 2000) in terms of natural risks (e.g., fluvial floods; Beniston, 2006). In these terms, alpine ecosystems are particularly susceptible to climate change because of the presence of species well adapted to cold temperatures and low anthropic impact (Korner, 1999; Thuiller, 2007) and endemic species.
Similarly, in the Arctic, surface temperatures have increased at a rate of 50% higher than the Northern Hemisphere in the last half-century (McBean et al., 2005), thus more pronounced impacts are expected in the future (Kattsov et al., 2005). Evidences lay in the diminishing extend of sea ice (Stroeve et al., 2012), glacier mass loss (Gardner et al., 2011), increasing river flows (Shiklomanov and Lammers,

2009), increasing groundwater flow (Smith et al., 2007), permafrost degradation (Brutsaert and Hiyama, 2012), ecosystem shifts (Karlsson et al., 2011) and shorter extend of snow cover season (Callaghan et al., 2011). Despite the differences among arctic, Antarctic and alpine areas due to their climate and radiation distribution all are characterized by the same high vulnerability to the RCC.

1.4.2 COLD REGIONS GEOMORPHIC PROCESSES

The geomorphic contribution to ground surface instability and modelling matches those processes related to permafrost creep, frost action, freezing and thawing cycles and snow action plus the gravitation process occurring in rocky areas. As a consequence, in presence of gentle to steep slopes in arctic-alpine environments, periglacial, cryotic and gravitational landforms occur and model the landscape depending on the ground temperature, soil texture and soil moisture (French, 2007). Thus, particular interests fall on rock glaciers and block streams that can be related to permafrost occurrence or solifluction lobes and terracettes, ploughing blocks, and scree slopes where permafrost presence cannot be relevant. Often these landforms are not the best representative of a single geomorphic process, rather more processes are involved in their formation (e.g., Rixhon and Demoulin, 2013).

1.4.2.1 Permafrost-related landforms

Rock glaciers are lobate or tongue-shaped bodies of frozen debris (interstitial ice or ice core) which creep downslope due to the deformation of the ice contained within it (French, 2007) and they are the best indicators of high mountain periglacial processes (Serrano et al., 2010). Further, they indicate the lower altitudinal limit of alpine permafrost, since the creep is due to warm permafrost (French, 2007). Even though the mean annual velocity of rock glaciers has been defined as 10-100 cm per year in many studies (Humlum, 1996; Haeberli et al., 2006; French, 2007), arctic rock glaciers show a reduced range (5-70 cm per year) (Haeberli et al., 2006; Kääb, 2006) than mountain ones (Kääb, 2006; Serrano et al., 2006). Also Barsch (1996) agrees with 1-2 cm per year minimum and 100-200 cm per year maximum, even though fastest movement have been recorded (up to 100 m per year) in Andes (Corte, 1987) and Asia (Gorbunov et al., 1992). Despite the knowledge of maximum horizontal velocities on the Alps (almost 7 m per year) (Chiesi et al., 1999; Krainer and Mostler, 2000), a focus is needed to the seasonal and interannual variation of velocity (Delaloye et al., 2008). Variations of velocity are likely due to the thermal state of permafrost (i.e. the rheological properties of warming ice) as the major component (Roer et al., 2008). In fact, the principal responsible of movement is the deformation of the frozen body, which can rely both on flow or creep (Whalley and Martin, 1992; Haeberli et al., 2006). However, secondary processes play a key role in the dynamic such as gravitational fall in the steepest sections (Lugon and Stoffel, 2010) or gravitation superimposed on the frozen body flow/creep (Ikeda and Matsuoka, 2006; Kääb, 2006). Therefore, “hybrid rock glaciers” (Evin et al., 1997; Delaloye, 2004) could be a correct term to indicate these features, principally formed by ice deformation, but also defined by several processes, all affected by ground temperature, ice

content, surface slope, mass advection processes, thaw settlement and frost heave (Lugon et al., 2004). Those are also processes directly influenced by climate change (Serrano et al., 2001, 2004, 2006; Lugon et al., 2004; Sanjosé et al., 2007).
Block streams are a particular type of periglacial blockfield characterized by downslope linear ribbons of blocks (Wilson, 2007) descending downslope as a stream (Washburn, 1979), consisting in angular and verticalized blocks (King and Hirst, 1964). Since they may develop on inclined slopes ranging between 1-2 (Hansom et al., 2008) and 30° (Barrows et al., 2004), velocities and processes involved in their formation are various. For instance, Andersson (1907) describes the life-cycle of block streams: block production processes, longitudinal transport by mass-wasting processes, vertical sorting, removal of interstitial fine material. Frost shattering and thermal stresses are responsible for the block production, while frost heave acts in the longitudinal movement (Boelhouwers, 1999) when turns into solifluction (frost creep) with the presence of a fine-grained matrix (Boelhouwers et al., 2002). Eventually, the flushing out of the fine matrix occurs when the block stream is no longer active (Clark, 1994, Boelhouwers et al., 2002) and water is free to percolate and flow underneath the blocks (Clark, 1994). Few studies focus on the dynamics of block streams, however they lay in a range of mean rate of 1 cm per year (White, 1981) and less than 60 cm per year (Harris et al., 1998). Climatic importance of block streams are highlighted in Harris (1994), especially related to air temperature and precipitation, but also with the snow cover distribution (Boelhouwers, 1999) and permafrost (Ballantyne, 2010), thus having an interest for future dynamics under a climatic change scenario.

1.4.2.2 Periglacial landforms

As described above, several landforms are associated with solifluction, however the most common are solifluction lobes and terracettes (Harris, 1981) and ploughing blocks (Tufnell, 1972). Solifluction lobes and terracettes are tongue-shaped accumulation of material distinguished by their morphometry (Matsuoka et al., 2005; van Everdingen et al., 2005) and they can be of 2 types: turf-banked if covered by vegetation or stone-banked if consisted of rocks (Benedict, 1970). Ploughing blocks instead, are boulders that "travel faster than their surroundings and which force up the ground before them and leave a depression to their rear" (Tufnell, 1972).
Solifluction describes a slow downslope movement of the soil due to several freeze-thaw cycle of the ground (Ballantyne, 2013) and, in non-permafrost areas it is divided into diurnal frost creep (needle ice creep) and annual frost creep (gelifluction), while in permafrost area it is called plug-like flow (Matsuoka, 2001; Harris, 2007). Thus, solifluction dynamics are dependent on the soil texture, ground temperature and water content (French, 2007), as well as ice lensing process or freeze-thaw frequency and depth (Benetict, 1970). Generally, solifluction rates are from 0.1 to 1 cm per year (Matsuoka, 2001; French, 2007) depending on the local conditions (e.g., slope, aspect, climate), but few studies are related to specific movement of lobes (Benedict, 1970) and ploughing blocks (Tufnell, 1972, 1976; Chattopadhyay, 1986; Hall et al., 2001). Solifluction process is partly controlled by climatic factors (Åkerman et al., 1996), thus having a direct influence on dynamics (Ballantyne, 1986; Elliot and Worsley, 1999).
One other evidence of solifluction, in particular diurnal creep (Matsuoka, 2001), is needle ice. Needle ice is an accumulation of slender, bristle-like ice crystals (needles) immediately beneath the surface

of the ground (Washburn, 1979). Generally, they form in particular conditions of soil texture, moisture, air (ground surface) temperatures and cooling rate (Grab, 2001), which occur in spring or autumn on the Alps. The necessary condition to have needle ice creep is the normal uplift of particles called “frost heave” (French, 2007; Rempel, 2010), that, after melting, turns into downslope displacement of the material (Matsuoka, 2001). This condition is reached when the freezing front does not penetrate deeply in the soil (Matsuoka, 1994), but remain at the uppermost centimeters. Even though needle ice creep accounts for one of the most rapid and significant processes of soil creep (Dylik, 1969), little has been studied, especially in recent years (Lawler, 1993; Vieira, 1996; Ballantyne, 1996; Grab, 2001; Grab, 2002; Vieira et al., 2003; Nel and Boelhouwers, 2013; Matsuoka, 2014). However, rates of surficial creep largely exceed average velocities of solifluction. In fact, higher movement rates occur with high freeze-thaw cycle frequency (Matsuoka, 2001), for instance the highest surficial rate (100 cm per year) has been recorded by Francou and Bertran (1997) on tropical mountains. Due to these rates and the linkage with microclimatic conditions, needle ice creep may be a major factor of slope evolutions (Perez, 1985) and in turn of soil disturbance (Meentemeyer and Zippin, 1981). As a consequence, they can affect the carbon cycle (e.g., Bockheim, 2007; Kaiser et al., 2007), soil nutrients (Walker et al., 2004), soil texture (e.g., Michaelson et al., 2008) and, therefore, the vegetation colonization (e.g., Boelhouwers et al., 2003; Groeneveld and Rochefort, 2005; Haugland and Beatty, 2005; Sutton et al., 2006; McGeoch et al., 2008; Haussmann et al., 2009; Cannone and Guglielmin, 2010; Makoto and Klaminder, 2012).

Scree slopes are massive accumulation of coarse, loose, angular rock debris at the foot of steep bare rock slopes (Luckman, 2007) with a “fall sorting”, namely an increase of particle size from the upper part to the lower section (Statham, 1976; Church et al., 1979). Their formation is prevailed by weathering and gravitational processes, where the balance of production and removal of debris is positive (van Steijn et al., 2002; Rixhon and Demoulin, 2013). In specific, the primary cause is rockfall (Francou, 1991; Dorren, 2003; Sass and Krautblatter, 2007) and its initiaitons (Blijenberg, 1998), such as rockwall retreat (Hutchinson, 1998; Curry and Morris, 2004), driven by freeze-thaw alternation (Matsuoka and Sakai, 1999; Matsuoka, 2008), thermoclastism (Luckmann, 1976; Delmonaco et al., 2013), weathering of the outcrop (Viles, 2013), pressure release and water availability (Luckmann, 1976). Then, secondary processes take place on the scree slope such as secondary rockfall (Luckmann, 1976; Krautblatter and Dikau, 2007), surface water flow (Lewkowicz, 1981; Strömquist, 1983), snow avalanches (Statham, 1976; Luckmann, 1977; Salm, 1993; Rixhon and Demoulin, 2013). Moreover, even creep-like displacement of single clasts have been recorded as a result of frost action or needle ice, especially on the upper parts of talus slopes where the particles are sandy (Pérez, 1993). Even though the mean gradient of talus slopes is 25-30°, this range may vary depending on the processes involved (Sauchyn, 1986) and thus also velocities. For example, 1-10 cm per year are recorded where fine sediments are present, while slower motions occur at coarser zones because direct impacts of rocks are required for dislodgement (Perez, 1993) and increased surface roughness acts as a frictional resistance (Luckman, 2007). However, few studies focus on the displacements of scree slopes, rather on rockwall debris production (Ballantyne and Eckford, 1984; André, 1997; French, 2007; Hoffmann and Schrott, 2002). Palaeoclimatic significance of scree slopes has been demonstrated (Hétu and Gray, 2000) and climate-controlled variations found (Hales and Roering, 2005). Thus, dynamics of scree slopes is considered an indirect indicator of the Pleistocene permafrost (Czudek, 2005a,b; Scapozza et al., 2011; Kenner et al., 2017).

1.4.3 DYNAMIC-ECOSYSTEM INTERACTIONS

Biogeomorphology is a new term referred to the study of the interactions between geomorphic processes with ecological processes (Viles et al., 2008; Haussman, 2011), especially in a context of disturbances coming from the climate change or human impacts (Naylor, 2005). In a context of climate change in fact, landscapes may be affected by remodeling of changing geomorphic processes as described above and ecosystems could experience direct impacts from the substrate dynamics. In these terms, vegetation ecosystems play a key role because they are permanently anchored to the substrate and are the first ring of the trophic chain in the primary production. As a consequence, polar and alpine ecosystems are the first aims because of their distance to human activities, particular susceptibility to climate change (Chapin et al., 2008) and representation of high topographic variability in short ranges.

Since the relationship between vegetation and geomorphic processes is bi-directional (Stallins, 2006), both the parts directly affect the other one. For example perturbation occurs in damaging the plant species but root systems also play a key role in stabilizing the sediment (Viles et al., 2008) and making a favorable niche for other species (Dickerson et al., 2013; Phillips, 2016). Hence, it is important to underline that surficial dynamics not only affect vegetation in a negative way (from single species damage to the altered community resilience; Evju et al., 2012) but sometimes substrate kinematics acts as a natural barrier against the upward migration of lowland species like shrubs (Cannone et al., 2007).

Geomorphic disturbance to vegetation may be related to a change of: a) microclimatic conditions (Körner, 2003; Malanson et al., 2012), b) species distribution (Randin et al., 2009) and community (Cannone and Pignatti, 2014), nutrient availability (Kreyling et al., 2008), or c) primary production (Nagy and Grabherr, 2009).

Due to the complexity of these systems, many facets of biogeomorphology have been investigated properly because of a large amount of interacting biotic and abiotic variables and geomorphic processes involved.

Among these, some authors preferred the field observation/sampling approach. As a result, interactions between vegetation and soil stability (Pohl et al., 2012), periglacial processes (Kozłowska and Rączkowska, 2002), alluvial fan (Lane et al., 2016), turf-banked solifluction lobe (Draebing and Eichel, 2016; Eichel et al., 2017), snow pack distribution (Evju et al., 2012), non-sorted circles (Kade and Walker, 2008), slope processes (Pérez, 2010), landslides (Cannone et al., 2010), active patterned ground (Cannone et al., 2004) and rock glaciers (Cannone and Gerdol, 2003; Burga et al., 2004) were found. However, so far it is not well known how vegetation communities respond to different surficial rates.

Other authors focused on the potential of statistical models, especially to aim at larger scale studies, able to comprehend many and easily accessible abiotic variables. For example, le Roux and Luoto (2014) found earth surface processes necessary for the prediction of species richness, distribution and community composition, while Randin et al. (2009) found difficult to assess plants distribution properly because of their high species-specificity with disturbance variables. Mod et al. (2016) underlined the importance of biotic and abiotic disturbances among other environmental variables for species distribution modelling.

Nevertheless, few studies focused on the relation between vegetation (or single species) and quantification of surficial movement tolerated (Cannone and Gerdol, 2003; Burga et al., 2004),

distinguishing among several periglacial/slope geomorphic processes (Kozłowska and Rączkowska, 2002). Rather, a simplification of surficial dynamics has been conducted by considering just topographic (Luoto and Hjort, 2005; Zinko et al., 2005; Lassueur et al., 2006; Kopecký & Čížková, 2010; Räsänen et al., 2016) or climatic variables (Aalto and Luoto, 2014).

It has already been demonstrated that geomorphic disturbance may change vegetation community over a long-term perspective (Lantz et al., 2013; Cray and Pollard, 2015). In this way, the whole ecosystem functions may be altered, as well as the local carbon cycle. In fact, some authors proved the importance of different vegetation communities as drivers of CO_2 uptake or release (Baldocchi, 2008; Cannone et al., 2012; 2016), but few demonstrated the linkage between disturbance and C cycle (Lantz et al., 2009; Pinzano et al., 2014; Cassidy et al., 2017). Thus, an insight into disturbance-vegetation-carbon cycle interrelationship is necessary to understand long-term feedbacks to climate change.

2. STUDY AREA

2.1 STELVIO PASS AREA

2.1.1 GEOGRAPHY AND CLIMATE

The study area is located around Stelvio Pass, a high alpine site in Stelvio National Park in the Italian Central Alps (Upper Valtellina) (Fig. 2.1). Along the Braulio Valley, the upper part of the Stelvio National road runs (SS38 “dello Stelvio”), built at the beginning of the XIX century to connect Lombardy and Tyrol territories though the Stelvio Pass (46°31’ N, 10°27’ E, 2757 m a.s.l.).

The study area is situated on the hydrological left side of the upper part of Braulio valley, in the western glacial cirque and northern slopes of Mt. Scorluzzo (3095 m a.s.l.). At the norh-eastern edge of the study area, the Stelvio Pass links the Valtellina and Braulio valley with the Venosta valley and the province of Bolzano, whereas at the north-west edge the Umbrail pass (46°32’ N, 10°26’ E; 2503 m a.s.l.) connects with the Müstair valley and the Swiss Confederation. The whole study zone is about 5.8 km^2, with an elevation range of about 900 metres, and spreads from the main road SS38 up to the summit of Mt. Scorluzzo. The hydrological catchment is defined by the Braulio river basin, which feeds the Adda river.

The study area is a typical alpine environment characterized by the presence of different habitats: from fen vegetation, pastures, grasslands and shrublands up to the characteristic habitats of the snowbeds and pioneer communities of the high alpine and nival belts. Indeed, it has been recognized has a site of community importance (SIC “Valle del Braulio-Cresta di Reit”; IT2040010) by the European Union, in the frame of the ecological network “Nature 2000”, established under the Habitats Directive (92/42/EEC).

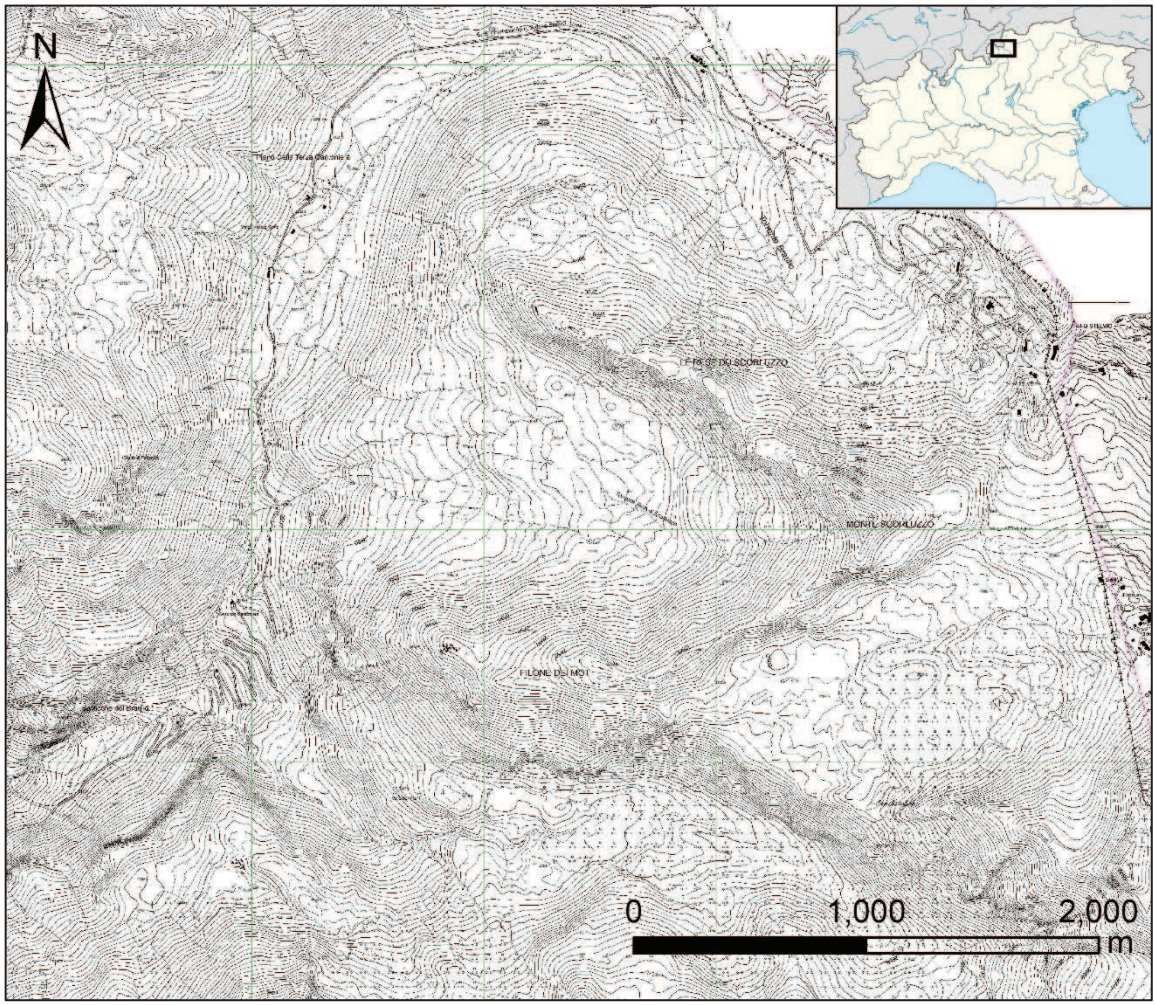

Figure 2.1. Study area location. The Mt. Scorluzzo cirque is in the central part, the Stelvio Pass at the top-right.

The climate is characterized by a continental regime (Ceriani and Carelli, 2000), with a highly variable values of precipitation because of the complex orography. Climate data for the 1978-2015 period from the nearest available meteorological station at Cancano (46°31.04' N, 10°19.25' E, 1948 m a.s.l., 9 km to E-SE) indicate a mean annual air temperature (MAAT) of +3.3 ± 0.75 °C; January is the coldest and driest month (-5.2 ± 1.8 °C; 38.9 mm) and July is the warmest and wettest (12.2 ± 1.6 °C; 94.7 mm). Mean annual precipitation sum is 810 mm, 56% of which falls between May and September. Snow can fall at any time, but lays continuously for 6 months, from mid November to May, reaching a mean maximum depth of 133 cm.

2.1.2 GEOLOGY AND GEOMORPHOLOGY

The geology and the lithology of the Stelvio Pass area is complex because several units of the Upper Austroalpine domain overlay and interact in this part of the Central Alps (Montrasio et al., 2012).
The study area is part of the Umbrail-Chavalatsch fault that belongs to the Upper Austroalpine domain. The bedrock is mainly acidic, consisting of granitic and granodioritic ortogneiss and of biotic or two

micas paragneiss, with some outcrops of dolomite in the south-west corner of the study area, from Bocca del Braulio (2280 m a.s.l.) upward to the south slope of Filone dei Mot (Giacomini and Pignatti, 1955; Guglielmin and Tellini, 1992) and a localised outcrop of andesite-basalts about 700 m West from Mt. Scorluzzo (Montrasio et al., 2012).

Glacial deposits, mainly composed of ablation till, are common and widespread up to 2850 m a.s.l., whereas inactive eluvial-colluvial and fluvial-stream deposits are mainly located below 2500 m a.s.l. Because the edges of the cirque scarps of Mt. Scorluzzo have been remodelled by degradational landslide processes, active scree slopes and talus cones are common within the study area at the base of the main rocky crest-line, especially in the western glacial cirque (Pozzi et al., 1990; Montrasio et al., 2012).

The soils are mainly Regosols, with only localized areas with Leptosols and mixed soils underneath the dolomite deposits and along the ridges that bring to Mt. Scorluzzo, respectively (Carta Pedologica Lombardia 1:25000; FAO, 2006).

The study area is composed of the western glacial cirque and the north side of Mt. Scorluzzo, that are characterized by the presence of several Holocene and Pleistocene moraine rigdes and of glacial erosional landforms (rocky crest-line, edge of cirque, roches moutonnées). Notwithstanding the abundance of historical documents, the Holocene glacial evolution of the Stelvio Pass area is not well known. Historical maps show that Platigliole and Vedretta Piana glaciers joint until 1872 (Hoffmann and Haushofer, 1872), with a maximum documented glacier extent in 1866 (Payer, 1868). The minimum elevation of the Little Ice Age (LIA) ice margins was 2780 m a.s.l. in Platigliole Valley and 2680 m a.s.l. in Trafoi Valley. It was not possible to date the glacier advance by dendrochronological, lichenometric or ^{14}C methods, but the ^{14}C age of 1580 AD obtained for the contiguous glacier of Trafoi Valley (Cardassi, 1995) provides an approximate date for the Vedretta Piana glacier maximum during the Little Ice Age. From geological and geomorphological surveys, the maximum extension of the glaciers during the Holocene reached 2610 m a.s.l. (Cannone et al., 2003). During this phase, the Vedretta Piana glacier crossed the Stelvio pass and joined with Scorluzzo glacier. A frontal morainic ridge at 2690 m a.s.l. represents the maximum advance of Scorluzzo glacier during the LIA. From the historical documents, it is possible to say that this position is lower than that reached in 1866 and documented by Payer (1868), which seems to correspond to the frontal morainic ridge at 2705 m a.s.l. The presence of Scorluzzo glacier in the northern cirque was documented until 1937 when the front reached a minimum altitude of 2820 m a.s.l. (Pelfini, 1992); around 1910 there were still two small tongues, reaching 2720 and 2730 m a.s.l. In the western glacial cirque of Mt. Scorluzzo, the iconography documented the presence of a glacier until 1872, further substituted by the actual active rock glacier (Guglielmin, 2007). Eventually, the reconstruction of the glacial history, especially the more recent, was investigated through vegetation survey (Cannone et al., 2003).

The Braulio valley is characterized by several geomorphological features (Pozzi et al., 1990), as evidenced by the presence of transversal U-shape section (upward than Bocca del Braulio), glacial circle edges and moraines in the valley and in their lateral tributaries. A large number of glacial, periglacial and gravitational features, relict, inactive or still active, are reported by several authors (Giorcelli and Pietracaprina, 1954; Nangeroni, 1954; Albertini, 1955; Pietracaprina, 1963; Guglielmin and Tellini, 1992; Guglielmin et al., 2001, 2003, Guglielmin, 2004; Cannone et al., 2003; Pozzi et al., 1990; Montrasio et al., 2012).

Here permafrost has a patchy and discontinuous distribution (Guglielmin and Siletto, 2000; Guglielmin et al., 2001; Cannone et al., 2003). Nevertheless, 1 km east from the study area at 3000 m a.s.l. the permafrost thickness exceeds 200 m (Guglielmin, 2004).

Permafrost distribution in the Stelvio pass area was little know before the PACE European Permafrost Monitoring Network project (Harris et al., 2001) commenced at Stelvio-Livrio area in 1998 (Guglielmin et al., 2001). Based on the distribution of active and inactive rock glaciers, the areas with actual potential permafrost occurrence were located above 2500-2600 m a.s.l., whereas those between 2300-2500 m a.s.l. represent the potentially permafrost distribution in the Holocene (Guglielmin and Siletto, 2000). In the upper part of Trafoi Valley, around Stelvio Pass and in Platigliole valley, bottom temperature of snow cover (BTS) measurements showed a patchy permafrost distribution above 2850 m a.s.l. From the first year of data (1998-1999) of the 100.3 m deep PACE borehole located at 3000 m a.s.l. (46°30' N 10°28' E), permafrost shows a mean annual ground surface temperature (MAGST) of -1.9 °C and an active layer thickness (ALT) of about 2.5 m (Guglielmin et al., 2001). Mean annual permafrost temperature (MAPT) was -1.7 °C with a total thickness of about 200 m (Guglielmin, 2004; Guglielmin et al., 2017). Two DC resistivity tomographies were carried out between 2680 and 2750 m a.s.l. on an active rock glacier and along the slope of the old glacier, where the ground was partly reworked for the construction of a ski run, in the north cirque of Mt. Scorluzzo. Results confirmed a patchy permafrost distribution with an active layer ranging from 3 to 5 m, and a permafrost thickness between 10 and 20 m (Cannone et al., 2003). Moreover, in the same area, a permafrost map was obtained by combining the ecological indications of vegetation. The areas with "permafrost absent" are mainly located in the lower part of the area, while areas with "possible permafrost" occurrences are distributed all over the area, without any particular link to altitude, even though the highest percentage of this category occurs between 2720 and 2750 m a.s.l. "Permafrost present" has a patchy distribution. In particular, in the ski area, permafrost occurs both in the upper and in the lower part, the middle area being "possible permafrost". On the rock glacier, permafrost is mainly in an area between 2700 and 2750 m a.s.l and on a little patch on the western side of the very upper part (close to 2800 m a.s.l).

Despite its limited extent, the study area is rich in periglacial features: 7 rock glaciers (4 active and 3 of uncertain activity; Guglielmin and Smiraglia, 1997; Guglielmin and Siletto, 2000), protalus ramparts, patterned grounds, turf hummocks (mainly localised on the northern slope of Le Rese ridge, at 2500-2600 m a.s.l.) and several solifluction lobes, (Pozzi et al., 1990). Small block streams are also present in the western glacial cirque (Albertini, 1955).

Characteristics are also landforms and deposits due to gravity: edge of cirque scarps and of glacially eroded scarps remodelled by degradational and landslide processes, active scree slopes and talus cones, active debris flows (Pozzi et al., 1990). Lot of gullies due to running water also characterize the area.

2.1.3 FLORA AND VEGETATION

The study area is located in the alpine and in the nival belts (Ellemberg, 1988), the latter colonised by discontinuous pioneer communities, especially by *Androsacetum alpinae, Oxyrietum digynae,* and by *Luzuletum spadiceae*, that accounts for a higher vegetation cover. In the alpine belt, the climax condition is reflected by alpine pastures with high vegetation cover: *Caricetum curvulae* and, in chionophilous conditions, *Salicetum herbaceae*.

The Stelvio Pass area is a suitable example of the characteristic vegetation of the central Alps and all the vegetation elevation belts typical of high elevation landscapes: subalpine (2200-2400 m a.s.l.), alpine (2400-2800 m a.s.l.) and nival belts (> 2800 m a.s.l.). Moreover the study area it is a unique case study where it has been possible to detect and assess the RCC impacts on the alpine flora and vegetation (Cannone et al., 2007; Cannone and Pignatti, 2014). The broad lineaments of the vegetation were drawn by Giacomini and Pignatti (1955) and, more recently, by Cannone (1997) and Cannone et al. (2007).

In 1953, a phytosociological map of the Stelvio pasture area was performed at scale 1:12500 (Giacomini and Pignatti, 1955), without the support of aerial photographs, and completed by phytosociological relevés describing all the communities observed. In 1953, no precedent examples of similar investigations on the alpine vegetation in the mountain regions of Italy existed, so that the aim of the investigation was to give a pioneering classification of the vegetation. In 2003 (Cannone et al., 2007) and 2014 (unpublished data) the vegetation of the Stelvio pass area was re-sampled to build new vegetation maps of the study area and new phytosociological relevés of the vegetation were performed.

Because of the difference in elevation, morphological features and edaphic conditions (e.g., long permanence of the snow cover, or limited drainage of water with consequent stagnation, or the presence of instability of the surface), the vegetation is composed of a mosaic of different plant communities. They belong to the high elevation alpine geosigmetum on acidophilous soils (*Caricion curvulae, Festucion variae, Androsacion alpinae, Caricion fuscae, Salicion herbaceae, Loiseleurio-Vaccinion, Nardion strictae*) and on calcareous soils (*Seslerio variae-Caricetum sempervirentis, Caricetum firmae, Potentillion caulescentis, Thlaspion rotundifolii*) (Blasi, 2010; Biondi and Blasi, 2013; Biondi et al., 2014).

2.2 SVALBARD

2.2.1 GEOGRAPHY AND CLIMATE

Svalbard is a 61000 km^2 Norwegian archipelago located in the Arctic Ocean. The group of islands range from 74° to 81° N, and from 10° to 35° E and consist of more than 500 islands where the islands of Spitsbergen, Nordaustlandet, Edgeøya and Barentsøya are the largest (Fig. 2.2).

The capital Longyearbyen is the biggest settlement in Spitsbergen with roughly 2000 inhabitants, followed by Barentsburg, Sveagruva and Ny-Ålesund.

Ny-Ålesund is the northernmost village on the Earth and it is situated in Kongsfjorden. It raises upon a coastal lowland of the Brogger peninsula. Here, during the Pleistocene glaciations, glacial sediments accumulated and underwent marine processes to form the actual deposits (Dallmann, 2015). The first small study area consists in a grid located at 78.92° N and 11.86° E upon a flat zone called Kolhaugen, between the coast and the Austre Broggerbreen glacial forefield (Fig 2.3).

The second study area is located in the Adventdalen valley (78°18' N, 15°92' E), in a glacially eroded valley located in Central Spitsbergen which was deglaciated around 10000 years BP (Mangerud et al., 1998) (Fig. 2.4).

The climate of Svalbard archipelago consists in an average July temperatures range from 4° to 6 °C and January temperatures are normally between -12° and -16 °C.

The amount of precipitation on the entire archipelago is generally low with averages along the western coast between 400 and 500 mm (Isfjord Radio - 480 mm). The fjord zone is extremely dry with an annual precipitation for Longyearbyen showing only 190 mm, even less than the average in the last few years (83 mm) (Elberling, 2007).

Ny-Ålesund, in detail, is characterised by a mean annual air temperature (MAAT) of -4.2 °C with the coldest month in January (-13 °C) in and the warmest in July (5 °C). The annual precipitation is 433 mm in w.eq. (Cannone et al., 2016).

Concerning Adventdalen valley, climate is a polar tundra climate (Kottek et al., 2006) with MAAT of -3.5 °C and annual precipitation of 191 mm, of which approximately 30% falls as snow (period 2000-2013; Svalbard Airport, data available at http://www.eklima.no).

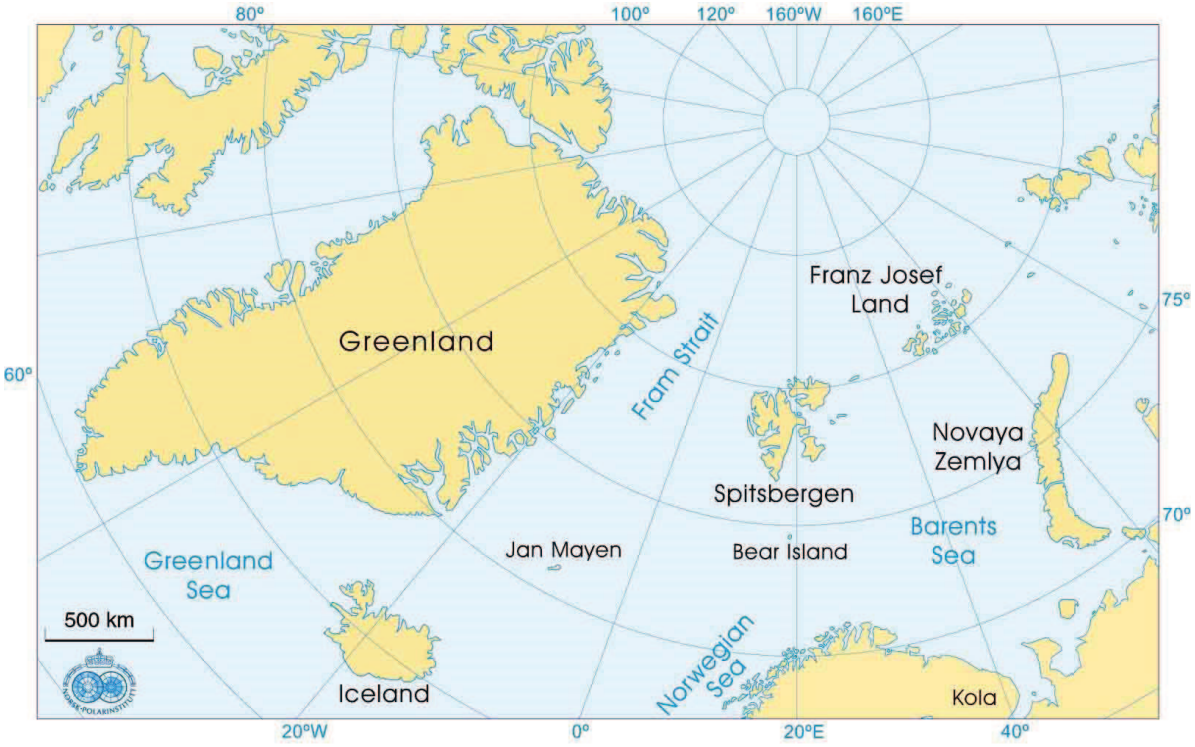

Figure 2.2. The Svalbard archipelago location in the Arctic Circle.

Figure 2.3. The investigated CALM grid location near Ny-Ålesund in Svalbard. a) aerial view of the town and the study site, b) Ny-Ålesund location in the archipelago.

Figure 2.4. The study area lays on the ice-wedge polygon site, in central Adventdalen valley in Svalbard.

2.2.2 GEOLOGY AND GEOMORPHOLOGY

Svalbard is an exposure of the northernwest domain of the Eurasian continental plate that was uplifted by late Mesozoic and Cenozoic crustal activity (Worsley and Aga, 1986). Exposed rocks on Spitsbergen's north and west coast show how the archipelago was located near today's South Pole during the Precambrian (Ingólfsson, 2008). Subsequently the islands crossed subequatorial areas during pre-Devonian and have migrated towards north over time (Worsley and Aga, 1986).
The coastal areas in North and West are deeply indented by fjords. Glaciers are the most characteristic landscape feature on the islands covering more than 60% of the land area (Johansen and Tømmervik, 2014), barren rocks cover the 30%, while vegetated areas the 10%.
The bedrock of Spitsbergen consists in flat lying sedimentary rocks of the Tertiary basin (Dallmann, 2015) composed of several formations showing alternation of sandstone and shale-stone layers (Hjelle, 1993).
Svalbard are known to have continuous permafrost, all over the landscapes (Christiansen et al., 2010) ranging from roughly 50 m in thickness near the coast to as 500 m at higher altitudes. The active layer, that is the seasonally-frozen ground (Muller, 1947; Burn, 1998; French, 2007), ranges from 0 to 3 m (Humlum et al., 2003). All the surfaces in the periglacial environment undergo active frost shattering, sorting, ice segregation (only in fine materials) and deformation. More specifically, the active layer shows features like sorted/unsorted circles, stripes, hummocks, boils, nets (Åkerman, 1980, 1996; Matsuoka et al., 2004), icings and frost blisters (Yoshikawa, 1998).
Geologically, Ny-Ålesund is generally covered by quaternary deposits, mainly marine beach deposits and weathered material or colluvium (André, 1993). Continuous permafrost underlies the area and ranges from 100 m of depth in coastal zones to > 500 m in montainous areas (Boike et al., 2008). Depending on the deposit and the topography, active layer thickness ranged between 0.3 and 1.8 m of thickness (André, 1993). Here several inactive sorted and unsorted stone circles are present.
The geology of Adventdalen valley shows flat-lying sedimentary rocks of Early Permian to Eocene age with increasingly younger rocks exposed towards the southwest (Dallmann et al., 2001). In its lowermost 15 km, the westward-draining valley bottom is covered by fluvial sediments with braided river flood-plain deposits, terraces (Tolgensbakk et al., 2000) and loess deposits covering the most exposed terraces (Bryant, 1982). Permafrost of the Adventdalen area is classified as continuous, with active layer thicknesses ranging between 74 and 110 cm in the UNISCALM site some 4 km west of the study site period 2000-2014 (Christiansen and Humlum, 2008; Schuh et al., 2017). A further data series was available also for the selected ice-wedge study area, which displayed a shallower active layer (70 to 81 cm) between 2012 and 2016 (Christiansen, unpublished data). Permafrost conditioned landforms occurring in the area include ice-wedge polygons (Christiansen, 2005), which are the most ice-rich lowland permafrost landform (Christiansen et al., 2016). The study site is located within a network of large, low-centered, hexagonal ice-wedge polygons (Watanabe et al., 2017), approximately 3-6 m above Adventelva river.

2.2.3 FLORA AND VEGETATION

The typical arctic vegetation is called Arctic Tundra which shows heterogeneous landscapes that can encompass a mosaic of wetland areas, riparian systems, well-drained heath lands, ridge-top vegetation and polar deserts (Sjögersten et al., 2006).
Five main vegetation types were established in the Svalbard islands (Walker et al., 2016):

- Graminoid, prostrate dwarf-shrub, forb tundra dominated by sedges and shrubs < 5 cm tall.
- Rush/grass, forb, cryptogam tundra dominated by grasses, rushes, forbs, mosses, lichens, and liverworts.
- Prostrate dwarf-shrub, herb tundra, a dry tundra with patchy vegetation. Prostrate shrubs < 5 cm tall (such as *Dryas* and *Salix arctica*) are dominant, with graminoids and forbs.
- Prostrate/Hemiprostrate dwarf-shrub tundra, a moist to dry tundra dominated by prostrate and hemiprostrate shrubs < 15 cm tall, particularly *Cassiope sp.*
- Sedge/grass, moss wetland dominated by sedges, grasses, and mosses

In particular, the study area at Ny-Ålesund lays in a polar semi-desert (Bliss and Svoboda, 1984) which 2 types of vegetation occur in: 1) graminoid tundra and 2) prostrate/hemiprostrate dwarf-shrub (Walker et al., 2016).
The Adventdalen study area instead lies in the middle-arctic vegetation tundra (Elvebakk, 1994) in the *Cassiope tetragona* zone (L.) D. Don (Rønning, 1996) and is characterized by the occurrence of a typical Arctic tundra vegetation mainly dominated by graminoids (*Dupontia pelligera* (Rupr.), *Luzula confusa* L., *Poa arctica* R. Br.) (Sjögersten et al., 2006). Within the Adventdalen area, study sites represent vegetation and geomorphological conditions widespread in the Arctic.

2.3 CONTINENTAL ANTARCTICA

2.3.1 GEOGRAPHY AND CLIMATE

The study area lays on the coast of Terra Nova Bay (Northern Victoria Land, Continental Antarctica), the ice-free area that includes the Italian Antarctic Research Station “Mario Zucchelli” (MZS) (74°42’ S, 164°60’ E) between Tethys Bay to the north and Adélie Cove to the south (Fig. 2.5).
The climate of the area surrounding MZS is characterized by a mean annual air temperature of -13.9 °C (Frezzotti et al., 2001). In the vicinity of MZS, at Boulderclay (74°43' S, 164°05' E), the mean annual air temperature for the period 1997-2003 ranged between -16.4 °C and -15.1 °C (Guglielmin 2006). Precipitation, always in the form of snow, is very low and ranges between 100 and 200 mm (Grigioni et al., 1992; Monaghan et al., 2006), favorable conditions for continuous permafrost.

Figure 2.5. Terra Nova Bay location in Continental Antarcica.

2.3.2 GEOLOGY AND GEOMORPHOLOGY

The area bedrock consists of Harbour Castle granite, Wilson Terrane meta-granite and high-grade metamorphics, and small areas of meta-sedimentary rocks, all Ordovician in age or older. Several large glaciers cut through the Trans-Antarctic Mountains in this area (the Reeves, Priestley and Campbell) and there are many smaller ones together with numerous snowbank or cirque glaciers (French and Guglielmin, 1999).

Two ancient glacial drifts TN I and TN II (Baroni, 1987; Orombelli et al., 1990) of a thin and discontinuous layer of till cover ice-free areas.

The area is also characterized by a very thick permafrost, around 400 m (Guglielmin, 2006). The active layer ranges between 2 and 92 cm in the deposits (Guglielmin et al., 2014) and it is strongly related to the surface conditions (generally thinner where mosses or lasting snow occur) while it can exceed 1.6 m in the granitic outcrops (Vieira et al., 2010). Active layer thickness in this area is increasing up to 1 cm yr^{-1} (Guglielmin and Cannone, 2012).

The geomorphology of the area was firstly describe by Baroni (1987) who included positions of rock glaciers along the coast of Adélie Cove and Tethys Bay. Among those, the interest fell on the rock glacier located at Tethys Bay close to the northern margin of the Strandline glacier and the rock glacier located on the southern side of Adélie Cove. Further studies have also identified patterned ground of thermal contraction cracking and frost mounds in periennially frozen lakes (French and Guglielmin, 2000) or tafoni (Strini et al., 2008).

2.3.3 FLORA AND VEGETATION

Continental Antarctica is dominated by the Antarctic non-vascular tundra formation that is composed entirely of microfungi, cyanobacteria, algae, lichens and bryophytes.

In the Antarctic non-vascular tundra formation, three principal subformations were described (Smith, 1988; 1990): short moss turf and cushion subformation (dominated by mosses), foliose and fruticose lichen subformation (dominated by macrolichens), crustaceous lichen subformation (dominated by crustose and microlichens).

In particular, the vegetation of Victoria Land is dominated by (a) mosses, (b) mosses encrusted by epiphytic lichens, (c) macrolichens, and (d) scattered epilithic lichens and mosses, respectively (Cannone, 2006; Cannone and Seppelt, 2008).

The vegetation of Boulderclay (the closest ice-free site to the study area) includes bryophyte communities dominated by *Sarconeurum glaciale*, *Bryum subrotundifolium* and *Syntrichia princeps* with terricolous and epiphytic lichens such as *Lecidella siplei*, *Caloplaca approximata* and *Candelariella flava* and, in some cases, with Cyanobacteria. The epilithic communities colonize the big erratic boulders which are very common throughout the site and is characterized by macrolichens as well as by crustose epilithic lichens. The macrolichen vegetation accounts for *Umbilicaria decussata*, *Usnea sphacelata*, and *Pseudephebe minuscula* as companion. The crustose lichen community is dominated by *Buellia frigida* mainly associated to *Xanthoria elegans* (Cannone, 2006).

3. CLIMATIC ANALYSIS

In this section, the most important climatic patterns for this study are presented. The automatic weather stations considered for this purpose are the following:

- Alps: Cancano (46.51729 N, 10.32076 E, 1948 m a.s.l.) (ARPA Lombardia)
- Adventdalen: Longyearbyen, Svalbard Lufthavn (78.2453 N, 15.5015 E, 28 m a.s.l.) (www.eklima.no)
- Ny-Ålesund: Ny-Ålesund weather station (78.9243 N, 11.9312 E, 8 m a.s.l.) (www.eklima.no)
- Terra Nova Bay: Eneide (74.683 S, 164.083 E, 92 m a.s.l.) (Guglielmin and Cannone, 2012).

The mean annual air temperatures (MAATs) are reported in Fig. 3.1. The longest records (from 1978 to 2016) were available for the Alps and the Arctic, while the shortest one (1989-2016) for the Antarctic. The arctic weather stations are not so far each other, therefore the pattern results very similar. Further, the arctic trend is positive: +1.03 and +1.39 °C per decade for Ny-Ålesund and Longyerabyen respectively, thus pronouncing a constant warming of these two arctic sites, comparable with the trends found by Førland et al. (2011) for the period 1975-2011 (0.99 and 1.25 °C per decade respectively). The same occurs for the alpine site but with a less detectable positive trend (+0.45 °C per decade). This support and updates what already found by Cannone et al. (2007), although the weather station was not the same, but close enough and at a similar elevation (Sils, 1798 m a.s.l.). In fact, they found a warming of 1.2 °C for the period 1980-2003, similar but slightly higher than the one obtained by applying the trend here described for the same period (1.03 °C). This warming also matches the one found by Begert et al. (2005) in Switzerland (+0.04 °C per decade), even though their dataset stops in 2000. Conversely, in Antarctica, despite the shorter record, a gentler trend of MAAT is visible (+0.24 °C per decade), higher than the stable trend illustrated by Guglielmin and Cannone (2012) and Chapman and Walsh (2007). However, in their studies, the periods considered were 1997-2009 and 1958-2002 respectively, and this might have changed the final considerations.

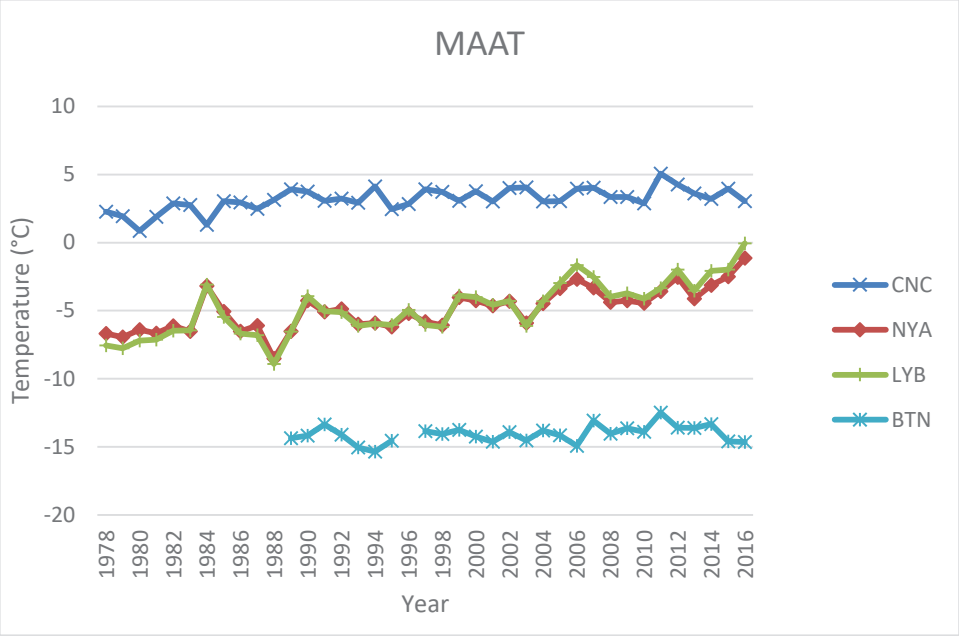

Figure 3.1. Graphic representation of the MAATs patterns from 1978 to 2016, except of the antarctic site (1997-2009). CNC = Cancano, NYA = Ny-Ålesund, LYB = Longyearbyen, Svalbard Lufthavn, BTN = Terra Nova Bay.

RCC also occurs in terms of mean annual snow thickness (cm) (Fig. 3.2). In fact, despite the lack of Antarctic data and some gaps in arctic ones, the general trends are decreasing since 1978. For the Alps (-2.4 cm per decade), this is consistent with Cannone et al. (2007) and Valt and Cianfarra (2010) for the whole Alps. In Svalbard the trend is more marked for Ny-Ålesund (-7.8 cm per decade), despite the incomplete data series, and less steep for Longyearbyen (-1.3 cm per decade), but generally in accordance to the American Arctic (Callaghan et al., 2011). Annual variations are well visible in the Alps and at Ny-Ålesund, while less evident in Longyearbyen. Nevertheless, the Alps annual averages remain higher than the Arctic because of the higher annual precipitations.

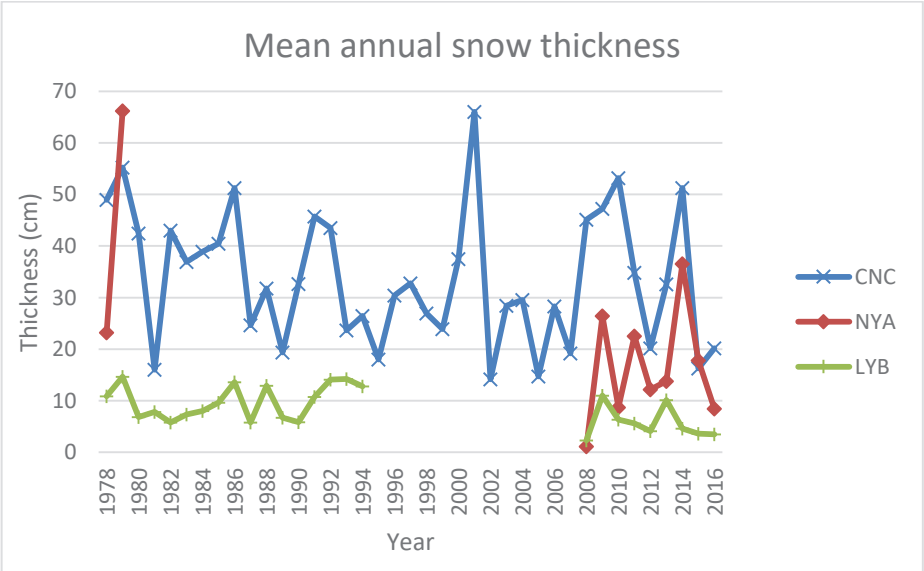

Figure 3.2. Graphic representation of the mean annual snow thickness patterns from 1978 to 2016. CNC = Cancano, NYA = Ny-Ålesund, LYB = Longyearbyen, Svalbard Lufthavn.

Trends of annual precipitations (both liquid and solid) show different variations in the study sites (Fig. 3.3) (data not available for Terra Nova Bay). On the Alps, the trend is positive (+23 mm w.e. per decade), following the trend of Cannone et al. (2007) and Walther et al. (2002), despite the very large interannual variations. In Svalbard the the precipitation trend is almost costant at Longyearbyen (+8.8 mm w.e. per decade), but with small interannual variations. Conversely, Ny-Ålesund shows an increasing trend (+45 mm w.e. per decade) with higher amounts compared to Longyearbyen, in accordance to Førland et al. (2011).

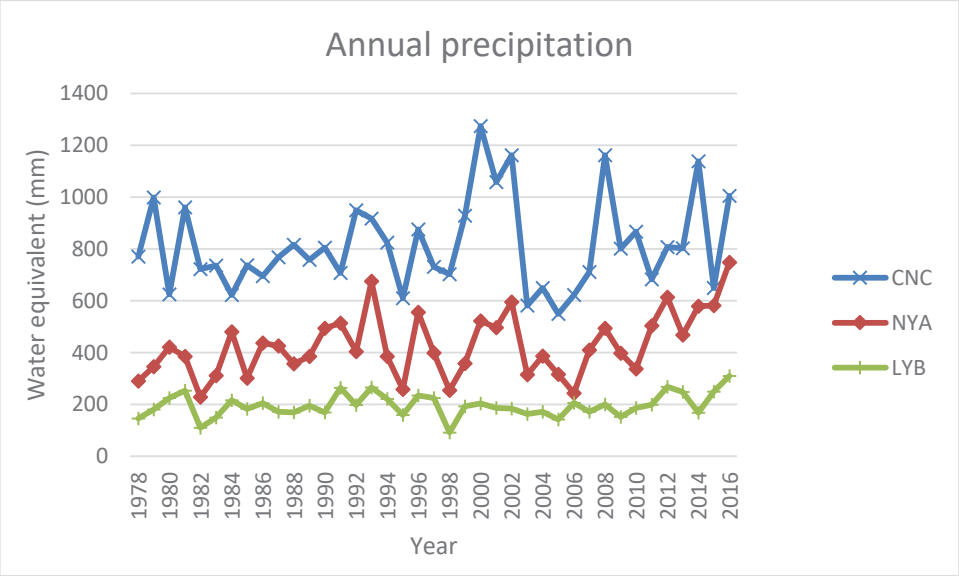

Figure 3.3. Graphic representation of the cumulative annual total precipitation patterns from 1978 to 2016 in mm of water equivalent. CNC = Cancano, NYA = Ny-Ålesund, LYB = Longyearbyen, Svalbard Lufthavn.

The simple representations of the climatic parameters described above aim to demonstrate how climate is changing, increasing in air temperatures especially in the Arctic and Alps. The snow pack distribution and duration is very important in interacting ground systems studies, even more than the single total precipitations. The intensity and frequency of snowfalls are strictly dependent on winter air temperature and precipitations, thus producing a mosaic of micro environmental future scenarios, even though a general diminution of snow is hypothesized below 3000 m a.s.l. on the Alps (Beniston, 2012).

4. MATERIALS AND METHODS

4.1 ALPS

4.1.1 LANDFORMS SELECTION

To study the landforms that experienced some vegetation changes related to RCC, the maps proposed by Cannone et al., (2007) were analysed through ArcGIS 10.3 (ESRI, 2011) in order to obtain three ecological indicators of the colonizing vegetation derived by the different original vegetation communities. The three ecological indicators are climax stage, pioneer stage and barren ground. Once obtained the ecological indicators for both the maps, an attribute query was computed to highlight the zones that experienced a regression change, for example: from climax to pioneer, from pioneer to barren ground and from climax to barren ground (Fig. 4.1). All the landforms ocurring, independently by their origin, where these three indicators were present, were selected.
Afterwards, for all the landforms selected at least one feature for each type was analysed also in areas where the vegetation regression was absent.
A total of 20 landforms (3 rock glaciers; 4 scree slopes; 5 block streams; 2 rock-banked solifluction lobes; 4 areas with turf-banked solifluction lobes and terraccetes and 2 areas with ploughing blocks) were analysed. In addition, 4 small areas affected by ice needles formation and 4 areas without evidences of particular landforms were also monitored.

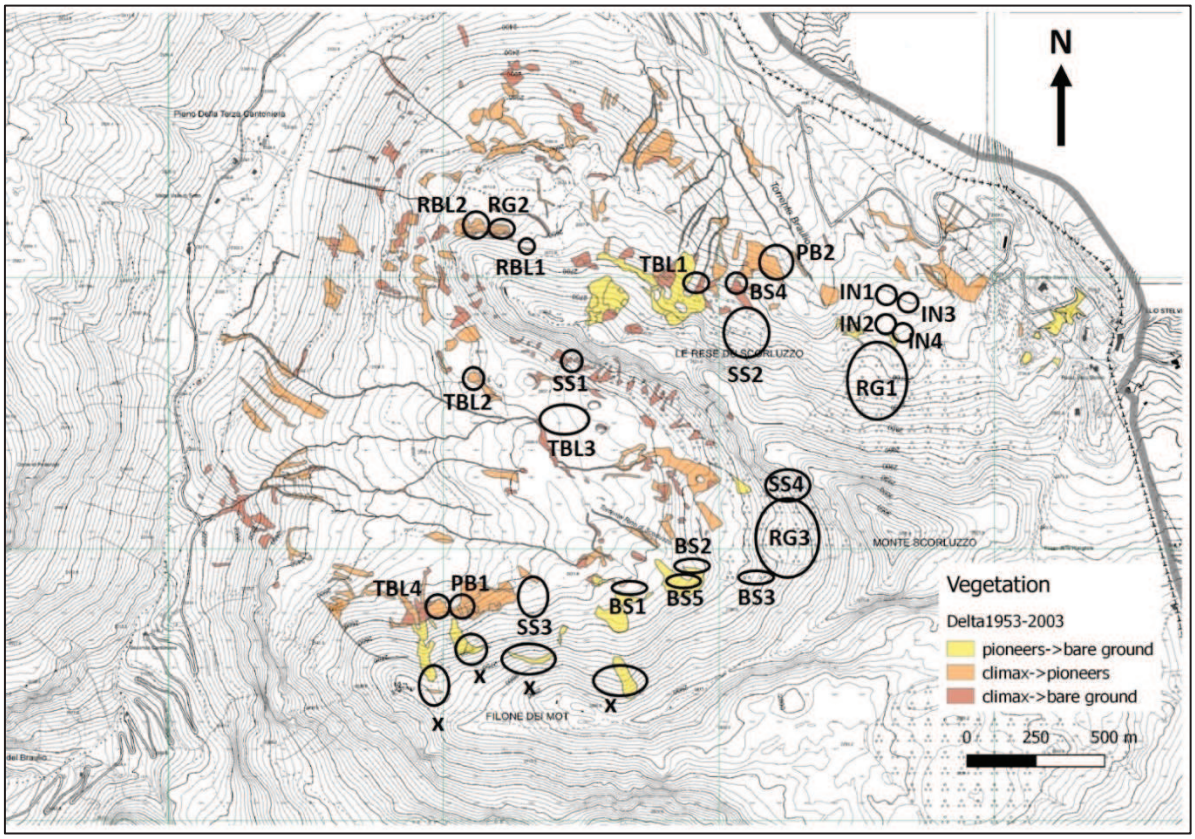

Figure 4.1. Distribution of the monitored landforms on the vegetation change map from 1953 to 2003. IN = ice needles, RG = rock glacier, DF = debris-flow, SS = scree slope, BS = block stream, TBL = turf-banked lobes, RBL = rock-banked lobes, PB = ploughing blocks, X = monitored lines without evidences of particular landforms.

4.1.2 SURFICIAL DISPLACEMENTS MONITORING

As diverse periglacial features were encountered in this study, different methods were used to study the surficial dynamics, besides the general description of the landforms (i.e. slope, aspect, average grain size, length, altitude).

In particular, for large to medium features (rock glaciers, rock-banked lobes, scree slopes, block streams) a minimum of 3 transversal lines per each feature were painted at the beginning of summer 2015 (after the snowmelt) and distributed within the features in a way to cover the total length of the landforms. As reference of the lines were chosen rock outcrops or big stable blocks (> 100 cm of diameter) according to the protocol proposed by Harris et al. (1998) to monitor movements of block streams. Generally, we tended to monitor each line twice per year, once after the snowmelt (mid to late July) and once at the end of the summer (end of September to beginning of October) for a total of 3 years (2015, 2016 and 2017) (see details in Tab. 4.1). The first survey indicated the dynamics occurred during the snow cover period (autumn, winter, spring), while the second survey indicated the dynamics occurred during the snow free period (summer). Displacements were surveyed by stretching a ribbon ruler along the painted lines and by counting the painted clasts moved down from the lines.

For each clast > 2 cm, the vertical distance from the line (cm), the horizontal distance from the beginning of the line (cm), the a axis dimension (cm), rotation (°), toppling (°) were recorded. Further, non-painted clasts that fell on the line were described with the same method. In addition, a description of the whole lines was conducted (i.e. distance of grain size change, slope, aspect) (Fig. 4.2).

Table 4.1. Survey dates for the largest landforms studied. Due to their unappreciable movements, block streams were monitored once per year. Other missing data ("-") in 2017 were due to an early snowfall that persisted during the season except on south-facing landforms. While RG3 and SS4 monitoring started in 2016. Instead, a survey of a previous monitoring project on old lines was conducted for SS1, SS2 and RG1.

	2015		**2016**		**2017**	
	First Survey	**Second Survey**	**First Survey**	**Second Survey**	**First Survey**	**Second Survey**
RG1	31-07-15	19-09-15	26-07-16	25-09-16	12-07-17	-
RG2	11-08-15	19-09-15	30-07-16	14-09-16	20-06-17	-
RG3	-	-	07-09-16	29-09-16	13-07-17	-
SS1	12-07-15	15-09-15	30-08-16	26-09-16	19-06-17	29-09-17
SS2	30-07-15	-	03-08-16	16-09-16	15-07-17	-
SS3	-	19-09-15	-	09-09-16	28-07-17	-
SS4	-	-	08-09-16	29-09-16	13-07-17	30-09-17
RBL1	06-08-15	19-09-15	01-08-16	28-09-16	20-06-17	-
RBL2	-	-	06-09-16	28-09-16	21-06-17	30-09-17
BS1	20-08-15	-	17-08-16	-	28-07-17	-
BS2	21-08-15	-	02-09-16	-	28-07-17	-
BS3	21-08-15	-	06-09-16	-	28-07-17	-
BS4	21-08-15	-	06-09-16	-	28-07-17	-
BS5	-	-	18-08-16	-	04-08-17	-

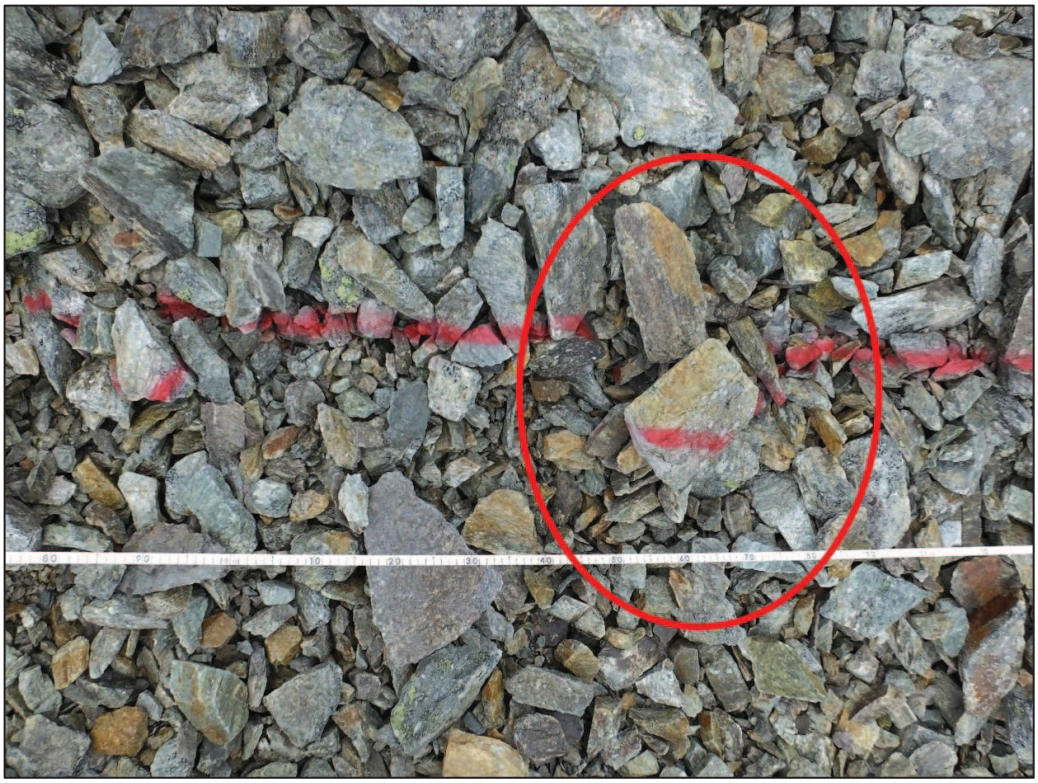

Figure 4.2. Example of a survey conducted on F2, Line 2. From 19.55 to 19.67 m the line moved downward due to a pebble of 19 cm of diameter, parallel to the line. This displacement was probably due to a push from above: a block of 26 cm of diameter covers the line from 19.55 to 19.65 m and overcomes it by 3 cm downward.

Some of the previously described displacement lines were used for the calibration of the surficial displacement model of the study area. Thus, the maximum cumulative movement (until summer 2016) of points (in cm) representing 10-meter sectors of the painted lines were extracted. A total of 85 points spread on 2 rock glaciers, 3 scree slopes, 3 block streams, 1 rock-banked lobe and 1 debris-flow (old monitoring) were selected. Roughly, the 30% (23) of those points has been taken apart to set up the validation set to calibrate the model. This method follows in part the “random partition” of Chung and Fabbri (2003) with the exception that the selection of the test set was not done randomly but by choosing 2 to 3 points placed at different altitudes on each landform to better represent all the landforms in the model (Fig. 4.3).

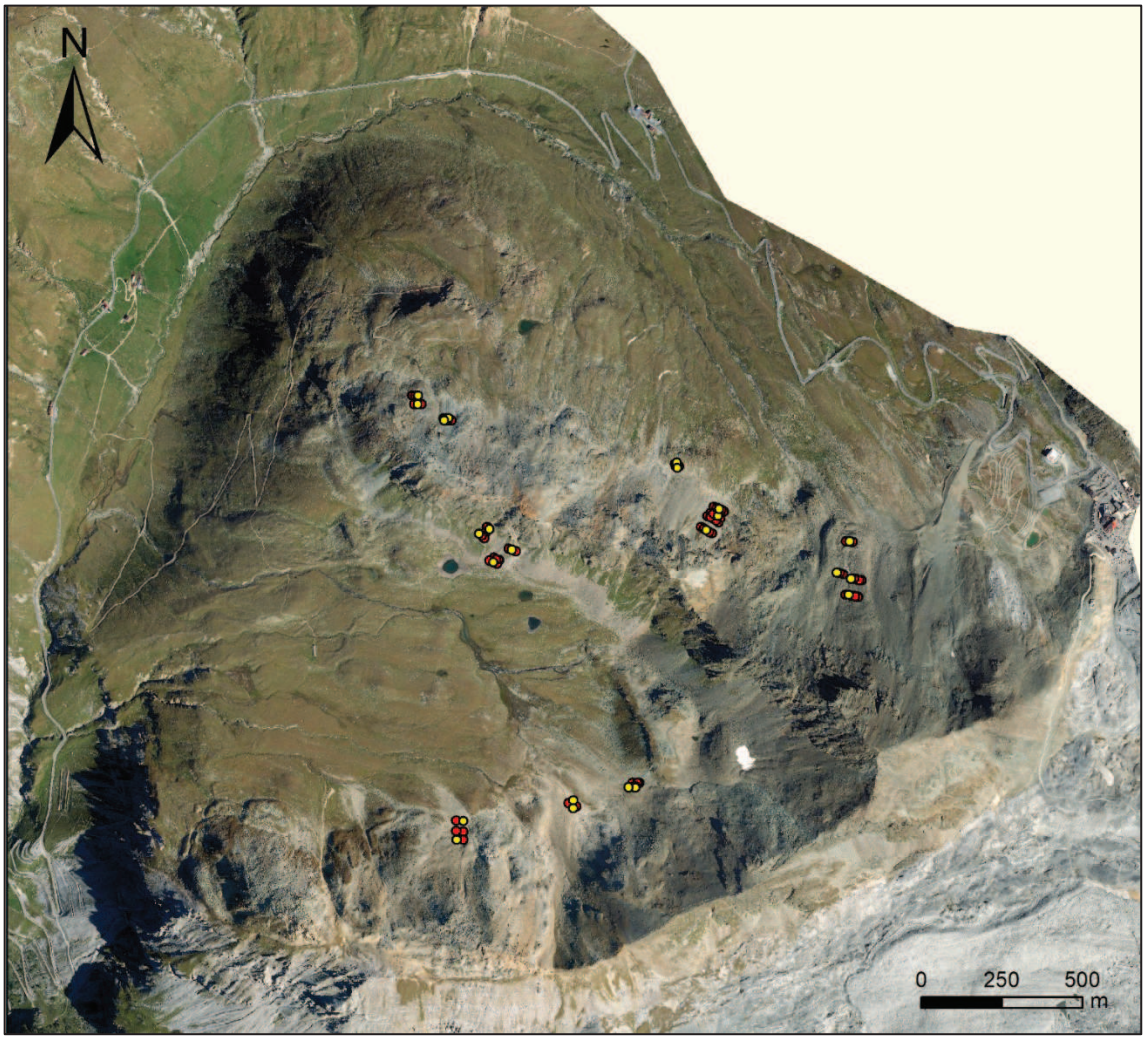

Figure 4.3. Distribution of the selected displacement points on the study area. They represent the different type of landforms present at the slope areas. Red dots indicate the training set, yellow dots the validation set.

For mid to small features such as turf-banked lobes and terracettes and ploughing blocks, a different approach was experimented. 6 vegetated sites were selected in different topographic conditions for a total of 3 lobes 2 terracettes and 2 ploughing blocks. Concerning the dynamics, 4 metal poles were anchored into the soil at the length and width extremes of lobes and ploughing blocks, 2 just at the width extremes of the terracettes. This helped to maintain a 3.2 m metal bar stable above the feature to move an electronic diastimeter (height-o-meter) and record the profile heights every 5 cm (Fig. 4.4). Since the movement is poorly appreciable in one year, the procedure was started in early summer 2015, repeated at the end of summer 2015 and in summer 2017 (Tab. 4.2). Beside this, a morphometric survey was conducted as described by Matsuoka et al. (2005). This method was also repeated for all the solifluction lobes and terracettes found on the whole study area, thus reaching a total of 110 features. To show evidences of motion inside the solifluction features, one per site was chosen to be excavated and described according to the soil taxonomy (USDA, 2010). To test solifluction action with a parallel method, an other site of lobes was selected and 2 lobes plus a control area free of features (all within 10 meters) to use a test pillars method already experimented by Benedict (1976), Matsuoka (2010) and Ballantyne (2013).

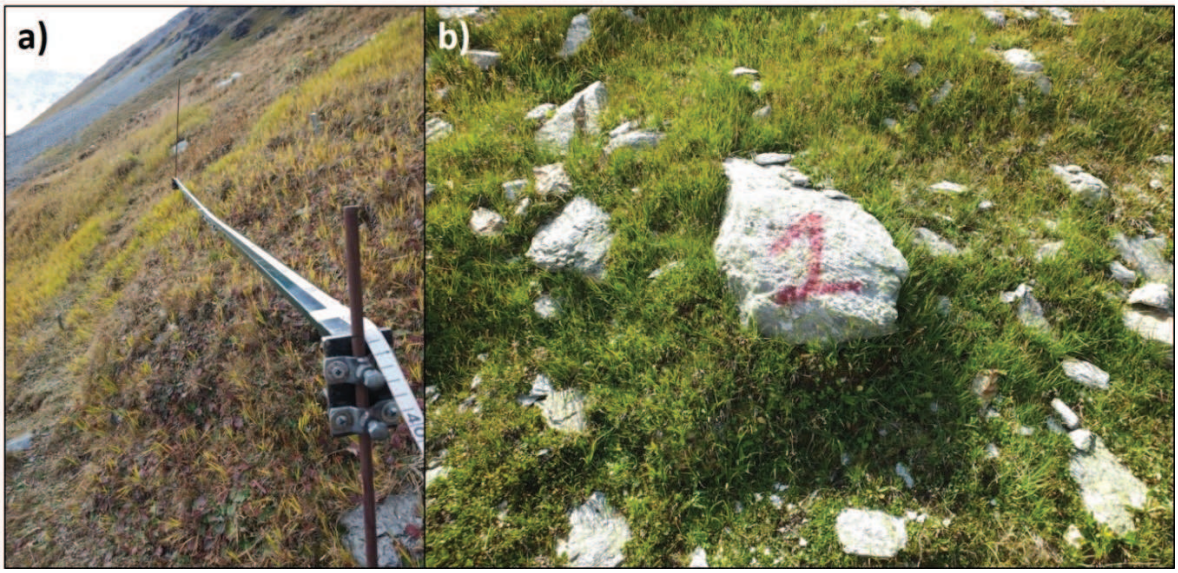

Figure 4.4. Examples of a) height-o-meter monitoring on the first terrace of TFL2 and b) one of the ploughing blocks present in PB1.

Table 4.2. Vegetated areas selected for mid to small features monitoring with the quantity of landforms and the survey dates.

		2015		2017
		First Survey	Second Survey	Survey
TBL1	Single lobe	11-07-15	15-09-15	14-07-17
TBL2	Two terraces	27-07-15	17-09-15	14-07-17
TBL3	Single lobe	03-08-15	19-09-15	14-07-17
TBL4	Single lobe	20-08-15	21-09-15	14-07-17
PB1	Single block	20-08-15	21-09-15	14-07-17
PB2	Single block	23-08-15	21-09-15	14-07-17

Small landforms, or better processes, treated in this thesis refer just to needle ice. For this process grain size, soil temperature and soil moisture are the major drivers. Thus, surficial grain sizes was assessed by visual estimation, while soil texture through sieving and sedimentation, according to Sheldrick and Wang (1993). Ground temperatures were recorded through thermistors (Onset HOBO U23, accuracy 0.2 °C) at different depths. Soil moisture was assessed as gravimetric content (%) by weighted, dried at 105 °C for 24 hours and re-weighted soil samples at different depths. The innovative technique used to monitor small heaves and creeps driven by needle ice has been a new application of the structure from motion (SfM) (Carrivick et al., 2016), a branch of the photogrammetry method. In fact, common digital cameras are able to acquire good images of an object and, if properly overlapped, they may produce good results. In this case, the object was a 1 meter square plot of which several converging images (James and Robson, 2012; James and Robson, 2014) were taken in different moments of the day/night to produce different dense point clouds (when the overlaps of the images is sufficient: 80% at least). In this way a digital elevation model (DEM) and orthophoto were obtained. However, DEM an orthophoto were usable only if georeferenced. To rectify the dense point cloud many studies have used differential GPS (Kääb et al., 2014) to get precise X, Y and Z coordinates of

stable ground control points (GCPs) spread homogeneously on the plot (Fonstad et al., 2013). In fact, thanks to the non-variability GCPs coordinates, it has been possible to acquire movements/changes of the surrounding areas with minimum errors. To do this and to avoid the expensive use of a differential GPS, small toothpicks were inserted into the soil in the plot as GCPs at the same depths. X and Y coordinates were calculated as distances in cm from the origin of the plot (bottom left corner) as the plots were placed north facing. The Z (elevations) was not necessary to build a dense point cloud because, for a triangulation principle, from the distances among GCPs tips, Z elevations are easily calculable automatically in the proper software. Agisoft Photoscan 1.2.6 was used to complete the bundle adjustment (Granshaw, 1980) of the taken images and the subsequent rectification and model building. This software is already known for the application of SfM in geomorphology studies (e.g., Eltner et al., 2016). Once the model was obtained, an automatic extraction of DEMs and orthophoto was used to manually identify horizontal displacement (creep) and vertical differences (frost heave) of clasts. Both of them were calculated in ArcGIS 10.3 (ESRI, 2011), in particular the latter was produced through the differencing of DEM (DoD) technique (i.e. Gardelle et al., 2012).

4.1.3 DATA ANALYSES

The average distance from the beginning of each line was considered as X coordinate of a point, the position of the points along the length of the landform was treated as Y coordinate and the average displacement of each clast (point) treated as Z coordinate. This scheme was repeated for the displacements occurred at the end of the first summer (2015), at the beginning of the second summer (2016) and at the last survey of 2017. The 3-axis tables of data were then imported in SURFER (Golden Software) and interpolated with a kriging algorithm (Oliver and Webster, 1990). In such a way, horizontal displacement contours have been computed to better visualize the surficial dynamics. Then, box and whiskers plots of the same corresponding periods were computed in the software STATISTICA® to understand means and ranges variations of gravel, pebbles and blocks.
Concerning data calculations, the cooling rate (°C h^{-1}) of needle ice plots was obtained at depth of 2 and 5 cm by dividing the amplitude of temperature recorded from sunset (6:30 p.m.) to the time of needles formation for the time past in the same interval. The potential freeze-thaw cycles (PFTC) were calculated as the numbers of time in which the minimum air or ground temperature at 2 and 5 cm goes through the threshold of 0 °C divided per two (Guglielmin et al., 2008). Moreover, the duration of the freezing during the ice needle formation has been indicated by the Freezing index (Fi), calculated as the sum of the temperature below 0 °C recorded every minute between the sunset and the time of ice needle maximum development.
To identify which environmental factors (minimum air temperature; minimum ground temperature at 2 and 5 cm of depth; minimum and maximum water content at 2 and 5 cm of depth) influenced the development and evolution of needle ice, we performed a general regression model (GRM which is an implementation of conventional linear regression models for a continuous response variable given continuous and/or categorical predictors, Hill and Lewicki, 2006) by selecting the significant factors with a backward stepwise method. The GRM was performed using the software STATISTICA®.
The extraction of topographic and geological information of the study area was possible by using a DEM at 5 m of resolution

(http://www.cartografia.servizirl.it/arcgis/services/wms/DTM5_RL_wms/MapServer/WMSServer) and a geological map (Montrasio et al., 2012). Therefore, a slope map and a solar radiation map were obtained. Then, from the geological map it was possible to extract a map of the deposit class types and a classified map of the age of the deposit with reference to the little ice age (LIA).
Beyond these surface data maps, climatic informations (in terms of mean air temperature per each pixel) were calculated with a linear regression equation deriving from the air temperatures of three closest automatic weather stations and their elevations. Thus, the DEM was converted into mean air temperature of different periods in 2015 and 2016: snow period (mean daily air temperature < 0 °C and snow coverage of the area > 90%), melting period (mean daily air temperature > 0 °C and snow coverage of the area < 90%), snow-free period (mean daily air temperature > 0 °C and snow coverage of the area < 10%), freezing period (mean daily air temperature < 0 °C and snow coverage of the area < 90%). Afterwards, daily snow maps at 250 m of resolution (Notarnicola et al., 2013a,b) of the study area were used to estimate the number of days per period at each pixel without snow coverage. Since the snow pack acts as a temperature insulator (Guglielmin et al., 2014), in this way it has been possible to assess which pixels and for how long have undergone a more direct effect of air temperature compared to other pixels. Thus, by excluding snow-free periods, several snow maps were selected to calculate an assessment of number of days without snow coverage all over the periods of 2015 and 2016 (snow period, melting and freezing). Hence, snow-free days maps and temperature maps of each period were multiplied in order to obtain an indication of ground temperatures. In these terms, the more a pixel have been uncovered, the more similar the ground temperature to the air temperature could have been. Furthermore, two snow-free days maps were made with the cumulative days without snow per pixel in 2015 and 2016. They were averaged to obtain a single map of average snow-free duration.
Since the index of the ground surface temperature is not enough to explain a trigger in surficial dynamics, indices of thawing degree days (TDD) and freezing degree days (FDD) (Carter et al., 1991; Fronzek et al., 2006) at the ground surface were calculated with the same principle described above. To do this, mean TDD and FDD were calculated per each period with the regression equation obtained from the three automatic weather stations. In this way, TDD and FDD maps were obtained per each period. TDD/FDD maps of freezing, snow-free and melting periods were then multiplied by the corresponding snow-free days maps and then periods of 2015 and 2016 averaged. The resulting periods were then summed to obtain mean annual maps of ground heating index (GHI) and ground cooling index (GCI).
All the maps operations described above were conducted through the raster calculator tool in ArcGIS 10.3 (ESRI, 2011). After the extraction of the maps variables at each of the remaining training set of points (62), a table of both categorical and continuous data was obtained. At this point, a multiple regression (Aiken et al., 1991) model was used to select the dominant variables with a backward stepwise option and it was run in STATISTICA©.
Afterwards, the fitness of the predicted movement with the measured one was run with a linear regression on the training set, while the predictability on the validation set.

4.1.4 VEGETATION CHANGES

In addition to geomorphic indications, a vegetation survey was conducted on the painted lines once per year, after the snowmelt. In fact, it has been supposed that the vegetation community structure does not change during few summer months. The measurement principle followed the same of Canfield (1941) called “line interception” then well described by Coulloudon et al. (1999) and repeated by McDonald (1980), Kaiser (1983), Kuchler and Zonneveld (1988), Muttlak and McDonald (1992), Zhou et al. (1998). Briefly, patches of vegetation on the painted line were measured as distance from the first extreme, length and width and floristic composition checked. For well vegetated features only patches touching the line were surveyed, for half-vegetated features an additional buffer range of 10 cm uphill and 20 cm downhill the line were surveyed, for poorly vegetated features an additional buffer range of 30 cm uphill and 50 cm downhill the line were surveyed. This has been helpful for identifying typical patches or species which have created micro-habitats for the downhill species by consolidating fine to coarse debris (Cannone and Gerdol, 2003). In addition, the frequency of species encountered on the line was treated as an indicator of: a) the scree association occurring on that landform (*Oxyrietum dyginae*, *Luzuletum spadiceae*, *Androsacetum alpinae*), b) the turn-over of species compared with previous surveys (Giacomini and Pignatti, 1954; Cannone and Pignatti, 2014). Lastly, the coupled information about species and clast displacements have been joint with box and whiskers plots in STATISTICA® to quantify the surficial movement tolerated by each species.

The vegetation change of mid to small solifluction features (turf-banked lobes and terracettes and ploughing blocks) was initiated by following the vegetation relevé (Braun-Blanquet, 1951; Cannone and Pignatti, 2014), conducted on the riser and the tread of the monitored forms.

Eventually, a recent vegetation map of the study area (2013, unpublished data) that followed the same methods of the two previous ones (Giacomini and Pignatti, 1955; Cannone et al., 2007) was simplified to obtain a coverage information in classes: 1 = bare ground (total coverage < 5%), 2 = discontinuous (total coverage 5-50%), 3 = continuous (total coverage >50%).

4.2 ARCTIC

4.2.1 EXPERIMENTAL SETUP

While on the Alps biogeomorphic interactions are more evident in slope processes (higher dynamic due to the gravity than flat and high vegetated areas), in the Arctic, periglacial processes join cryotic processes also at flat areas due to the shallower permafrost table (French, 2007). This is evident when encountering patterned grounds (stone circles), soil stripes, frost hummocks or vertical sorting of grains. Here, apparent stable flat zones undergo frost heave depending on the soil moisture, grain size and temperatures (Outcalt, 1971; Grab, 2001). Therefore, we decided to study vegetation in relation to surficial dynamics likely driven by thaw and melt cycles with a circumpolar active layer experiment (CALM) grid (Brown et al., 2000).

In Ny-Ålesund, an almost flat homogeneous area was selected to build a 50 x 50 m grid with 36 nodes and a span of 10 m. Despite the smaller dimensions than those provided by the CALM experiment due to the topography of the area, it was possible to remain close to the climatic change tower (CCT), a 30-meter high tower, designed to monitor energy balance and exchange between the air and the surface and thus useful to get air temperatures. At each node of the grid, a plastic snow stake was anchored into the soil with its height fixed at 1.2 m from the surface. Plastic stakes were useful for several reasons: a) coupled with reflex camera installed on the CCT (9 m of height) equipped with a time-lapse system (Harbotronics) able to take photos of the whole grid every hour, it was possible to calculate the snow thickness at any time by measuring the length of the stakes remaining outside of the snow (Fig. 4.5). These values were also calibrated with several manual measurements probing the snow cover carried out in different times during the experiment. b) assess the days of snow presence/absence for each node. c) the length of the stakes from the surface was measured at the beginning of each summer and then the stakes were replaced at the original depth (leaving 1.2 m outside) in order to measure also the total frost heave (FH).

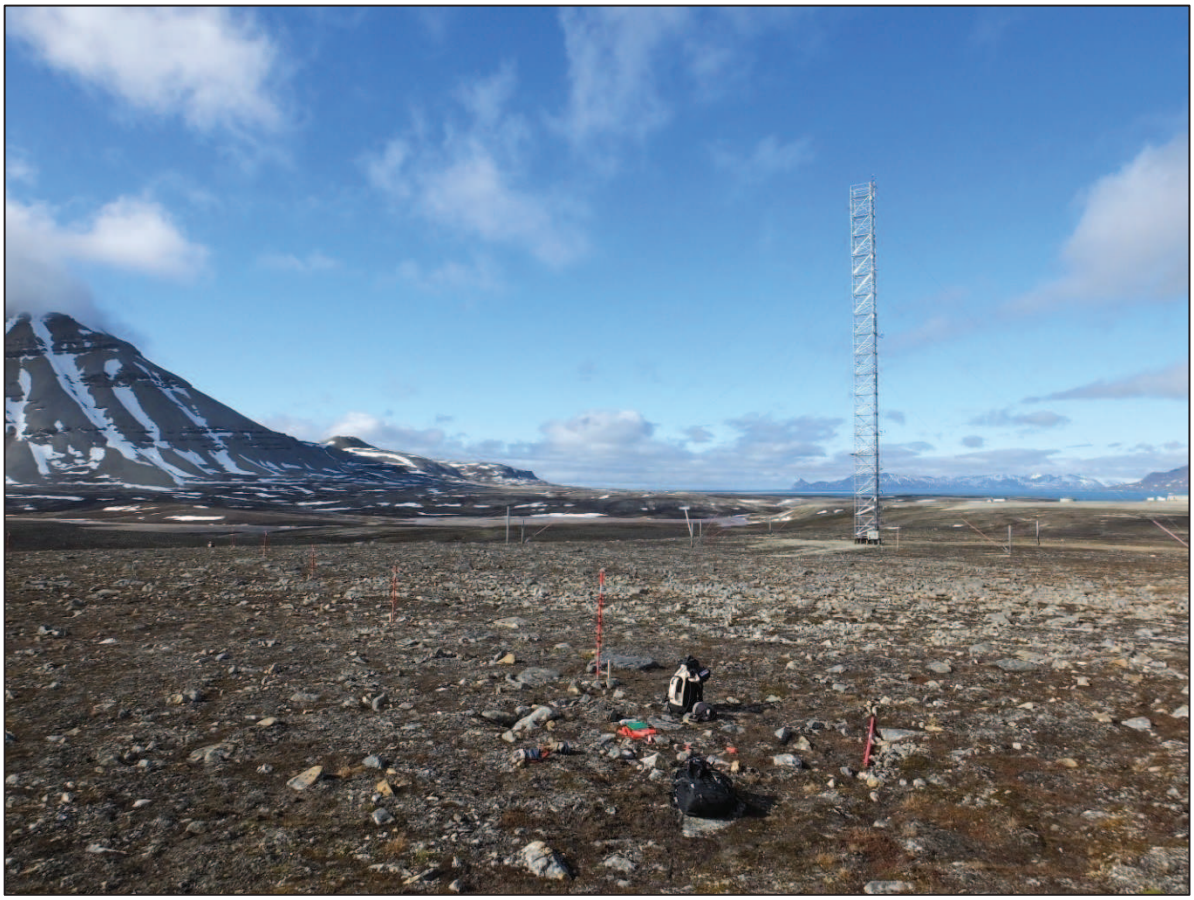

Figure 4.5. View of the CALM grid under construction and the CCT where the camera was placed.

12 of 36 nodes were equipped with 4 thermistors (Hobo U23, 0.2 °C of accuracy) inserted at 2, 30, 60 cm and at the maximum available depth (ranging between 79-101 cm). They have been recording soil temperature every 30 minutes since July 2014.

Also single field observations were conducted: a) inclination and aspect of the plots (measured through a compass), b) surficial grain size through visual estimation, c) litter height and A0 horizon thickness through a caliper.

In addition, SfM method used for ice needles on the Alps was applied to monitor micro-changes at the plot scale. Each plot has been equipped with toothpicks as GCPs and converging images acquired every summer.

Since toothpicks are not stable and findable after the arctic winter, they were replaced every summer at the surveying moment. Thus, to bypass the problem of vertical errors in GCPs coordinates likely obtained with the FH of the whole plot and thus toothpicks, one multiannual GCP with a stable elevation was chosen at each plot, corresponding to the fixed wooden picks at one corner of the quadrat. Its height was controlled each summer and replaced in case of heaves (Fig. 4.6).

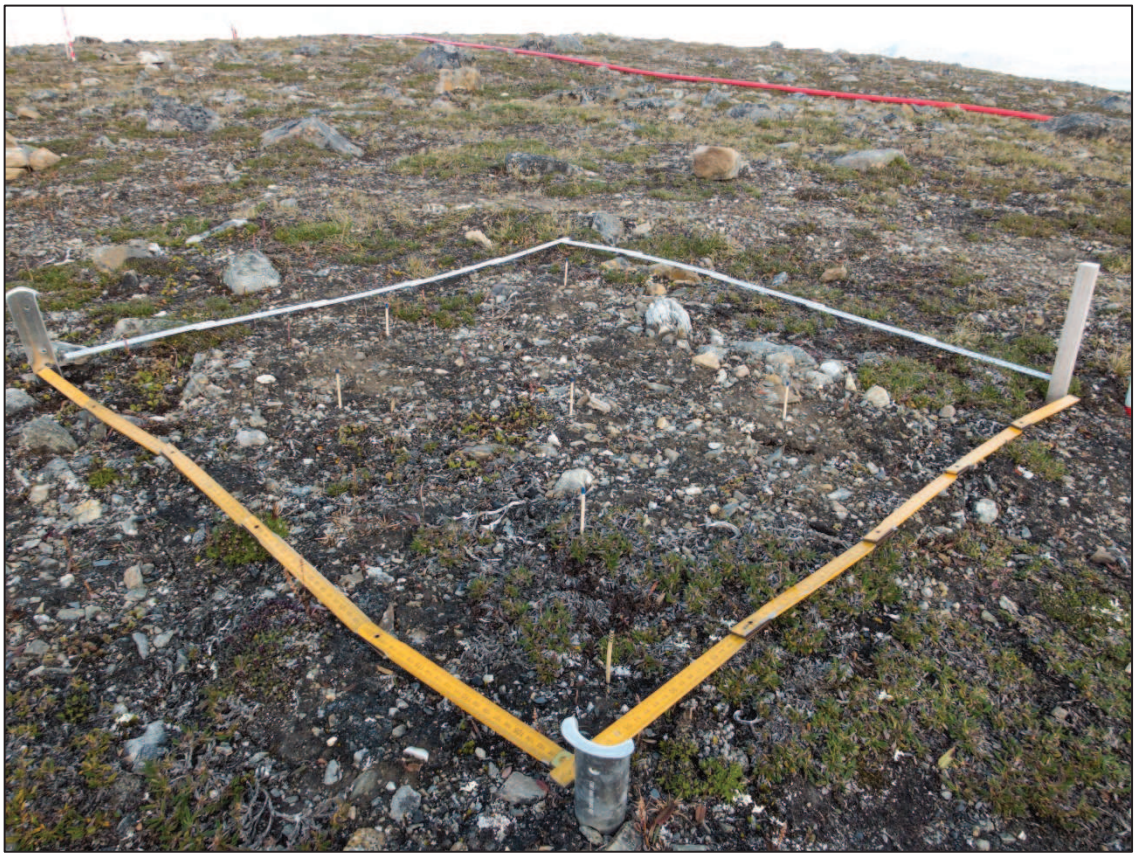

Figure 4.6. Example of one plot adjacent to the snow stake. Inside the quadrat, several toothpicks used for GCPs are visible. This is one of the pictures also used for the SfM reconstruction.

To investigate ecosystem feedbacks in terms of carbon fluxes, seven small circular plots (23 cm diameter) were installed within a ray of 200 m from other on the ice-wedge polygon site (Adventdalen valley) in order to represent the environmental variability but keeping comparable topographic conditions (slope, elevation, aspect) (Fig. 4.6). In fact, beyond topographic characteristics, also the geomorphology (distance from the polygon border, active layer thickness (ALT)) was recorded. Hence, ALT was measured by probing with a metal probe according to the CALM experiment (Brown et al., 2000) 4 points around the plot and within 50 cm and averaging them.

A portable automated CO_2 exchange instrument (ACE, ADC BioScientific Ltd., http://www.adc.co.uk) was used to get carbon dioxide fluxes from the ecosystem represented by the plot through an infra-red gas analyzer (IRGA) system. A typical data acquisition was represented by 10-minute assays, 2 consecutive in light conditions and a following one in darkness condition (by covering the chamber with a dark blanket). Light conditions indicated the net ecosystem exchange (NEE), while darkness conditions the ecosystem respiration (ER), both expressed as µmol CO_2 $m^{-2}s^{-1}$. ER values were always positive (showing a release of CO_2 from the ecosystem to the atmosphere), while NEE showed both positive and negative values: when NEE < 0 the ecosystem incorporates CO_2 from the atmosphere, when NEE > 0 there is a release of CO_2 from the ecosystem to the atmosphere. Using the measured values for NEE and ER we calculated gross primary production (GPP) using the equation GPP = NEE − ER. The ACE machine system was coupled with a thermistor (ADC Bioscientific), a soil moisture (moisture sensor Decagon Echo) and a photosynthetically active radiation (PAR, µmol $m^{-2}s^{-1}$) (a silicon photocell) sensor. They acquired data at the same time of flux exchanges at 2 cm of depth for the

formers and at 30 cm of height for the latter. Stainless steel soil collars (10 cm height, 23 cm diameter) delimited the plots and remained inserted in the soil for the whole study period, which started on 17 June 2013 and ended on 4 October 2013 for a total of 775 assays.

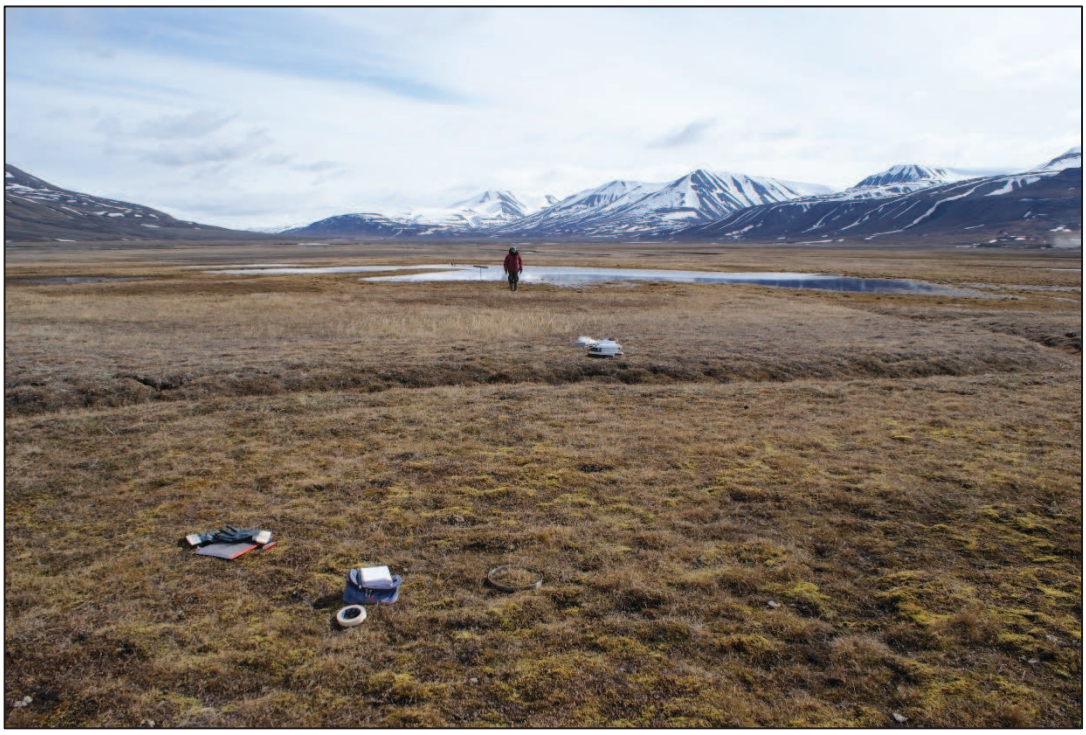

Figure 4.6. View of the ice-wedge polygons site at Adventdalen valley. At the bottom a soil collar is visible, while the operator indicates the farthest plot position.

4.2.2 DATA ANALYSES

Concerning the CALM grid, ALT has been calculated according to Guglielmin (2006) by interpolating the two lowermost daily maximum ground temperatures available at each shallow monitored borehole and therefore represents the yearly maximum depth of 0 °C isotherm. In fact, the coarse nature of the sediments in this site exclude the possibility to use the classical probing method to define the maximum thawing depth. In this view, spatial and temporal variability of ALT was assessed with the the normalized index of active layer variability (INV) according to Hinkel and Nelson (2003). Moreover, ground temperatures were used to calculate: a) thawing degree days (TDD), b) freezing degree days (FDD) according to the international tundra experiment (ITEX) manual (i.e. Molau and Mølgaard, 1996) and c) N-factor according to Klene et al., (2001) for understanding the effects of the snow and of the vegetation on the ground surface temperature.
Samples of the topsoil (0-5 cm of depth below the A0 horizon) for each stakes were sieved (ASTM, 2003), tested with a pH-o-meter at 1 M solution, desiccated for 24 hours at 105 °C and organic matter content calculated through the LOI method (Loss on Ignition at 550 °C) (Heiri et al., 2001).

Maps of the grid were obtained by interpolating the grid nodes in ArcGIS 10.3 (ESRI, 2011) with the natural neighbor algorithm (Sibson, 1981) and successively 3D maps were generated in ArcScene 10.3 (ESRI, 2011). While the photogrammetric procedure was conducted in Agisoft Photoscan 1.2.6.
At Adventdalen, by analyzing our phenological observations, we divided the growing season in three periods: early season (from snow melt to the completion of greening phenophases), peak season (during the reproductive phenophases) and late season (during leaf senescence).
Preliminary analyses (through linear regression) allowed us to avoid redundancy in selecting the variables to be used for further analyses.
As both NEE and ER had a normal distribution, we performed a general regression model (GRM) to identify the relation of the main abiotic and biotic factors (thaw depth, PAR, soil temperature, soil moisture, daily precipitation, as continuous variables; plant phenology and plot as categorical variables) with NEE and ER (Cannone et al. 2012, 2016). Te selection of the significant factors followed a backward stepwise method for the full season, as well as separately for early, peak and late season. In addition, to analyse also the effect of fixed and random factors we performed a generalized linear mixed model (GLMM). For both GRM and GLMM we selected the model with the best fit based on Akaike's information criterion (AIC), in particular, models having $\Delta AIC < 2$ (Burnham et al. 2011). Considering the similar results of the two analyses in the results and discussion we focused on the GRM. Both GRM and GLMM were performed using the software STATISTICA®.
At the end of the field campaign, above ground and below ground phytomass and soil samples were collected for each plot to carry out laboratory analyses. In fact, water content for the 3 types of samples was determined by weighting, oven drying at 105 °C for 24 hours, and then re-weighting the sample. In addition, soil samples were air dried and their fine fraction (sieved < 2 mm) was used to measure: a) total organic matter (TOM) through loss on ignition (Heiri et al., 2001), b) pH, c) carbon and nitrogen contents by using a CHN-S analyzer to assess the C/N ratio of each sample, d) Munsell color determination by using the Munsell color chart, e) soil texture with an automated sifter (Tecnotest, 2006) and a sedimentation test for the finest fractions (< 0.075 mm) (Sheldrick and Wang, 1993). Eventually, the soil classification was achieved following the Soil Taxonomy (USDA, 2010).

4.2.3 VEGETATION DATA

Considering the CALM grid, every summer the vegetation has been estimated on each plot (1 x 1 m) installed at side of each stake according to the Braun-Blanquet method (Braun-Blanquet, 1951; Cannone and Pignatti, 2014) to get information on the community structure, coverage change, species richness and composition in relation to ALT, snow and surficial dynamics.
A similar method was used for the small plots in Adventdalen: the vegetation (% coverage and dominant species) (Braun-Blanquet, 1951; Cannone and Pignatti, 2014) was surveyed at the beginning of summer. Since vegetation phenology affects ecosystem CO_2 fluxes (Cannone et al., 2016), also phenophases of the vascular plants were recorded once a week according to the international tundra experiment (ITEX) protocol (Molau and Mølgaard, 1996) with special reference to the following phenophases: first shoots, new leaves, main shoots (greening phenophases), first flower, first visible stigma, first visible anther, main blooming, start developing seeds, mature seeds (reproductive phenophases), leaf senescence. Also snow cover occurrence and depth were recorded.

4.3 CONTINENTAL ANTARCTICA

Since the dynamics of a rock glacier are related to the internal properties of the material, two different methods were used to assess: a) the internal structure in the upper 10 m with the ground penetrating radar (GPR) and b) the distribution of ice/water content, typology and grain size with the electrical resistivity tomography (ERT). In fact, ERT displays high resistivity in presence of frozen materials, while it decreases in presence of free water. The instruments used were: for GPR a ProEx GPR (Malå Geoscience) equipped with 250 MHz shielded antennas, and triggered every 10 to 15 cm by an electro-mechanic odometer, collecting 9 profiles with a total of about 1800 m; for ERT a 16G electro-resistivity meter (Pasi Geophysics) connected with 48 electrodes having a constant separation equal to 2 m and adopting a standard Wenner electrodes configuration. Moreover, a GPS was used for absolute data positioning, with decimetric horizontal accuracy and metric vertical accuracy. In order to calibrate the automatic geophysical data described above, a long core (6.1 m) was drilled and extracted from Adélie Cove rock glacier with a widia bites core auger (Beretta T21) in November 2003. Thank to a stratigraphic description, the gravimetric ice content (Black, 1965) and the electrical conductivity with an electrical conductivity meter (Hanna Instruments-HI 98360, accuracy of ± 0.5%), it was possible to compare the core with the digital acquisition and to calibrate them.
GPR data have been processed by a standard processing flow that included: drift removal (zero-time correction), background removal, geometrical spreading correction and exponential recovery, spectral analysis and bandpass filtering, topographic (static) correction and depth conversion. In order to provide a more constrained GPR data interpretation, we used a technique routinely used for reflection seismic data (e.g., Chopra and Marfurt, 2007). Further, phase- and frequency-related GPR attributes were used to improve discriminations between zones with different attenuation properties. Apparent resistivity obtained from ERT were associated with the topographic profile into RES2DINV software (Loke and Barker, 1996), which also adopts a smoothness-constrained least-squares inversion algorithm to recover the true resistivity model. Into the software it was also possible to cancel noisy and out-of-range data. Thus, the 14% of ERT data was removed. Additional factors to be considered in ERT interpretation are: a) ice content, b) temperature, c) salt and related unfrozen water (e.g., brines).

5. RESULTS

5.1 Vegetation tolerance to the surficial dynamic, a case study of three active rock glaciers in Central Alps.

5.1.1 INTRODUCTION

Rock glaciers are the most visible and widespread permafrost-related landform of cold environments. They have been the object of several studies related on: palaeoclimate (Konrad et al., 1999; Frauenfelder and Kääb, 2000), responsiveness to recent temperature increase (Roer et al., 2005, Kääb et al., 2007; Delaloye et al., 2008), rheology (Kääb, 2006; Serrano et al., 2010), sediment transfer rates (Gärtner-Roer, 2012), discharge through ice melt (Azócar and Brenning, 2010), hydrological effects (Roer et al., 2008), permafrost distribution (French, 2007; Serrano et al., 2010).
Concerning the rheology, the horizontal displacements of alpine rock glaciers typically range between several centimetres to around 1 m per year (Haeberli et al., 2006), 0.05-0.7 m per year in the Arctic (Haeberli et al., 2006; Kääb, 2006) but up to 100 m per year in Andes (Corte, 1987).
This have been studied because surface measurements appear to be good indicators of the whole rock glacier body (Wirz et al., 2016). However, recent studies have majorly focused on rock glacier surficial dynamics at different temporal scales (e.g., Kääb et al., 2007; Perruchoud and Delaloye, 2007; Delaloye et al., 2010) but few of them at intra-annual resolution (Krummenacher et al., 2008; Buchli et al., 2013; Wirz et al., 2016).
Further, the study of rock glacier dynamics as dependent on climate conditions have been addressed (Haeberli et al., 2006; Kääb et al., 2007; Bodin et al., 2009). In fact, the linkage between rock glaciers and permafrost creep (Haeberli, 2006), gravitation (Lugon and Stoffel, 2010), mass advection processes, thaw settlement and frost heave (Lugon et al., 2004) are thought to be directly related to climate change (Serrano et al., 2001, 2004, 2006; Lugon et al., 2004; Sanjosé et al., 2007).
However, the impact of the change of alpine rock glacier dynamics could not only be addressed to the entire geosystem but also to alpine ecosystems as fundamental part of the mountain landscape. In this view, few studies focused on vegetation as indicator of surficial dynamics in cold systems such as solifluction lobes (Eichel et al., 2017), glacier forefields (Moreau et al., 2008) and rock glaciers (Cannone and Gerdol, 2003; Burga et al., 2004; Gärtner-Roer et al., 2013).
Therefore, in this section 3 scientific questions will be treated: a) understand the spatial distribution of surficial displacements of 3 alpine rock glacier at seasonal and annual scale; b) assess the geomorphic processes involved in such displacements; c) define the frequency of occurrence and quantify the surficial displacement tolerated of some alpine tundra species growing on the studied rock glaciers.

5.1.2 STUDY AREA

The study area is located around Stelvio Pass (46°31’ N, 10°27’ E, 2757 m a.s.l.), a high alpine site in Stelvio National Park in the Italian Central Alps (Upper Valtellina).
More specifically, the site is situated on the hydrological left side of the upper part of Braulio valley, in the western glacial cirque and northern slopes of Mt. Scorluzzo (3095 m a.s.l.). At the norh-east edge of the study area, the Stelvio Pass links the Valtellina and Braulio valley with the Venosta valley and the province of Bolzano, whereas at the north-west edge the Umbrail pass (46°32’ N, 10°26’ E, 2503 m a.s.l.) connects with the Müstair valley and the Swiss Confederation. The whole study zone is about 5.8 km^2, with an elevation range of about 900 metres, and spreads from the main road SS38 up to the summit of Mt. Scorluzzo. The hydrological catchment is defined by the Braulio river basin, which feeds the Adda river (Fig. 5.1.1).
The climate is characterized by a continental regime (Ceriani and Carelli, 2000), with a highly variable values of precipitation because of the complex orography. Climate data for the 1978-2015 period from the nearest available meteorological station at Cancano (46°31.04’ N, 10°19.25’ E, 1948 m a.s.l., 9 km to E-SE) indicate a mean annual air temperature (MAAT) of +3.3 ± 0.75 °C. January is the coldest and driest month (-5.2 ± 1.8 °C; 38.9 mm) while July is the warmest and wettest (12.2 ± 1.6 °C; 94.7 mm). Mean annual precipitation sum is 810 mm, 56% of which falls between May and September. Snow can fall at any time, but lays continuously for 6 months, from mid November to May, reaching a mean maximum depth of 133 cm.
The bedrock is mainly acidic consisting of granitic and granodioritic ortogneiss and of biotic or two micas paragneiss, with some outcrops of dolomite and a localised outcrop of andesite-basalts about 700 m West from Mt. Scorluzzo (Montrasio et al., 2012).
Here permafrost has a patchy and discontinuous distribution (Guglielmin and Siletto, 2000; Guglielmin et al., 2001; Cannone et al., 2003), despite a thickness exceeding 200 m at 1 km east from the study area at 3000 m a.s.l. (Guglielmin, 2004).
Despite its limited extent, the study area is rich in periglacial features: 7 rock glaciers (4 active and 3 of uncertain activity; Guglielmin and Smiraglia, 1997; Guglielmin and Siletto, 2000), protalus ramparts, patterned grounds, turf hummocks (mainly localised on the northern slope of Le Rese ridge, at 2500-2600 m a.s.l.) and several solifluction lobes, (Pozzi et al., 1990). Small block streams are also present in the western glacial cirque (Albertini, 1955).
The study area is located in the alpine and in the nival belts (Ellemberg, 1988), the latter colonised by discontinuous pioneer communities, especially by *Androsacetum alpinae, Oxyrietum digynae,* and by the more densely vegetated *Luzuletum spadiceae*. In the alpine belt, the climax condition is reflected by the alpine grasslands with high vegetation cover: *Caricetum curvulae* and, in chionophilous conditions, *Salicetum herbaceae.*

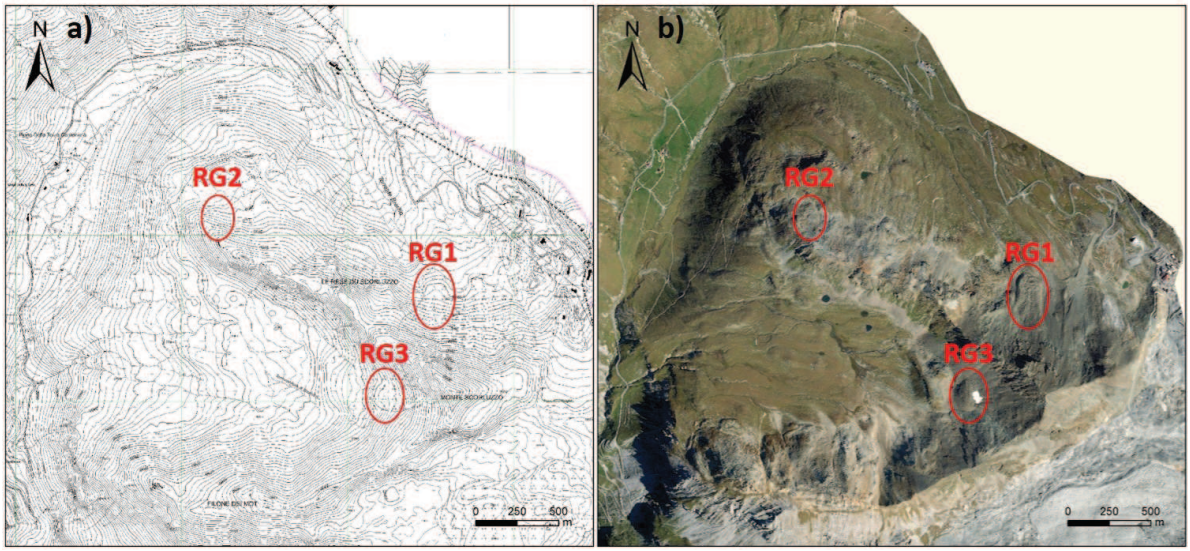

Figure 5.1.1. Individuation of the 3 studied rock glaciers at the study area. a) topographic map, b) orthophoto year 2015.

5.1.3 METHODS

5.1.3.1 Fieldwork

Three rock glacier (RG1, RG2, RG3) situated in the study area were selected as representative of various morphology, aspect and dynamic evidences (Fig. 5.1.1).

A minimum of 4 transversal lines per each feature were painted at the beginning of summer 2015 (after the snowmelt) and distributed within the features. As reference of the lines extremes, big stable blocks were chosen (> 100 cm of diameter). The decision of the positions of the lines followed previous monitoring in case of RG1 (Cannone, 1997), while for RG2 and RG3 followed the way to better represent the whole landform, namely to cover locations such as ridges, fronts and furrows (Fig. 5.1.2). Generally, we tended to monitor each line twice per year, once after the snowmelt (mid to late July) and once at the end of the summer (end of September to beginning of October) for a total of 3 years (2015, 2016 and 2017) (see details in Tab. 5.1.1). The first survey indicated the dynamics occurred during the snow cover period (autumn, winter, spring), while the second survey indicated the dynamics occurred during the snow free period (summer). Displacements were surveyed by stretching a ribbon ruler along the painted lines and by counting the painted clasts moved down from the lines. The ASTM grain size classification was considered: fine material (< 2 mm), gravel (2 – 64 mm), pebbles (64 – 256 mm), blocks (boulders) (> 256 mm) (ASTM, 2003).

For each clast > 2 cm, the vertical distance from the line (cm), the horizontal distance from the beginning of the line (cm), the a axis dimension (cm), rotation (°), toppling (°) were recorded. Further, non-painted clasts that fell on the line were described with the same method. In addition, a description of the whole lines was conducted (i.e. distance of grain size change, slope, aspect) (Tab. 5.1.2).

In addition to geomorphic indications, a vegetation coverage was conducted by visual estimation on the whole rock glaciers. Further, a more detailed survey was conducted on the painted lines once per year, after the snowmelt. In fact, it has been hypothesized that the vegetation community structure does not change during few summer months. The measurement principle followed the same of Canfield (1941) called "line interception" then well described by Coulloudon et al. (1999) and repeated by McDonald (1980), Kaiser (1983), Kuchler and Zonneveld (1988), Muttlak and McDonald (1992), Zhou et al. (1998). Briefly, patches of vegetation on the painted line were measured as distance from the first extreme, length and width and floristic composition checked. For well vegetated features only patches touching the line were surveyed, for half-vegetated features an additional buffer range of 10 cm uphill and 20 cm downhill the line were surveyed, for poorly vegetated features an additional buffer range of 30 cm uphill and 50 cm downhill the line were surveyed. This has been helpful for identifying typical patches or species that have created micro-habitats for the downhill species by consolidating fine to coarse debris (Cannone and Gerdol, 2003). In addition, the frequency of species encountered on the line was treated as an indicator of: a) the scree association occurring on that landform (*Oxyrietum dyginae*, *Luzuletum spadiceae*, *Androsacetum alpinae*), b) the turn-over of species compared with previous surveys (Giacomini and Pignatti, 1954; Cannone and Pignatti, 2014).

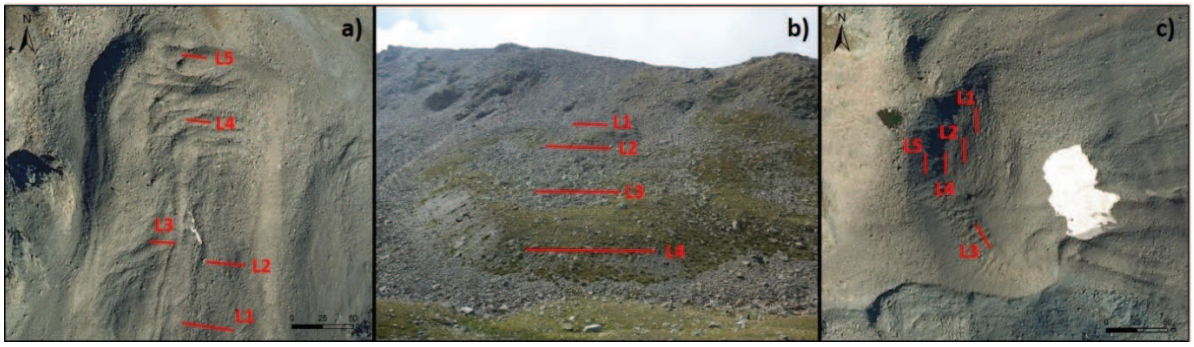

Figure 5.1.2. Shape and distribution of the monitored lines on the studied rock glaciers: a) RG1; b) RG2 and c) RG3.

5.1.3.2 Data analysis

The average distance from the beginning of each line was considered as X coordinate of a point, the position of the points along the length of the landform was treated as Y coordinate and the average displacement of each clast (point) treated as Z coordinate. This scheme was repeated for the displacements occurred at the end of the first summer (2015), at the beginning of the second summer (2016) and at the last survey of 2017. The 3-axis tables of data were then imported in SURFER (Golden Software) and interpolated with a kriging algorithm (Oliver and Webster, 1990). In such a way, horizontal displacement contours have been computed to better visualize the surficial dynamics.
Then, box and whiskers plots of the same corresponding periods were computed in the software STATISTICA® to understand means and ranges variations of gravel, pebbles and blocks.
Eventually, the coupled information about species and clast displacements have been joint with box and whiskers plots in STATISTICA® to quantify the surficial movement tolerated by each species.

5.1.4 RESULTS

5.1.4.1 Rock glacier characteristics

Whilst RG1 and RG2 are tongued-rock glaciers, RG3 is a lobate rock glacier due to their length/width ratio. The latter is located at a higher altitude than the other two, it is the only one West-facing and its average slope is more pronounced (36° compared to 25.2° and 29.3° of RG1 and RG2 respectively). The average surficial grain size results very similar for RG1 and RG2 except for a larger amount of blocks on RG1 (29%). Unlikely, RG3 shows a different surficial grain size with no fine material and a higher amount of gravel (24%) compared to RG1 and RG2.
Further, RG3 accounts for the most poorly vegetated rock glacier, followed by RG1 and RG2 (Tab. 5.1.1).

Table 5.1.1. General characteristics of the monitored rock glaciers.

	RG1	**RG2**	**RG3**
Length (m)	275	141	165
Witdh (m)	160.6	60	195
Aspect	N	N	W
Average Slope (°)	25.2	29.3	36
Front Slope (°)	38	35	40
Elevation (m a.s.l.)	2716	2647	2805
Average Surficial Fine Material (%)	6.8	15.75	0
Average Surficial Gravel (%)	6.2	18.75	24
Average Surficial Pebbles (%)	58	50	56
Average Surficial Blocks (%)	29	15.5	20
Vegetation Cover (%)	5	30	< 5

The characteristics of single lines are shown in Table 5.1.2. Lengths are not similar because they depend from the location of stable extremes to use as reference points, such as big anchored blocks, which defined the line length. The steepest lines occurred at the frontal scarp of each rock glacier with rather similar slopes, but on RG2, despite its smaller dimensions, also L2 is quite steep (30°). This is due to the particular shape of RG2 with 2 major ridges and 2 furrows. Generally, finer material is distributed on the fronts (and on the second furrow of RG2) except of RG3 that did not show surficial presence of fine particles. The same occurs for gravel, but in this case RG3 has a large amount of gravel on the ridge (20 to 50%). Pebbles and blocks are similarly distributed in RG1 and RG2 because furrows and fronts showed a lack of this grain size. Conversely, RG3 showed a higher concentration of pebbles and especially of blocks at the front (40 and 45% respectively).
The monitoring period was similar in RG1 and RG2 (from summer 2015 to summer 2017), while in RG3 from summer 2016 to summer 2017 due to the larger time required in 2015 to set up all the experiment.

The fallen parts of each line were considerably larger at the steeper part of all the rock glaciers. In particular, even in a shorter period (one year), the frontal line of RG3 fell completely. Instead, a particularity was observed in RG2 that showed a larger part (69.1%) of fallen line at the furrow rather than at the front (36.4%), despite its higher slope (35°).

As a result, highest annual rates occurred at the front of RG1 (up to 57.8 cm yr^{-1}) and RG3 (up to 76.5 cm yr^{-1}) and at the furrow of RG2 (18.5 cm yr^{-1}). In particular, RG1 accounted for the highest frontal rates for each grain size, with a large difference of speed between its front and ridge. RG2 accounted for the highest rates at the furrow, followed by the front, but in any case these rates were not comparable to RG1 unlike the ridge velocities. Averagely, ridge velocities of RG3 (3.4 cm yr^{-1}) were smaller than the other rock glaciers (5.3 cm yr^{-1} for RG1 and 5.4 cm yr^{-1} for RG2), despite a lack of movements in several grain sizes, but the front rates reached the maximum value. In another point of view, among all the lines, the highest rates occurred in gravel for RG1 (57.8 cm yr^{-1}) and blocks for RG2 (18.5 cm yr^{-1}) and RG3 (76.5 cm yr^{-1}) (Tab. 5.1.2).

Table 5.1.2. Topographic and dynamic characteristics of the monitored lines on the rock glaciers. Total Displacements refer to the percentage of moved line on the total length, while the annual rates are averages of the displacements per each grain size divided by 2 years.

	RG1					RG2				RG3				
	L1	L2	L3	L4	L5	L1	L2	L3	L4	L1	L2	L3	L4	L5
Position	Ridge	Ridge	Furrow	Ridge	Frontal Scarp	Ridge	Scarp	Ridge	Frontal Scarp	Ridge	Furrow	Ridge	Frontal Scarp/Ridge	Frontal Scarp
Length (m)	40	37	20	21.7	20	35	20.7	21	21	14	20.6	18	15.6	16
Slope (°)	30	26	22	10	38	27	30	25	35	5	15	22	30	40
Elevation (m a.s.l.)	2747	2731	2733	2704	2681	2658	2639	2619	2599	2806	2800	2801	2790	2733
Fine Material (%)	5	4	0	0	25	0	24	0	39	0	0	0	0	0
Gravel (%)	5	1	0	0	25	0	36	0	39	50	30	20	5	15
Pebbles (%)	60	75	60	50	45	90	40	50	20	50	65	75	50	40
Blocks (%)	30	20	40	50	5	10	0	50	2	0	5	5	45	45
Total Displacement (%)	4.5	1.6	2.5	0.5	82.0	12.6	69.1	1.2	36.4	3.2	7.8	0	9.9	100
Annual rate Gravel (cm yr^{-1})	3.8	2.5	1.3	-	57.8	-	17.9	2.5	5.4	2.5	-	-	2.5	-
Annual rate Pebbles (cm yr^{-1})	6.6	4.4	4	-	55.5	4.9	18	6.7	11.9	-	4.3	-	2	-
Annual rate Blocks (cm yr^{-1})	7	-	12.5	-	35.8	7.5	18.5	-	5	-	-	-	5	76.5

5.1.4.2 Spatial distribution of rock glaciers dynamics

Spatialization of surficial displacements has been calculated in Surfer with the kriging interpolation method to obtain horizontal displacement contours (Fig. 5.1.3, 5.1.5, 5.1.7). Overall, an increasing trend of displacements is visible per each rock glacier from the first survey to the last one. Concerning RG1, within-summer displacements occurred only at the front (up to 110 cm), while, after one winter, also L1, L2, L3 and L4 moved up to 15, 19.5, 13.5 and 5 cm respectively. The highest displacement occurred on L5 (302.5 cm), almost three times the intensity of the previous season. After 2 years, other displacements occurred except at L4 but of the order of few centimeters (ranging from 2.5 to 25 cm). Conversely, the front increased the intensities, especially at the central part reaching 450 cm (Fig. 5.1.3).

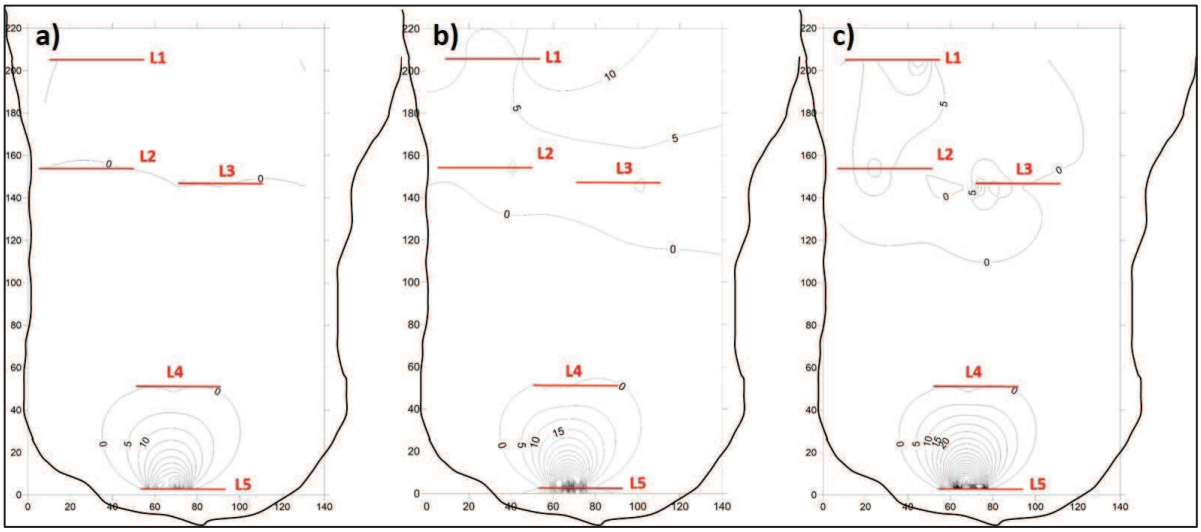

Figure 5.1.3. Diagram of horizontal displacement contour occurred on RG1 with the position of the monitored lines. a) 19-09-2015, b) 26-07-2016, c) 12-07-2017. Axes show distances in meters.

Despite this general increase of displacements, displaced clasts varied in 2 years and not after one season (winter). In fact, gravel accounted for the highest average displacements (from 49.4 to 17.5 to 81.7 cm). Blocks behaved in the same way but with shorter movements (from 32.6 to 8.3 to 54.2 cm). Instead, a slight decrease occurred for pebbles that varied from 49.6 to 18 to 46.2 cm (Fig. 5.1.4). The decreased averages occurred in 2016 compared to 2015 may be related to the fact that the number of displaced clasts increased (frequency) but with lower intensities, thus decreasing the average displacement.

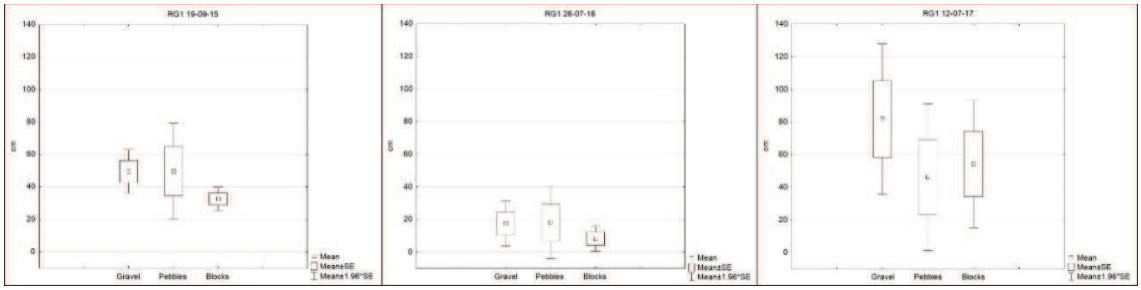

Figure 5.1.4. Ranges of horizontal displacements occurred on RG1 divided in grain size classes per the monitored dates. SE refers to standard error.

RG2 showed a particular distribution of displacements. Little displacements occurred on the front at the end of summer 2015 (up to 12 cm), while larger displacements on the furrow (L2) (up to 107 cm). After the winter, namely at the first survey in 2016, also L1 and L3 showed displacements up to 6.5 and 17.5 cm respectively. Instead, L2 and L4 considerably increased intensities up to 150 and 300 cm respectively. After 2 years, little movements occurred at all the lines (up to 20, 110, 26 and 80 for L1, L2 L3 and L4 respectively). L2 and L4 decreased the maximum intensity (110 and 80 cm respectively), but new spots of considerable movements appeared, conversely to summer 2015 and 2016 (Fig. 5.1.5). Such a decrease on L2 and L4 may be related to the fact that the previously highly displaced

clast fell farther enough to not be visualized. Thus, L2 and L4 displacements in 2017 could be higher than showed in Figure 5.1.5.

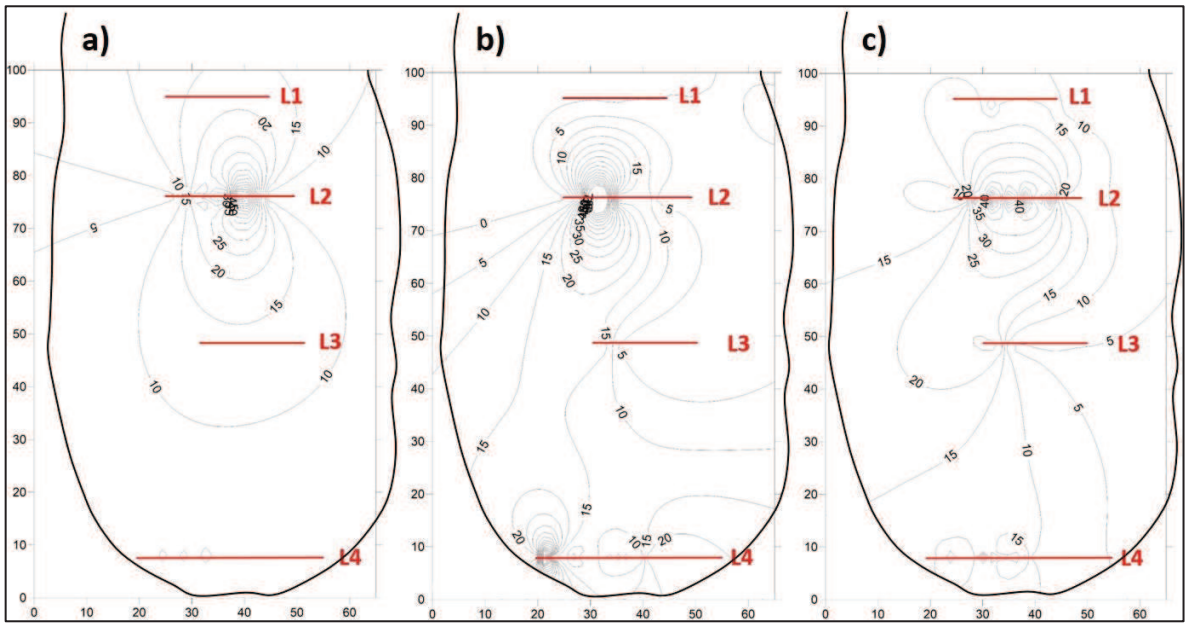

Figure 5.1.5. Diagram of horizontal displacement contour occurred on RG2 with the position of the monitored lines. a) 19-09-2015, b) 30-07-2016, c) 20-06-2017. Axes show distances in meters.

The first grain sizes to have undergone RG2 dynamics in 2015 have been pebbles with an average of 25 cm, followed by gravel with an average of 18 cm. Apparently, the short monitoring period was not sufficient to appreciate blocks displacements. Gravel did not vary the average dynamic after the winter (average of 20 cm). In addition, one block displaced by 14.5 cm, while average pebble displacements decreased from 25 to 8 cm due to an increased frequency of moved clasts with lower intensities. In 2017, while gravel and pebbles did not vary considerably from the first survey (17.5 and 24.8 cm respectively), blocks displaced with an average of 24.7 cm (Fig. 5.1.6).

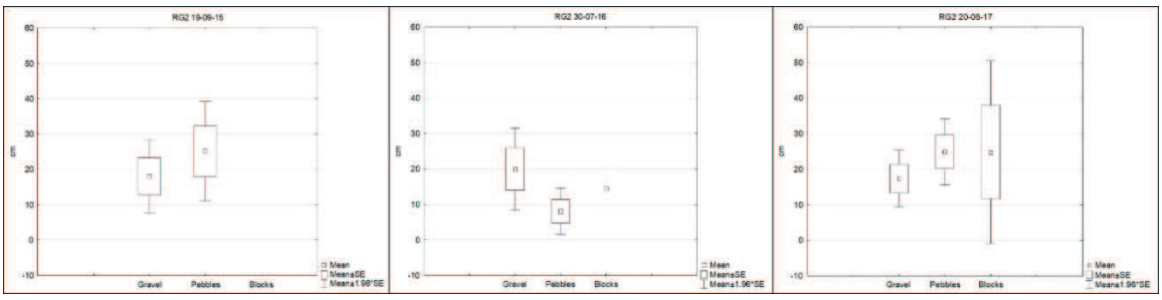

Figure 5.1.6. Ranges of horizontal displacements occurred on RG2 divided in grain size classes per the monitored dates. SE refers to standard error.

Due to the lobate shape of RG3, the distribution of the monitoring lines is occurs at similar elevations rather than along the downslope flux. During summer 2016, the only displacements recorded occurred

at the front with localized movements of coarse material (up to 70 cm). In summer 2017, after one year, displacements occurred also at other lines except of L3 (up to 5, 25, 10 and 200 cm for L1, L2, L4 and L5 respectively). However, it is important to notice that the shape of the displacement contours is different from the other rock glaciers because L5 totally collapsed, thus producing a homogenized displacement, intense enough to hide minor movements of the ridge (Fig. 5.1.7).

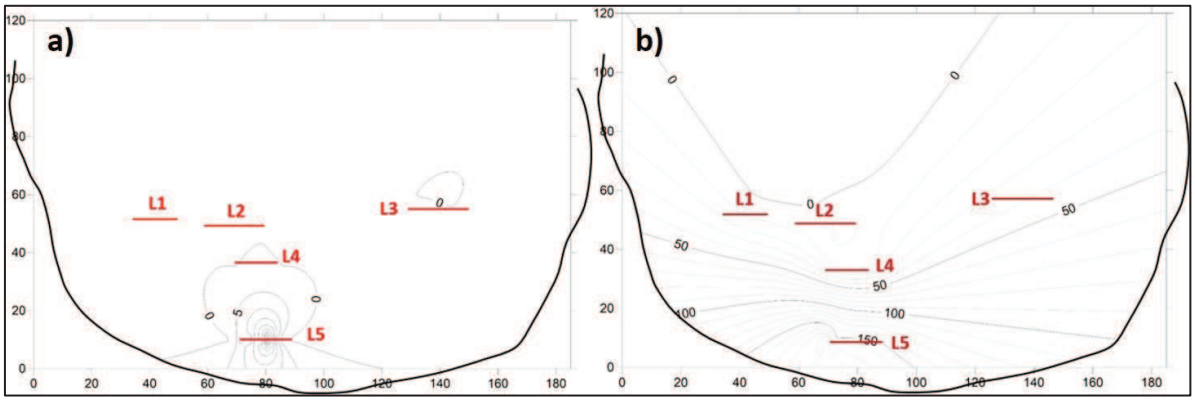

Figure 5.1.7. Diagram of horizontal displacement contour occurred on RG3 with the position of the monitored lines. a) 29-09-2016, b) 17-07-2017. Axes show distances in meters.

Gravel, principally present at the ridge, did not displace in 2016 but only coarser grains fell at the front, namely pebbles (averagely by 12.4 cm) and blocks (averagely by 23.7 cm). It has been sufficient just one year of span to firstly appreciate little movements of gravel (averagely by 5 cm) and pebbles (averagely by 6.2 cm) on the ridge and secondly to see how the big blocks at the front hid the previous displacements of pebbles. In fact, such an intense and homogeneous displacement of coarse material (145 cm) did not occur at the other rock glaciers. In addition, the slight average decrease of pebbles (from 12.4 to 8.5 cm) may be associated to the increased frequency of displaced pebbles with lower intensities (Fig. 5.1.8).

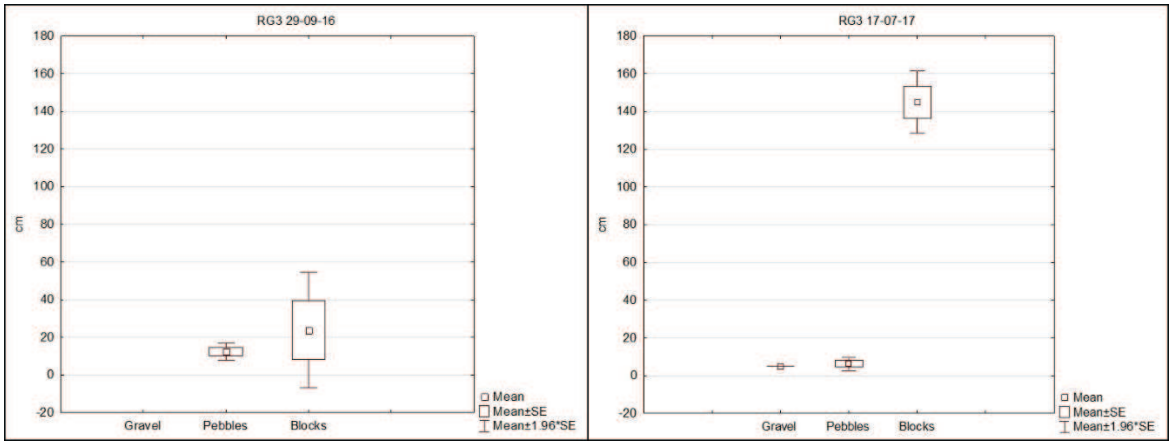

Figure 5.1.8. Ranges of horizontal displacements occurred on RG3 divided in grain size classes per the monitored dates. SE refers to standard error.

5.1.4.3 Vegetation distribution

The vegetation occurring at the study area has been well described by Giacomini and Pignatti (1955). The important note on that is to differentiate pioneer communities (such as *Androsacetum alpinae* (AA), *Arabidetum caeruleae* (AC), *Luzuletum spadicae* (LS), *Oxyrietum dyginae* (OD)) from climax communities (such as *Caricetum curvulae* (CC) and *Salicetum herbaceae* (SH)). At these altitudes stable presence of shrubs community has not been registered yet, therefore the only 2 climax communities can be divided into alpine grassland (CC) and snowbeds (SH). Differently, among the pioneer communities, only 3 of them can be also encountered on screes, thus suggesting surficial dynamic tolerance: AA, LS and OD (Cannone, 1997).

As expected, the vegetation growing on the rock glaciers is different in terms of floristic composition and abundance. In fact, probably due to the higher vegetation coverage, RG2 accounted for the highest number of species (22), followed by RG1 (12 species) and RG3 (9 species). Also, the communities differed but always displaying the presence of both pioneer and climax vegetation. Moreover, in RG2 we were able to appreciate the differentiation of climax communities with snowbed and grassland species.

Overall, a common trend of decreasing frequencies from the first to the last yearly survey is visible at all the rock glaciers. This may be related to the fact that several vegetation patches underwent the direct effect of rock displacements, namely total cutoff or burial. However, this is partly true for RG3 that shows several species with increased frequency in 2017 but with low values and RG2 that showed significant increases. This is likely due to the fact that a single patch of vegetation could have been counted as single or double depending on its shape. Otherwise, it is possible that a fallen clast might have exposed the species previously hidden by it. Notwithstanding, it is also likely that some new individuals could have growth in just one year.

Concerning RG1, a prevalence of pioneer species and the absence of snowbed species is visible. In 2015, there were localized species such as *Leucanthemopsis alpina* and *Saxifraga bryoides* (L5) and well distributed species such as *Poa alpina* and mosses (L1, L3, L5). *P. alpina* resulted as the most widespread species, while *Oxyria dygina* occurred only once. Generally, the highest decrease of individuals occurred for *Cardamine resedifolia* (-94.1%), *Leucanthemopsis alpina* (-75.4%) and *Poa alpina* (-60.6%) especially located at the front line, the most dynamic one (L5). Also slight increase of individuals occurred (*Linaria alpina* +100%) but not statistically significant (one individual) (Tab. 5.1.3).

Table 5.1.3. Vegetation surveys of the monitored lines (L1-L5) on RG1. The column ALL refers to the summatory of the individuals encountered throughout the lines. The first column refers to the vegetation associations: AA = *Androsacetum alpinae*, AC = *Arabidetum caeruleae*, LS = *Luzuletum spadicae*, OD = *Oxyrietum dyginae*, CC = *Caricetum curvulae*, PionComp = species occurring in all the pioneer associations, CCComp = species associated to CC. Colors indicate pioneer associations (green), alpine grassland (orange), snowbed associations (blue).

		2015						2017					
	Species	L1	L2	L3	L4	L5	ALL	L1	L2	L3	L4	L5	ALL
AA	*Linaria alpina*	0	0	0	0	0	**0**	1	0	0	0	0	**1**
AC	*Arabis alpina*	0	0	0	0	7	**7**	0	0	0	0	4	**4**
	Saxifraga oppositifolia	1	0	0	0	0	**1**	0	0	0	0	0	**0**
LS	*Cerastium uniflorum*	0	0	0	0	15	**15**	0	0	2	0	1	**3**
OD	*Cerastium pedunculatum*	0	0	5	0	0	**5**	0	0	0	0	1	**1**
	Geum reptans	0	0	0	0	10	**10**	5	0	0	0	4	**9**
	Oxyria digyna	2	0	0	0	0	**2**	1	0	0	0	0	**1**
PionComp	*Cardamine resedifolia*	0	0	0	0	17	**17**	0	0	0	0	1	**1**
	Ranunculus glacialis	8	0	0	0	27	**35**	4	0	0	0	13	**17**
	Saxifraga bryoides	0	0	0	0	21	**21**	0	0	0	0	10	**10**
CCComp	*Leucanthemopsis alpina*	0	0	0	0	65	**65**	0	0	0	0	16	**16**
	Poa alpina	17	0	1	0	53	**71**	9	0	1	0	18	**28**

RG2 presented all the already mentioned communities and well distributed between pioneer and climax. Similarly to RG1, also here localized species such as *Doronicum clusii* and *Oreochloa disticha* (L4) and well distributed species such as *P. alpina* and *L. alpina* (all the lines) were present in 2015. Here *L. alpina* was the most frequent, while many species occurred only once. In fact, those species vanished during 2 years. Nevertheless, the most decreased species were *O. disticha* (all 13 individuals disappeared), *C. uniflorum* (-64.3%), *Leucanthemopsis alpina* (43.5%) and *Poa alpina* (46.2%) all prevalently located at the furrow and the front, the most dynamic part of the rock glacier (L2, L4). Also slight significant increase of individuals occurred for *Carex curvula* (appearance of 13 individuals) and *Polygonum viviparum* (appearance of 7 individuals), even though they grew at the most dynamic zones (L2, L4), thus indicating a good tolerance to movement (Tab. 5.1.4).

Table 5.1.4. Vegetation surveys of the monitored lines (L1-L4) on RG2. The column ALL refers to the summatory of the individuals encountered throughout the lines. The first column refers to the vegetation associations: AA = *Androsacetum alpinae*, LS = *Luzuletum spadicae*, SH = *Salicetum herbaceae*, CC = *Caricetum curvulae*, PionComp = species occurring in all the pioneer associations, CCComp = species associated to CC, Comp = species associated to whatever association. Colors indicate pioneer associations (green), alpine grassland (orange), snowbed associations (blue).

		2015					2017				
	Species	L1	L2	L3	L4	ALL	L1	L2	L3	L4	ALL
AA	*Gentiana bavarica*	0	0	0	0	**0**	0	0	0	1	**1**
	Linaria alpina	0	1	0	0	**1**	0	0	0	0	**0**
	Saxifraga seguieri	0	2	0	2	**4**	0	0	0	3	**3**
LS	*Cerastium uniflorum*	0	14	0	0	**14**	0	5	0	0	**5**
	Doronicum clusii	0	0	0	8	**8**	0	0	0	6	**6**
	Luzula alpino-pilosa	0	1	0	6	**7**	0	1	0	6	**7**
PionComp	*Cardamine resedifolia*	0	2	0	1	**3**	0	0	0	0	**0**
	Ranunculus glacialis	0	32	0	9	**41**	0	11	0	13	**24**
	Saxifraga bryoides	0	2	0	9	**11**	0	5	0	10	**15**
	Poa laxa	1	1	0	0	**2**	0	0	0	0	**0**
SH	*Sagina saginoides*	0	0	0	4	**4**	0	0	0	0	**0**
	Salix herbacea	0	0	2	0	**2**	0	0	0	0	**0**
	Veronica alpina	0	0	1	0	**1**	0	0	0	0	**0**
SH/CC	*Sedum alpestre*	0	0	0	1	**1**	0	0	0	0	**0**
CC	*Carex curvula*	0	0	0	0	**0**	1	0	0	12	**13**
	Euphrasia minima	0	0	0	1	**1**	0	0	0	0	**0**
	Oreochloa disticha	0	0	0	13	**13**	0	0	0	0	**0**
CCComp	*Leucanthemopsis alpina*	0	12	3	31	**46**	0	5	1	20	**26**
	Poa alpina	1	29	6	3	**39**	0	12	4	5	**21**
	Homogyne alpina	0	0	0	0	**0**	0	0	0	1	**1**
Comp	*Polygonum viviparum*	0	0	0	0	**0**	0	0	0	7	**7**

Although also RG3 showed the presence of all the ecological stages (pioneer and climax), the prevalence of pioneer species is visible. Here no species were present on L5, however the localized ones were for example *P. alpina* (L3) and *L. alpina* (L4), while the most widespread *Ranunculus glacialis* (L1, L2, L3) and *Geum reptans* (L1-L4). In RG3, beyond *G. reptans*, which considerably decreased its occurence in one year (-46.5%, well distributed at lines L1-L4), it is hard to define tolerant species because the frequencies were very low and thus not statistically significant. Rather, it is possible to say that probably intense displacements at the front do not permit the colonization of plants on that area (Tab. 5.1.5).

Table 5.1.5. Vegetation surveys of the monitored lines (L1-L5) on RG3. The column ALL refers to the summatory of the individuals encountered throughout the lines. The first column refers to the vegetation associations: AA = *Androsacetum alpinae*, OD = *Oxyrietum dyginae*, PionComp = species occurring in all the pioneer associations, SH = *Salicetum herbaceae*, CCComp = species associated to CC. Colors indicate pioneer associations (green), alpine grassland (orange), snowbed associations (blue).

		2016						2017					
	Species	L1	L2	L3	L4	L5	ALL	L1	L2	L3	L4	L5	ALL
AA	*Androsace alpina*	0	0	0	1	0	**1**	0	0	0	0	0	**0**
	Linaria alpina	0	0	0	1	0	**1**	1	0	0	0	0	**1**
OD	*Geum reptans*	17	17	2	7	0	**43**	7	11	2	3	0	**23**
PionComp	*Agrostis rupestris*	0	0	0	0	0	**0**	1	0	0	0	0	**1**
	Saxifraga bryoides	0	0	1	0	0	**1**	2	0	0	0	0	**2**
	Poa laxa	0	0	0	0	0	**0**	2	0	0	0	0	**2**
	Ranunculus glacialis	1	1	2	0	0	**4**	1	0	0	0	0	**1**
SH/CC	*Sedum alpestre*	0	0	0	0	0	**0**	1	0	0	0	0	**1**
CCComp	*Poa alpina*	0	0	2	0	0	**2**	1	0	1	1	0	**3**

5.1.5 DISCUSSION

5.1.5.1 Rock glacier dynamics

Our findings suggest interesting explanations concerning rock glaciers dynamics. The studied rock glaciers show different shapes and topographic conformations but similar surface displacements. Generally, the largest amounts of collapsed/displaced line occurred at the steepest part, namely the fronts or the ridges scarps. Further, except for RG3, the displacements occurred more frequently on lines with a high percentage of fine material. This may be related to the fact that fine material decreases the roughness compared to coarser material, able to increase frictional resistance to displacement (Luckman, 2007; Rixhon and Demoulin, 2013). As a consequence, fine material may undergo several geomorphic processes such as solifluction and running water transportation independently to the major process that form a rock glacier (permafrost creep) (Kääb et al., 1997; Haeberli et al., 2006; Rixhon and Demoulin, 2013). Unlikely, the blocky front of RG3 totally moved probably due to the steeper position of L5 compared to the other rock glaciers (Lugon and Stoffel, 2010).

Concerning the surficial rates, all the investigated rock glaciers show typical surficial velocities among worldwide rock glaciers (Humlum, 1996; Haeberli et al., 2006; French, 2007). Rates recorded at each line of the gentler parts also well represent rates of similar studies in the Alps (Kääb et al., 1998; Frauenfelder and Kääb, 2000; Cannone and Gerdol, 2003; Roer, 2007). However, frontal/scarp rates

exceed the above cited studies, thus laying in the larger and latest ranges found by Delaloye et al. (2008). Due to this discrepancy between fronts and main bodies of the studied rock glaciers, we would prefer not to talk about mean annual velocities. In fact, involved processes may be largely different in a small spatial scale. In support of this theory, the interpolation of surficial displacement occurred after one winter (in presence of snow) displayed changes not only at the steepest parts but also on the main body (RG1 and RG2). Therefore, we claim that in presence of snow, despite the frozen ground that inhibit the rock glacier creep (Delaloye et al., 2008), surficial nivation processes (Ballantyne, 1985) act in terms of meltout water slopewash (Lewkowicz, 1981; Strömquist, 1983; Thorn and Hall, 2002) on finer materials and debris + snow avalanche ("mixed avalanche") (Statham, 1976; Washburn, 1979; Salm, 1993) on coarser material. Indeed, many perched blocks (Luckman, 1977) have been spotted especially on RG3 and "mixed avalanches" near RG1 (Fig. 5.1.9). Hence, we would distinguish a creep displacement occurring on ridges and visible during the summer period that ranges between 1.3 and 7.5 cm yr^{-1} among all grain size classes and a polygenic displacement occurring on fronts/scarps ranging between 5 and 76.5 cm yr^{-1}. The latter could be likely related to creep but also to solifluction (frost heave + needle ice creep) on fine material during spring/autumn (Fig. 5.1.10), nivation during winter, slopewash during spring and gravitation on coarse material during summer.
With a detailed look at the grain size class ranges of displacement during the study period, we can hypothesize the increase in gravel displacements occurred on RG1 to be related to processes acting on fine material egual or smaller than gravel, mainly present at the front. In this case, RG1 would be a good representative of frost/solifluction/slopewash action. Oppositely, the increase of blocks displacements on RG2, mainly present on the ridge, could be related to creep of the frozen body during winter or a "mixed avalanche", rather than gravitation processes on such a gentle slope. Unlikely, the same considerable increase of blocks displacements on RG3, mainly present at the front (already moved at the end of the first season), may be associated to gravitational forces that acted at a such steep slope (40°) at the angle of repose (Wahrhaftig and Cox, 1959) and encouraged by freezing/thawing during spring and autumn.

Figure 5.1.9. Evidences of "mixed avalanches" on the slope above RG1. Picture taken on 13-06-2017.

Figure 5.1.10. Evidences of needle ice activity on the top part of a scree slope, very similar to the grain size of rock glacier fronts. Note the voids structure of the fine material at the right of *Cerastium uniflorum* after the melting of ice needles. Picture taken on 30-09-2017.

5.1.5.2 Rock glacier – vegetation interactions

The vegetation observed on the rock glaciers showed different colonization patterns. While on RG1 only species belonging to pioneer and grassland communities are present, on RG2 and RG3 also snowbed species grow, despite the large difference in floristic composition. In fact, pioneer species richness is high on RG1 and RG2 but scarse on RG3. Grassland species are more present on RG2 than RG1 and RG3. Snowbed species are present only on RG2 and RG3 (few). This colonization distribution could be related to the total vegetation coverage of each landform: RG2 (maximum coverage) results as the most biodiverse, where pioneer species have partially created establishment zones or sub-niches for climax species; RG1 and RG3 (minimum coverage) result as the most pioneer-species dominated, index of a harsher environment not only related to the surficial displacement (Cannone and Gerdol, 2003).

Generally, a decrease of species frequency was expected and observed due to the surface substrate instability (Chapin, 1993) provoked by the falling clasts or a “burial” effect, but also an appearance of new species or increase of frequencies was observed. This is true for *Linaria alpina* on RG1, *Gentiana bavarica*, *Carex curvula*, *Homogyne alpina* and *Polygonum viviparum* on RG2, *Agrostis rupestris*, *Poa laxa* and *Sedum alpestre* on RG3. Although a detectable growth could be expected for pioneer species on unstable situations (Bliss, 1958), it is less likely that a stable-community species have grown in a

short period. On the contrary, it is possible that in certain cases some individuals appeared after the removal of a clast because they were living hidden underneath.
For the issue explained above, it is more reliable to take in consideration the highest-frequency species occurred on the lines. Averagely, those species did not vary their distribution on the rock glaciers (among the lines) at the end of the monitoring, but rather little variations occurred in terms of frequency at the same lines. This means that no catastrophic event totally removed a species from their niche, neither a large colonization of distant areas was possible in such a short period.
The largest disappearance on RG1 happened for *Cerastium uniflorum*, *Cardamine resedifolia*, *Ranunculus glacialis*, *Leucanthemopsis alpina* and *Poa alpina*, all of which grow at the front. Since the front has been the most dynamic sector of the rock glaciers, we can assume that these species are surface-instability tolerant, especially for those processes regarding fine material (solifluction and slopewash).
On RG2 the largest disappearances accounted for *C. uniflorum*, *R. glacialis*, *Oreochloa disticha*, *L. alpina* and *P. alpina*, all of which grow on the front/scarp except for *L. alpina* and *P. alpina* both occurring also on the ridge, on which no fine material occurred. In this case, we can suppose that all the above species tolerated solifluction or slopewash of the steepest parts, while *L. alpina* and *P. alpina* also tolerated coarser displacements related to creep.
Unlikely, on RG3, the only largest disappearance happened for *Geum reptans*, which lays on the more stable lines, associated with coarse material.
The above cited species were already investigated by Cannone and Gerdol (2003) and many of them were already attributed to be dynamic-tolerant species. However, a direct analysis on rock glacier vegetation is necessary to quantify the occurrence of species interested by surficial displacement (Fig. 5.1.11) and the tolerated displacements (Fig. 5.1.12).
Overall, displacement-affected species distributed (in terms of horizontal extension of the patch in cm) homogeneously on the investigated lines with medians ranging between 15 (*R. glacialis*) and 80 cm (*C. uniflorum*).

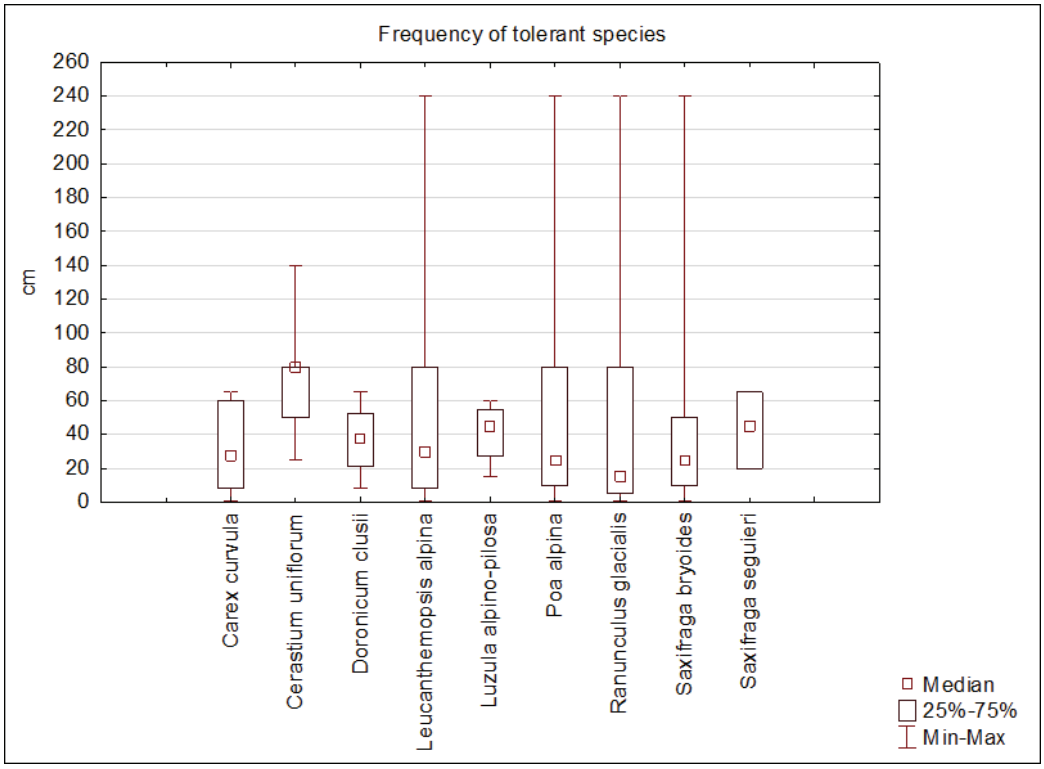

Figure 5.1.11. Frequency of displacement-tolerant species growing on rock glaciers. Centimeters refer to horizontal dimensions of the vegetated patch containing or the single individual of the indicated species considering all the investigated lines.

An other way to use vegetation species as ecological indicators of surface disturbance is to detect the species that are related only to displaced clasts. In this way, rather than quantify the dynamic of each species, it is possible to associate them to areas of defined rates. Even though this analysis should be coupled with the distintion of the geomorphic process that produced the displacement, some of these species had a defined range of displacement tolerance (e.g., *C. uniflorum* and *P. alpina*), other tolerated more various displacements (e.g., *Doronicum clusii* and *Saxifraga seguieri*). Hence, in this study, displacement-associated species occurring on rock glaciers showed the following average velocities:

- *Carex curvula*: 168 cm yr^{-1}
- *Cerastium uniflorum*: 37.5 cm yr^{-1}
- *Doronicum clusii*: 126 cm yr^{-1}
- *Leucanthemopsis alpina*: 90 cm yr^{-1}
- *Luzula alpino-pilosa*: 66 cm yr^{-1}
- *Poa alpina*: 70 cm yr^{-1}
- *Ranunculus glacialis*: 87 cm yr^{-1}
- *Saxifraga bryoides*: 106 cm yr^{-1}
- *Saxifraga seguieri*: 167.5 cm yr^{-1}

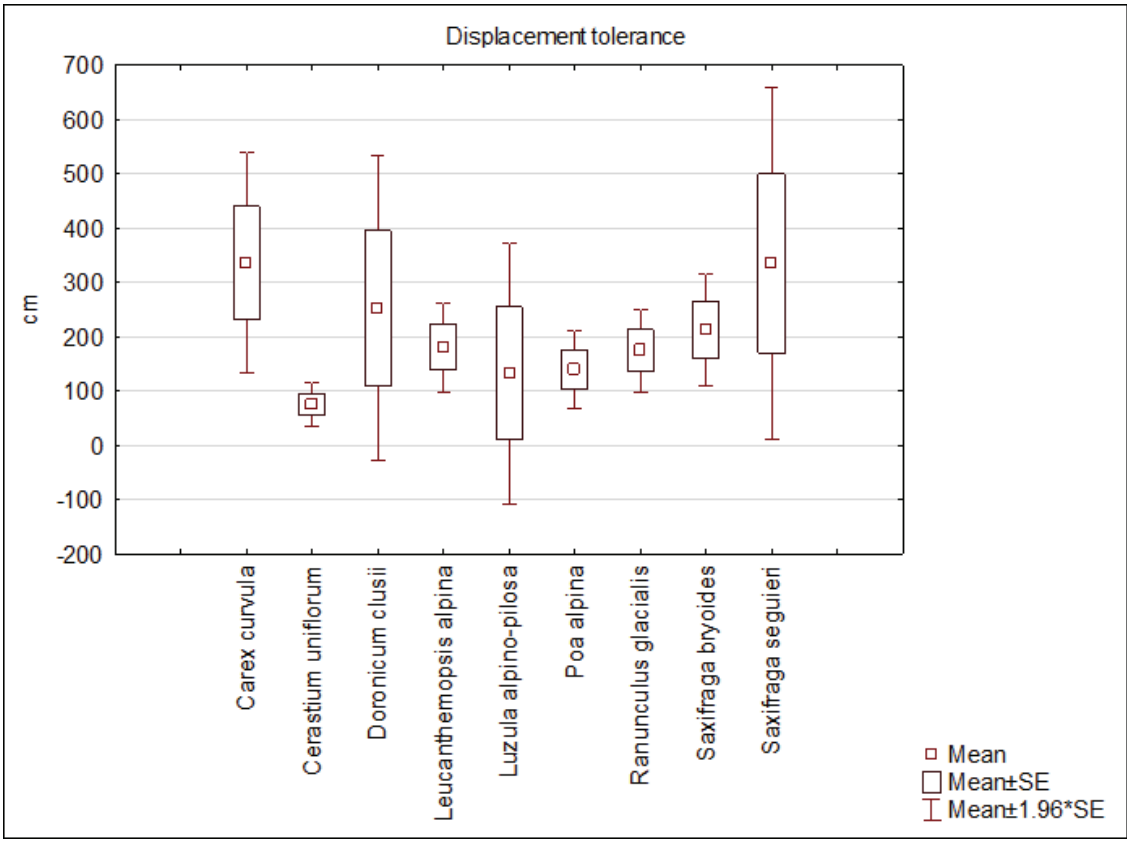

Figure 5.1.12. Tolerance of the cumulative surficial movement in cm associated to the stress-tolerant species. For collapsed sectors of line a high value of 500 cm was given. Since standard error (SE) is represented in this panel, also negative values are possible.

Carex curvula is a species typical of alpine grasslands and not associated with a pioneer behavior. The velocity associated to it could be interpreted as an ongoing dynamic at the zone previously established by a pioneer species rather than a pure and direct tolerance. In fact, *C. curvula* was always present as big patches on fine and stable material with other species such as *Luzula alpino-pilosa* and *Poa alpina*. *L. alpino-pilosa* showed the same behavior but it is associated with lower velocities because of the presence of denser and more stable patches. The well-defined velocity associated with *C. uniflorum* is consistent with Cannone and Gerdol (2003) and, considering its slightly higher frequency, this species could be directly related to displacements. In fact, rarely *C. uniflorum* occurred on stable and vegetated patches but rather as dense individuals anchored to the substrate. *Doronicum clusii* could be defined as a resilient species due to its ability to rapidly regenerate aboveground stems every year (Cannone and Gerdol, 2003). Indeed, it always occurred as large individuals on unstable but fine material (gravel maximum) that is not able to damage its fragile root system. *L. alpina* and *P. alpina* were often associated, very frequent and always growing on fine unstable sediment as single individuals and thus directly associated with displacements (debris holder) (Somson, 1984). Similarly, *R. glacialis* occurred as small individuals on fine material, less frequent but able to trap sediments and thus initiate a stable sub-niche (Schröter, 1926). *S. bryoides* often occurred as big mono-specific patches on stable fine material, thus its tolerance towards coarser material coming from above is a resistance due to its compact growth form. *S. seguieri* was rare and always associated with other taller species that created a stable sub-niche for it. Hence, its strategy is an avoidance strategy like *C. curvula* (Cannone and Gerdol, 2003).

With these results it is possible to demonstrate that vascular species are present at rates higher than 30 cm yr^{-1} in contradiction to Burga et al., (2004), despite they locate at finer zones of rock glaciers which moved considerably. In fact, *Geum reptans*, known as colonizer of unstable coarse material (Stöcklin and Bäumler, 1996) was not associated to displacements in this study. Further, properly the higher frequency of vegetation on the most dynamic parts (fine grained) could be an indicator that not only displacement affects the vegetation distribution but also grain size of the substrate (Rieg et al., 2011) and their relations with plant species.

5.1.6 CONCLUSION

In the alpine environment, rock glaciers occur as complex systems that join the vegetation distribution and the surficial kinematics. In this section, 3 alpine rock glaciers have been considered to demonstrate that their main body creeps with velocities in the range found by several authors throughout the world and on the Alps. However, the steepest parts of the studied rock glaciers (ridges scarps or front) largely exceed the main body average, thus being in accordance to other solely alpine researches. The discrepancy of such velocities might be related to the multiplicity of processes involved in horizontal displacements. Thank to the intra-annual survey it has been possible to detect and differentiate processes occurring in winter and summer. Some of them acted throughout the main body (permafrost creep, see RG2), others speeded up the displacements of fine material (solifluction, nivation, slopewash, see RG1) or coarser material at the front (gravitation, see RG3).
In such a dynamic frame, the vegetation communities growing on the rock glaciers are majorly pioneer, except on RG2 that showed also climax community species. A decrease of species frequency occurred at the highest dynamic parts of each rock glacier after burial events, even though large decreases did not occur. *Cerastium uniflorum* was the species majorly associated with surficial displacements, oppositively to *Ranunculus glacialis*. Among the displacement-tolerant species, also stable community species occurred. This could be interpreted as a consequence of micro-habitat creation by pioneer species. Many velocity ranges associated to species has been defined, but in the future a complete consideration of other landforms could improve those ranges. In addition, for a future perspective, an analysis of the spatial distribution of each geomorphic process within the landform associated to the zonal vegetation could emphasise the role of alpine tundra in determining and differentiate, as ecological indicator, the ongoing processes.

5.2 Surface dynamic in paraglacial and periglacial mountains of the Central Alps: a simple topo-climatic model. (Manuscript)

Ponti Stefano[1], Cannone Nicoletta[2], Guglielmin Mauro[1]

[1]Department of Theoretical and Applied Sciences, Insubria University, Varese, Italy;
[2]Department of Science and High Technology, Insubria University, Como, Italy.

5.2.1 ABSTRACT

Climate change is occurring at rapid rates in alpine areas due to the susceptibility and the heterogeneity of these environments. A poorly studied impact in such areas is the surficial displacements yielded by periglacial and paraglacial processes. For this reason, the need of a prediction model that take into account both topographic and climatic variable rises to connect future climate change scenarios with quantified surficial dynamics.
Observed points of surficial displacements have been associated to non-climatic (altitude, till deposit type, deposit age, vegetation coverage, solar radiation, slope) and climatic (days of snow permanence, ground surface temperature index, ground heating index, ground cooling index) variables through a multiple regression model in Central Alps.
The model output shows the importance of altitude, slope and ground heating index to predict surface displacements. The quality of the predictability has been tested through the splitting of the observation points in a training and validation set, which both displayed good results.
Our findings demonstrate how low elevated areas with low ground heating index and steep slopes are the most susceptible to undergo surface displacements. This could be explained by the snow accumulation and the permafrost occurrence in specific altitudinal belts.

5.2.2 INTRODUCTION

Large parts of the mountains at middle latitude are currently not more glaciated (Oerlemans, 2005; Zemp et al., 2006; Paul et al., 2007; Diolaiuti et al., 2011) and many others are rapidly becoming ice-free. In the frame of the current Climate Change scenario, the landscape is changing and paraglacial and/or periglacial conditions are widespread. Despite of an intuitive relation between climate change and landscape changes only a few works have focused on the climate change and landscape modelling (Coulthard, 2001; Tucker et al., 2010). In mountain regions of middle or low latitudes, the spatial variability is very high mainly due to the topography (Becker and Bugmann, 1997) and therefore even little changes in climatic drivers on a meso- to micro-scale could have large effects on the landscape

and on the related ecosystems (Chapin et al., 2008; IPCC, 2013). Moreover, surface dynamic at micro-scale can exert an additional impact to the ecosystems and to the vegetation development. Indeed the surface dynamic, known also as “physical disturbance” or “disturbance”, has been demonstrated to be one of the controlling factor with evidences such as: unexpected vegetation altitudinal shifts (Cannone et al., 2007), species composition, richness and productivity (Virtanen et al., 2010), tolerance of surface velocity (Cannone and Gerdol, 2003; Burga et al., 2004).

Probably due to the logistical constraints, the monitoring of landforms dynamic at meso- to micro-scale are not so abundant (e.g., Harris et al., 1998; Ballantyne, 2013; Matsuoka, 2006) and in many cases focused on a single geomorphic process such as solifluction (Matsuoka, 2001a; Ballantyne, 2013), needle ice (Grab, 2001; Nel and Boelhouwers, 2013), frost wedging (Tharp, 1987; Matsuoka, 2001b), rill erosion (Govers, 1992; Cai et al., 2004), nivation (Ballantyne, 1985; Thorn and Hall, 2002). In order to improve the knowledge on the spatial variability of the surface dynamic many studies tried to focus on coupling the remote-sensing with geographic information systems (GIS) (Kääb et al., 2003; Micheletti et al., 2015; Necsoiu et al., 2016; Arenson et al., 2016; Kääb et al., 2014; Westermann et al., 2015). In many cases, the GIS approach results as a rapid solution for expanding the investigated area or generating models when coupled with a reliable data validation (Marmion et al., 2008; Lee, 2005; Dymond et al., 2006; Pradhan, 2010).

Several predictive/distribution models have been produced concerning both the susceptibility of certain areas to undergo slope processes (Messenzehl et al., 2017; Brenning, 2005; Bai et al., 2010; Carrara et al., 2008; Das et al., 2010; Frattini et al., 2008; Komac, 2006; Saito et al., 2009) or periglacial processes (Luoto and Hjort, 2004, 2005; Hjort, 2014; Marmion et al., 2008). However, few of them integrate the models with climatic variables (Aalto and Luoto, 2014; Fronzek et al., 2006; Hjort et al., 2007), often forgetting the importance of snow distribution (Guglielmin et al., 2003; Randin et al., 2009). Further, previous studies focused on the risk assesment without a quantification of the process involved in each zone (Pelletier, 2008; Baas, 2013). In fact, the importance of a quantification of the effects beyond a probability could be treated as a quantitative risk assessment especially of mountainous non-anthropic areas. These areas have already been investigated as highly susceptible to the recent climate change concerning the vegetation shifts/colonizations (Walther et al., 2005; Keller et al., 2000; Cannone et al., 2007; Theruillat and Guisan, 2001; Gottfried et al., 2012). Therefore, the role of surficial dynamics modelling could also be implemented in vegetation distribution models (Zinko et al., 2005; Mod et al., 2016; Räsänen et al., 2016; Pfeffer et al., 2003).

The aim of the presented research is to produce a simple surface dynamic prediction model that takes into account both the topographic and climatic informations of an alpine area. Here, the dynamic prediction is not only treated as probability of occurrence but also as numerical quantification. In this way, the potentiality of this model could be used as predictor of surface displacements under future climatic scenarios.

5.2.3 STUDY AREA

The study area is located around Stelvio Pass (46°31' N, 10°25' E; elevation 2230-3094 m a.s.l.), a high alpine site in Stelvio National Park located between Stelvio Pass (2758m a.s.l.) and M. Scorluzzo (3095 m a.s.l.) close to the border between Italy and Switzerland in the Central Alps (Fig. 5.2.1).
The climate is characterized by a continental regime (Ceriani and Carelli, 2000), with a highly variable values of precipitation because of the complex orography. Climate data for the 1978-2015 period from the nearest available meteorological station at Cancano (46.51729 N, 10.32076 E, 1948 m a.s.l., 9 km to E-SE) indicate a mean annual air temperature (MAAT) of +3.3 ± 0.75 °C; January is the coldest and wettest month (-5.2 ± 1.8 °C; 38.9 mm) and July is the warmest and wettest (12.2 ± 1.6 °C; 94.7 mm). Mean annual precipitation sum is 810 mm, 56% of which falls between May and September. Snow can fall at any time, but lay continuously for 6 months, from mid November to May, reaching a mean maximum depth of 133 cm. Despite the patchy and discontinuous permafrost distribution (Guglielmin and Siletto, 2000; Guglielmin et al., 2001; Cannone and Gerdol, 2003), at 3000 m the permafrost thickness exceeds 200 m (Guglielmin, 2004; Guglielmin et al., 2017).
The area is characterized by bedrock outcrops, as well as some Holocene till and talus deposits.
The Holocene glacial evolution of this area is not very well known. The presence of Scorluzzo Glacier was documented until 1937 when the front reached a minimum altitude of 2820 m a.s.l. (Pelfini, 1992).
Despite its limited extent (ca. 3 km^2), the area is rich in periglacial features: several types of patterned ground, solifluction lobes, scree slopes, protalus ramparts, block streams, debris-flows and at least two active rock glaciers (Guglielmin and Tellini, 1992).
The vegetation is typical of the alpine and nival belt (Ellemberg, 1988) and it was firstly mapped by Giacomini and Pignatti (1955) in 1953, then by Cannone (1997). In the nival belt, the most representative communities of discontinuous pioneer species colonizing the screes are *Androsacetum alpinae*, *Oxyrietum digynae* and *Luzuletum spadiceae*. In the alpine belt, continuous climax communities dominate alpine meadows (*Caricetum curvulae*) and chionophilous areas (*Salicetum herbaceae*).
At the elevations of the study area, the effects of anthropogenic land use change on vegetation are mostly negligible (Keller et al., 2005) with extensive summer pasturing being the only anthropogenic land use in our study area (Cannone et al., 2007).

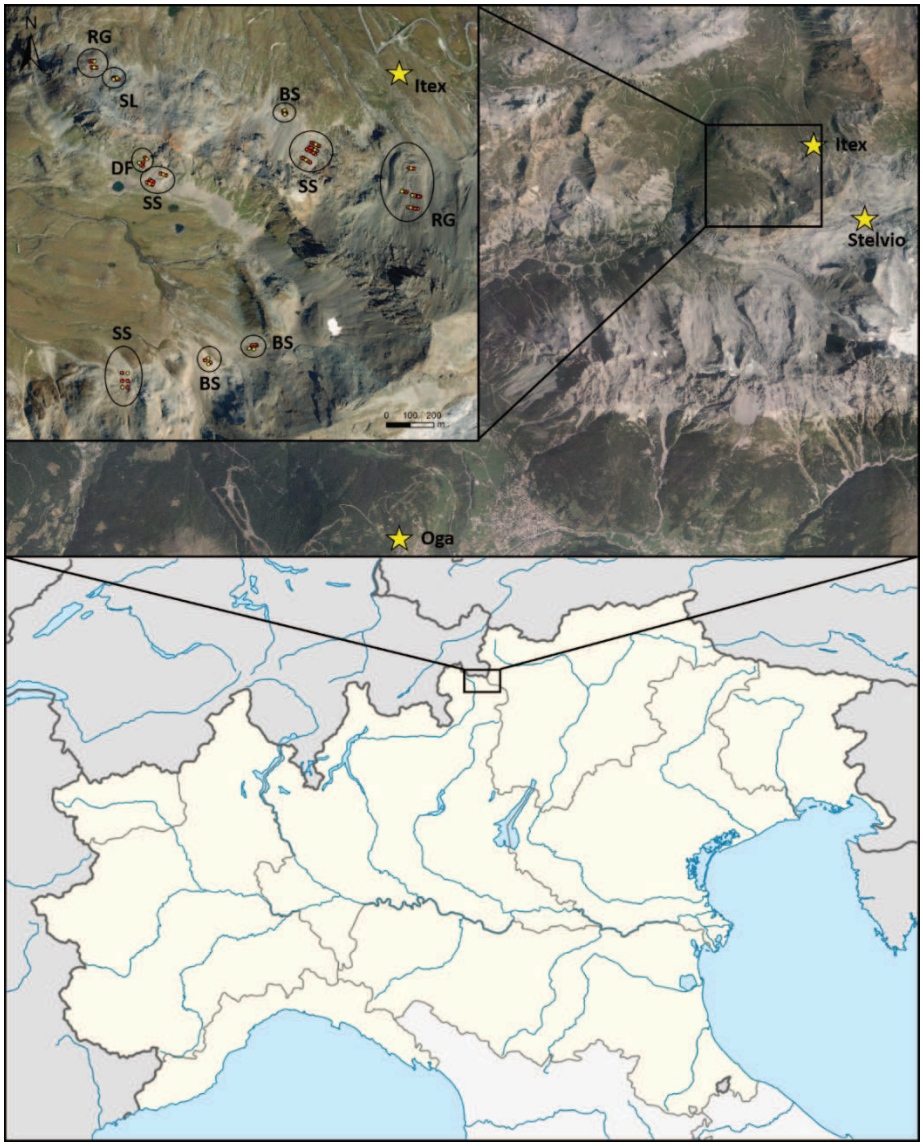

Figure 5.2.1. The investigated area and the locations of the automatic weather stations (AWS) (yellow stars). The colored dots are the monitoring points for the observed movements (red = training set, yellow = validation set). They are circled to indicate the landform type of the substrate: RG = rock glacier, BS = block stream, SS = scree slope, SL = solifluction lobe, DF = debris-flow.

5.2.4 METHODS

5.2.4.1 Surface data

Topographic information were obtained from the digital elevation model (DEM) of the study area available with 5 x 5 m of resolution (http://www.cartografia.servizirl.it/arcgis/services/wms/DTM5_RL_wms/MapServer/WMSServer) in ArcGIS 10.3, with which were developed also a slope map and the radiation maps (Area solar

radiation tool) of the two snow-free periods (2015 and 2016), subsequently averaged to produce a single mean solar radiation map.
The new geological map by Montrasio et al., (2012) and a new unpublished vegetational map surveyed on 2013 that follows Giacomini and Pignatti (1955) and Cannone et al. (2007), were re-classified and rasterized at 5 m of resolution as summarized in Table 5.2.1.
Furthermore, measurements of surface displacements were added as point data. In detail, the maximum cumulative movement (between summer 2015 and 2016 and measured in cm) recorded on 10 m long painted lines located on selected periglacial landforms spread all over the study area were considered in order to calibrate the model with direct measurements. A total of 85 points spread on 2 rock glaciers, 3 scree slopes, 3 block streams, 1 solifluction lobe and 1 debris-flow were selected. Roughly, the 30% (23) of those points has been taken apart to set up the validation set to calibrate the model. This method follows in part the "random partition" of Chung and Fabbri (2003) with the exception that the selection of the test set was not done randomly but by choosing 2 to 3 points placed at different altitudes on each landform to better represent all the landforms occurring in the modeled area.

Table 5.2.1. Classification of the characteristics deriving from the geological and vegetation map. Classes are represented by the numbers at the first row and only the totality of classes (6) were used for the deposit types. LIA refers to Little Ice Age.

	1	**2**	**3**	**4**	**5**	**6**
Age of Deposits	Postglacial unit (post-LIA)	LIA	Ancient postglacial unit (pre-LIA)			
Deposit Type	Glacial till	Slope deposit	Lacustrine deposit	Landslide deposit	Debris flow deposit	Alluvional deposit
Vegetation Coverage	Bare ground (< 5%)	Discontinuous (5-50%)	Continuous (> 50%)			

5.2.4.2 Climatic data

Climatic data refers to air temperatures and solid precipitations occurred during the study period: from 06-11-2014 to 06-11-2016. The first step was to build a detailed map of air temperatures occurring at each pixel (5 x 5 m) of the DEM. Secondly, the seasons of the 2-year period have been defined in terms of snow coverage as shown in Table 5.2.2, assuming that when snow is present it insulates completely the ground from the radiation air temperature (although we are conscious that snow should be at least 80 cm thick to exert this complete insulation, i.e. Haeberli, 1985; Guglielmin et al., 2003).

Table 5.2.2. Definition of the year periods based on the snow presence and the mean daily air temperature. It is interesting to underline that in 2016 two freezings occurred, one at the end of the snow period and one at the end of the snow-free period.

Periods	**Snow Coverage (%)**	**Mean Daily Air Temperature (°C)**	**Number of periods**
Snow	> 90	< 0	2
Melting (MT)	< 90	> 0	2
Freezing (FT)	< 90	< 0	4
Snow-free (SFT)	< 10	> 0	2

The periodic mean air temperature has been calculated from data series belonging to the 3 closest available automatic weather stations (Stelvio = 3000 m a.s.l., Itex = 2616 m a.s.l. and Oga = 2295 m a.s.l.). Subsequently, a linear regression was calculated between mean temperatures for each defined period and the elevation of the correspondent station allowing to extrapolate maps of mean air temperatures (all of them with $R^2 > 0.75$ and $p < 0.05$) for each pixel of the examined area for all the defined periods.
The third step was to generate the snow free maps for each defined period starting from the MODIS daily snow maps (250 m of resolution; Notarnicola et al., 2013a,b) of the study area. For each defined periods the sum of the snow free days was computed for each pixel obtaining maps of the snow free duration for each defined periods. Finally, the latter maps were multiplied for the mean temperature of each correspondent defined periods obtaining the maps of Ground Surface Temperature Index (GSTI). Moreover, thawing degree days (TDD) and freezing degree days (FDD) (Carter et al., 1991; Fronzek et al., 2006) were calculated for each period through the linear regressions obtained from the three automatic weather stations as explained above. These values were multiplied by the snow free days for each pixel for each periods obtaining the maps of Ground Heating Index (GHI) and of Ground Cooling Index (GCI).

5.2.4.3 Statistical analyses

All the maps operations described above were conducted through the raster calculator tool in ArcGIS 10.3 (ESRI, 2011).
From all the maps of the variables listed in Fig. 5.2.2, at each 62 training points both categorical and continuous data were extracted and used to run a multiple regression (Aiken et al., 1991) model in order to select the dominant variables with a backward stepwise option through the software STATISTICA©.
Afterwards, the fitness of the predicted movement with the measured one was tested with a linear regression on the training set, while the evaluation on the validation set. A schematic reconstruction of the utilized variables is visible in Fig. 5.2.2.

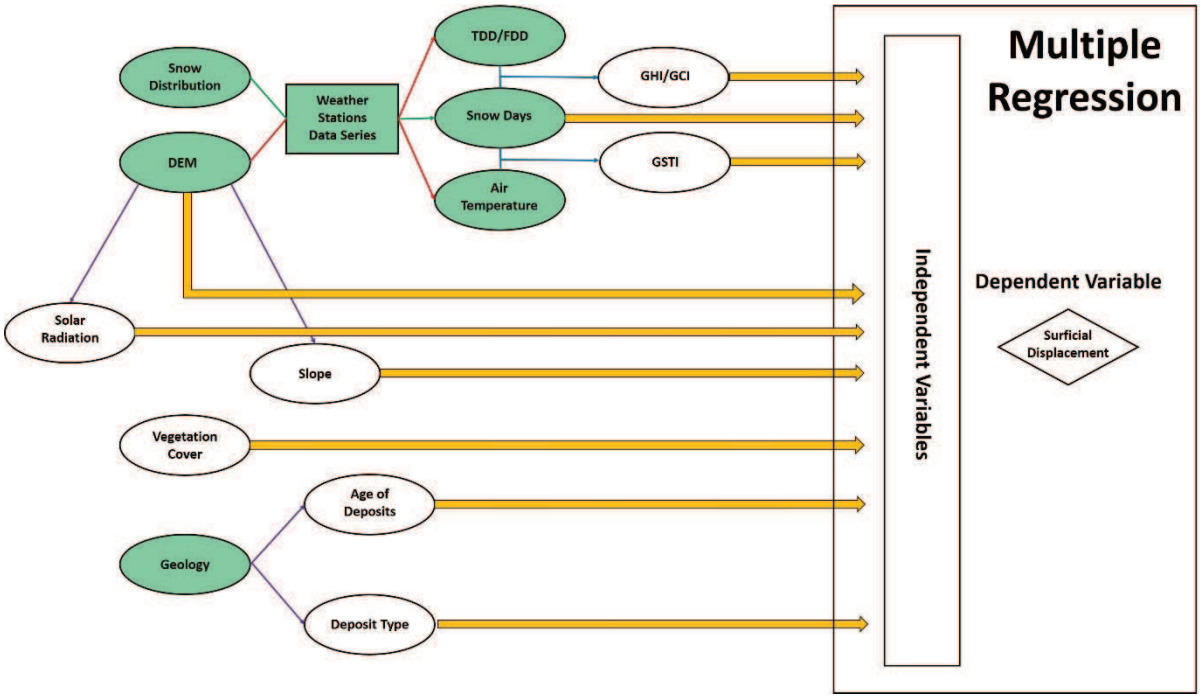

Figure 5.2.2. Flow chart representing the calculation conducted until the multiple regression analysis. Green backgrounds represent data used as source of secondary maps. Circles are raster maps, some of which derive from a parental map calculation in ArcGIS (see violet arrows). The quadrat indicates a data time series, thank to which the spatial distribution of air temperature, TDD and FDD derived from the DEM (see red arrows) and the number of days with snow cover derived from the snow distribution (see green arrows). Multiplication of snow-free days per TDD, FDD and air temperature (see blue arrows) produced the indices of heating (GHI), cooling (GCI) and surface temperature at the ground surface (GSTI). Yellow arrows tell which variable has been used for the multiple regression input (independent variables). The rhombus (surficial movement record) indicates the dependent variable of the multiple regression analysis.

5.2.5 RESULTS

The distribution of the surface components of the model is shown in Fig. 5.2.3. The elevation ranges between 2210 and 3094 m a.s.l while the slope between 0 and 72° with the steepest areas corresponding to the rockwalls. The cumulative radiation of the snow-free period ranges between 10^5 to $1.2*10^6$ Wh m^{-2} with the lower values occurring on the north-facing slopes, while higher radiation on the south-facing slopes and almost flat areas as expected. All the rock outcrops were not considered in the model because are generally avoided by vegetation and affected by completely different processes respect the deposits. The deposits are classified according their age respect the last main recent glacial event occurred during the Little Ice Age (LIA) that in this area occurred sometime between 1580 and 1834 AD (Guglielmin et al., 2001; Guglielmin et al., 2017). The deposits Post-LIA are quite rare and are completely free by any soil coverage while in the LIA areas only discontinuous soil occur whereas in Pre-LIA areas soil is generally present and in many cases quite well developed with spodosoils that can exceed 50 cm of thickness. If the age of the deposits give an idea of the weathering and of the stability of the surfaces, the typology (glacial till, slope deposits etc.) give an indication of the average grain size (till generally sandy vs. alluvial generally gravelly), of the

selection of the deposits (alluvial well selected vs. till massive). Among the different typology, till is the most widespread while scree slope are concentrated at the foot of the rockwalls. The vegetation was classified in three classes according to its coverage in percentage and gives an information about the stability of the surface but also the time of deglaciation. Continuous vegetation is abundant in flat areas at mid to low elevations while in proximity of streams or at the foot of scree slopes vegetation becomes discontinuous.

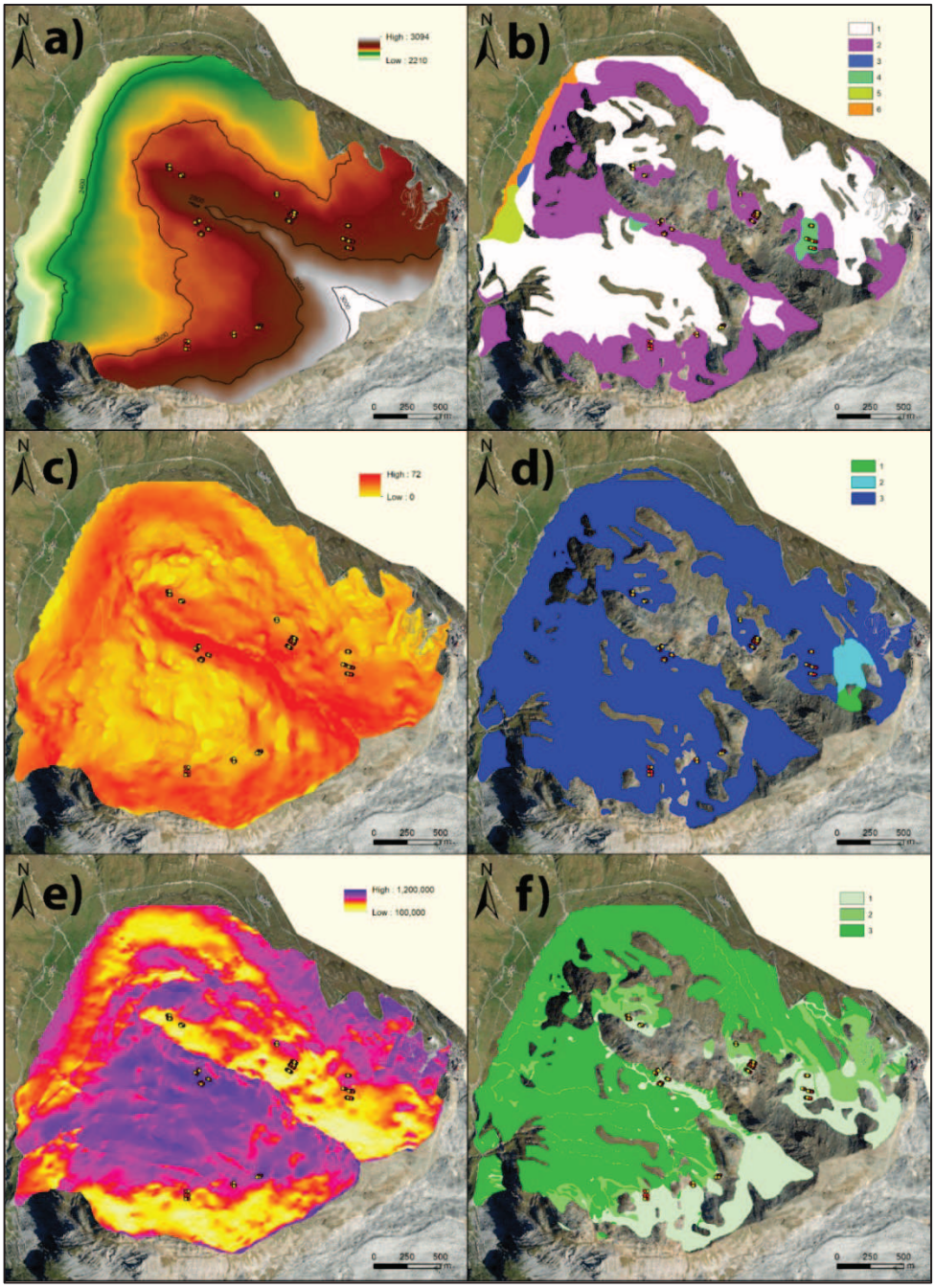

Figure 5.2.3. Surface components as inputs for the multiple regression. a) DEM in m a.s.l.; b) deposit type: 1 = till, 2 = scree slope t, 3 = lacustrine deposit, 4 = landslide deposit, 5 = debris flow deposit, 6 = alluvional deposit; c) slope (°); d) age of the deposits: 1 = post-LIA, 2 = LIA, 3 = pre-LIA; e) solar radiation (Wh m^2); f) vegetation coverage (%): 1 = bare ground (< 5%), 2 = discontinuous (5-50%), 3 = continuous (> 50%). Red dots indicate the training set, yellow dots indicate the validation set.

The climatic indices included in the model are shown in Fig. 5.2.4. Because the snow map have a larger pixel size (250 m), all these maps have the 250 m resolution. The snow persistence ranges between 156 and 262 days per year, generally it lasted longer at the higher elevations although sometimes in depressed and shady areas at lower altitude is possible to have quite long snow persistence. The GSTI for the FT, MT and SFT is expressed in °C day. FT shows low values for higher elevations (ranging from 5.7 to 113 °C day), even though maximum is not reached at the most elevated place. The GSTI for MT is not available for all the area due to a consistent presence of clouds during that period. However, it ranges between 0.6 and 143.5 °C day with lower values at higher elevations. The GSTI for SFT has a higher resolution (5 m) because no snow-free duration maps were used to compile these maps and the values ranges between 233 to 381 °C day.

The GHI and the GCI are also both strongly controlled by DEM although the range of the variability is much wider for GCI (between $-2.4*10^6$ °C day^2 to $-5.58*10^4$ °C day^2) respect to the GHI that ranges between $2.4*10^6$ °C day^2 to $1.2*10^6$ °C day^2 (Fig. 5.2.4d,f).

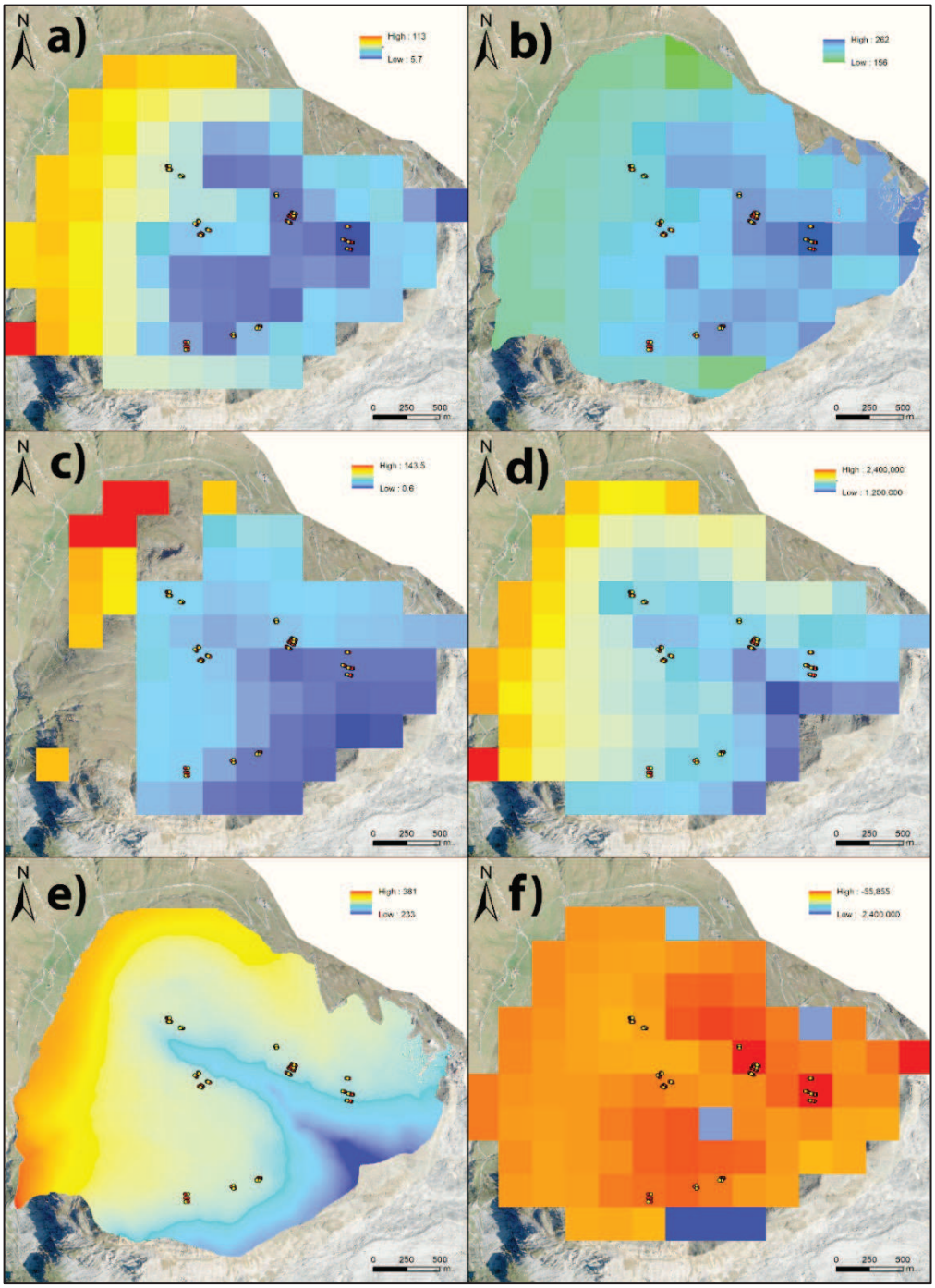

Figure 5.2.4. Climatic components as inputs for the multiple regression. a) mean annual number of days with snow coverage; b) GSTI for FT (°C day) c) GSTI for MT (°C day); d) index GSTI for SFT (°C day); e) GHI; f) GCI. Red dots indicate the training set, yellow dots indicate the validation set.

A multiple regression model with stepward backwise option was applied to the training set points of measured surface displacements considering as independent variables all the values of the variables listed in Table 5.2.6 (Supplementary Material) and as dependent variables the measured values of surface displacement. A good result was achieved (Table 5.2.3). In particular, the R-square value (0.61) suggests a good estimate of the strength of the relationship between the model and the response variables. The relationship is significant because the p-value (< 0.001) is considerably lower than the

F-value (30.67), suggesting that the model fits the data better than the model with no independent variables.

Table 5.2.3. Overall characteristics of the multiple regression analysis.

Model Characteristics	
Dependent Variable	Observed movement (cm)
Multiple R	0.78
F	30.67
R^2	0.61
Adjusted R^2	0.59
p	< 0.001
Std.err. Estimates	91.8

The results of the model indicated that DEM, Slope and GHI are statistically significant driver factors (Table 5.2.4). The model indicated that there is a direct linear relationship between Slope and Surface Displacement and reverse relationships between DEM, GHI and the displacement as expressed by the Equation 1.

Table 5.2.4. Statistically significant variables characteristics as outputs of the multiple regression analysis. B = standardized regression coefficient, b = unstandardized regression coefficient, t(58) = t-test results.

	β	**Std.Err.β**	**b**	**Std.Err.b**	**t(58)**	**p-value**
Intercept			13363.418	1946.090	6.86680	< 0.001
DEM	-0.90234	0.142459	-3.811	0.602	-6.33405	< 0.001
Slope	0.58834	0.087091	10.499	1.554	6.75543	< 0.001
GHI	-1.14111	0.138894	-0.002	0.000	-8.21564	< 0.001

Equation 1: Surface Displacement (cm) = -3.811*DEM + 10.499*Slope - 0.002*GHI + 13363.418.

The fitness of the model was tested through a simple linear regression between the observed movements (cm) and the predicted surface displacement (cm). The same procedure was applied to the validation set of points that has never been used in previous calculations. Good R-square values were obtained both in the fitness (0.61) and in the validation (0.71) regression with statistical significance ($p < 0.001$). Thus, the plots suggest a good predictability of the tested model (Fig. 5.2.5).

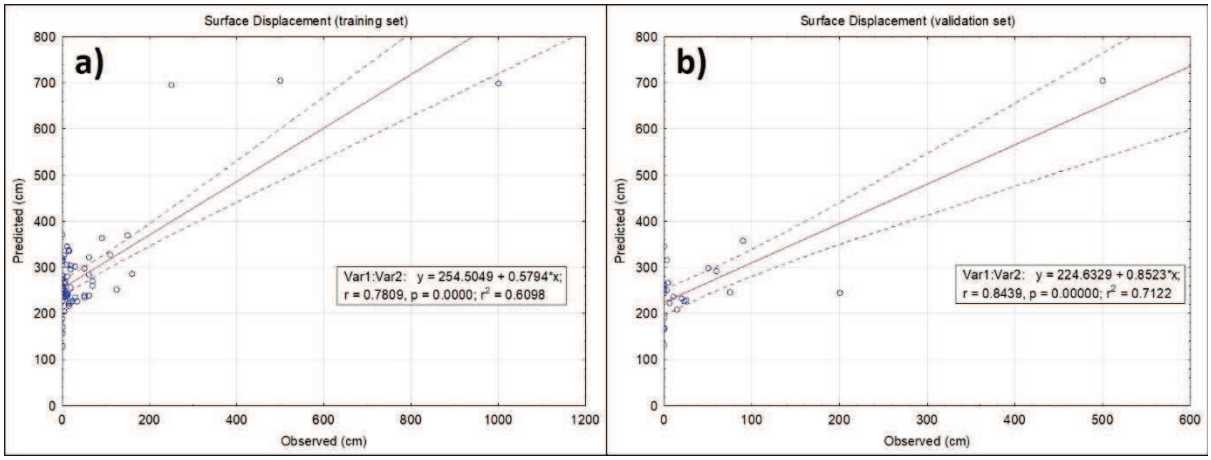

Figure 5.2.5. Plots of the linear regression model run on the a) training set (62 points) and b) validation set (23 points).

By applying the Equation 1 at the whole study area, a map of predicted surficial displacement was generated (Fig. 5.2.6).

Unfortunately, the 250 m resolution pattern deriving from snow maps depicts abrupt changes within few meters in certain zones (Gottfried et al., 1999; de Lannoy et al., 2010; James et al., 2017) that are not realistic. The surficial displacement ranges between 0 to 913 cm with an average value of 254 cm and a median of 240 cm. The model predicts as highly dynamic areas the foot of the rockwalls as expected but also some well-vegetated slopes. Conversely, stable areas are mainly distributed in flat vegetated zones as expected and on north-facing ridges.

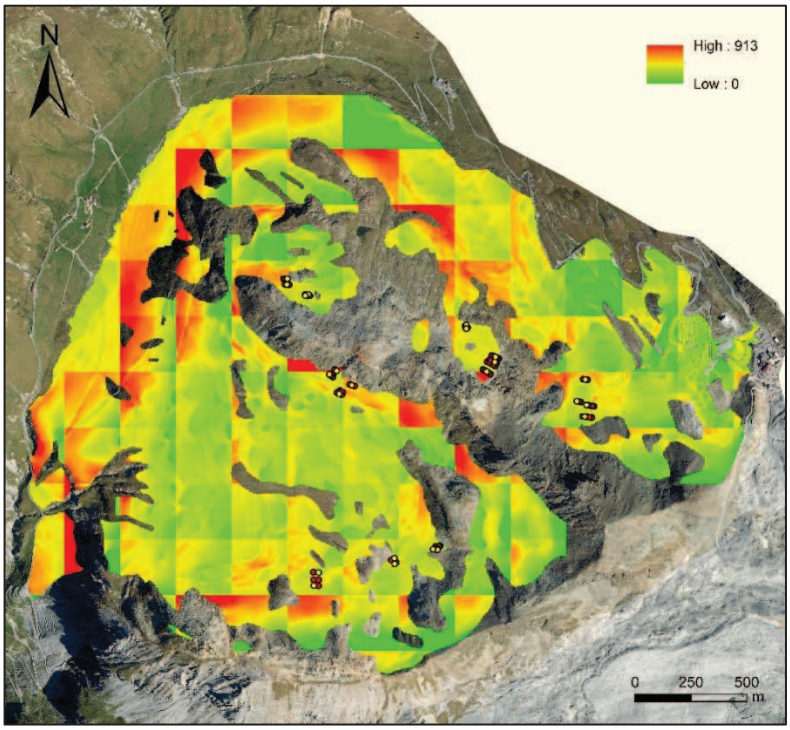

Figure 5.2.6. Graphic visualization of the final model derived (Surface Displacement, cm) from the multiple regression equation. Red dots indicate the training set, yellow dots indicate the validation set.

5.2.6 DISCUSSION

In the mountain areas of the middle and low latitudes, slope processes dominate and could be related to gravitation, nivation, periglacial and cryotic processes and their interactions (Pérez, 1993; Kääb et al., 1997; Haeberli et al., 2006; Rixhon and Demoulin, 2013).

Among the factors that we take into account, it is remarkable that the grain size of the sediments seems not so important. This can be explained probably by the general coarse size of the sediment occurring in the area and where the monitoring points, that reflect the general grain size pattern of the deposits in the area, were selected. Also the vegetation cover seems to be not important probably because here we used classes of coverage (Cannone et al., 2007) and not specific vegetation species indicators of differential movement such as *Cerastium uniflorum*, *Geum reptans* or *Saxyfraga bryoides* (Cannone and Gerdol, 2003; Burga et al., 2004). In fact it is difficult to have vegetation map at species level at the examined scale due to the scarcity of mono-specific detectable patches, even though species-specific distribution models have been developed (e.g., Zimmermann et al., 1999; Guisan and Thuiller, 2005; Guisan et al., 2006; Guisan et al., 2013). Probably at a more detailed scale this factor can be considered.

On the contrary, it is quite obvious that the slope is a relevant parameter, indeed all the geomorphic processes that characterize the mountain periglacial belt are dependent in a such way by the gravitational force and therefore by the slope angle (Matsuoka, 1998; Harris et al., 2001; Matsuoka, 2001a; Harris and Smith, 2003; French, 2007).

Beyond the slope, the other two statistically significant factors, DEM and GHI, showed an inverse relation with the surface displacement. Indeed, the areas at higher elevation and with higher GHI showed the lowest surface displacements. These two factors generally have an opposite spatial pattern because lower GHI (and thus higher surface displacements) occurred at higher elevation (because GHI depends primarily by the air temperature) but sometimes also at lower elevations in shaded position and/or in leeward slope where snow cover can remain for longer time and consequently the GHI is lower. However, a general decrease of surface displacement is visible with higher elevations.

Since elevation and GHI together could be treated as permafrost indicators, we assume that permafrost occurence might be the key to understand the surface displacement in relation to 2 oppositively distributed variables such as elevation and GHI.

According to the alpine permafrost index map (APIM) (Boeckli et al., 2012a,b), we found that the area in which permafrost is more probable is between 2500-3000 m a.s.l. For each altitudinal belts belonging to that range, the percentage of pixels that matches both low GHI with permafrost occurrence has been calculated (Table 5.2.5). At lower elevations (< 2500 m a.s.l.), where permafrost does not occur, the increased slope (> 24° as median) is the responsible for higher surface displacements (data not shown). Between 2500-2600 m a.s.l., less than 2% of the area has a low GHI and permafrost occurrence. On the contrary, between 2600-2900 m a.s.l. there is a good matching between low GHI and permafrost occurrence (ranging between 31.85-75.47%). Maybe this behavior is related to a thinner ALT due to the low GHI that can trigger periglacial processes (Matsuoka, 1998, 2001; French, 2007). At high elevations (2900-3000 m a.s.l.) permafrost decreases its matching with the low GHI (29.78%) probably because the scarce accumulation of snow on the wind-exposed ridges sufficiently enhances the radiation and warming (spring) or cooling (winter) at the surface. In summary, the highest surface dislacements are concentrated at the lower altitudes but rather high

surface displacements occur also in the intermediate zone (2600-2900 m a.s.l.), while at higher elevation are significatively lower. This trend can be axplained by: i) the surface displacement decrease with the elevation; ii) the low GHI and permafrost occurrence that mantain the surface displacements at higher elevation; iii) the steep slopes at low elevations acting as the major driver of displacements; iv) the low GHI at higher elevations acting as the only responsible for slow processes (Table 5.2.5).

Table 5.2.5. This table shows the amount of area interested by the predicted surface displacement at different altitudinal belts. The surface displacement has been divided per altitudinal belts and per areas showing both low GHI (smaller than the mean GHI of the whole altitudinal belt) and permafrost occurrence (> 50%).

		Whole altitudinal belt			Low GHI matching permafrost zones			
	Altitudinal belt in permafrost zone (m a.s.l.)	**Mean Surface Displacement (cm)**	**Min Surface Displacement (cm)**	**Pixel amount**	**Mean Surface Displacement (cm)**	**Min Surface Displacement (cm)**	**Pixel amount**	**Percentage of pixel compared to total**
Low	**2500-2600**	196.97	0	41235	325.73	170.99	604	1.46
	2600-2700	272.02	0	40354	267.40	0	12852	31.85
	2700-2800	226.22	211.75	16320	271.06	0	6337	38.83
High	**2800-2900**	84.36	61.98	10204	217.72	0	7701	75.47
	2900-3000	0.95	0	732	53.18	0	218	29.78

As the model does not aim to distinguish and predict single geomorphic processes (Messenzehl et al., 2017; Hjort, 2014; Fronzek et al., 2006; Luoto and Hjort, 2004), the key role is played by the environmental parameters common to alpine processes, that are the variables used in this model (the multiple regression output). In fact, elevations directly affect those environmental parameters that influence permafrost occurrence (Haeberli, 1978; French, 2007) and thus DEMs result to be the basics for permafrost modelling (Guglielmin et al., 2003; Keller et al., 1996; Boeckli et al., 2012) and permafrost creep related dynamics (Haeberli et al., 2006). Slope angle, instead, is fundamental in periglacial processes such as solifluction (Goodfellow and Boelhouwers, 2013; French, 2007; Benedict, 1970; Matsuoka, 2001) and gravitational processes related to debris accumulation (Statham, 1976; van Steijn et al., 2002; Luckmann, 1976). Further, ground temperatures are necessary to initiate periglacial processes, especially solifluction (French, 2007; Matsuoka, 2001). However, the most important variable in these environments is the snow distribution because it drives several processes (Ridefelt et al., 2010; Thorn and Hall, 2002; Salm, 1993; Berrisford, 1991; Luckmann, 1977), also by altering the energy transfer to the ground (Guglielmin et al., 2014; Guglielmin et al., 2008; Mazhitova et al., 2004). Further, to our knowledge, it is the first time that a snow distribution information has been used to model the activity of geomorphic processes, rather, it has been utilized for plant species distribution (Randin et al., 2009) or permafrost distribution (Guglielmin et al., 2003; Etzelmüller et al., 2001; Gisnås et al., 2016) or avalanche prediction (Lehning et al., 2006).

The model presented in this study showed a good predictability despite the relative small number of observation points. They laid from the farthest bottom to the middle part of the ridges slopes in presence of landforms. Since they do not well represent the totality of the study area, it would be better to focus on the slope areas. However, in the extrapolated areas some zones resulted rather dynamic despite their poor slope in correspondence of small solifluction lobes (central part of the cirque), others very dynamic without the evidence of periglacial features (western border of the model), maybe suggesting other environmental ongoing processes (i.e. vegetation shifts, Cannone et

al., 2007). Nevertheless, the prediction details obtained on slope features (rock glaciers and scree slopes) are evident. Indeed, the selected observation points in this study belong to a larger study of monitored landforms dynamics (unpublished data) and many features (or the most dynamic parts of features) lay in highly dynamic predicted zones. This is true for the front of a large rock glacier, a large rock-banked solifluction lobe and several scree slopes.
The other variables taken into account in this study were not significant: vegetation coverage may be interpreted as a consequence of surficial dynamic activity (Cannone et al., 2007); deposit type and age are not relevant since the processes involved are various; radiation is less fundamental when indices of ground temperature are available.
In addition, our results demonstrate how it is possible to use dated but simple statistical models such as the multiple regression for geoscientific purposes and hazard evaluation (Carrara, 1983; Carrara et al., 1991; Brunori et al., 1996) instead of novel and sophisticated techniques (Hjort, 2006; Hjort and Luoto, 2013).
To conclude, the potentiality of this type of models (that include climatic variables) aims to be related to the Climate Change (Harris et al., 2009). In particular, it is possible to focus on surficial dynamics connected to vegetation shifts (Cannone et al., 2007) or ecosystem feedbacks (Chapin et al., 2008) under future climatic scenarios, especially in highly heterogeneous environments such as alpine areas (Gobiet et al., 2014).

5.2.7 CONCLUSIONS

The development of a simple topo-climatic model for predicting surficial dynamics in mountain regions has been presented in this manuscript. Our findings suggest that slope, DEM and GHI are the best predictors of surficial displacement in alpine areas. In particular, the multiple regression model show how steep zones with low GHI and not much elevated are more susceptible to undergo periglacial and paraglacial processes. Further, there is a trend of decreasing surficial displacement with the increasing elevation. According to us, at lower elevations, slope processes are the main responsible for the high surface displacements. At mid elevations, the combination of a low GHI, snow accumulation and a considerable elevation provides a good distribution of permafrost, able to act as driver of surficial displacement through the water contened in the shallow active layer. At high elevations the displacements are minimum and majorly driven by the low GHI driven by the low air temperatures rather than the permafrost distribution.
In a future perspective, the novel usage of climatic data for this type of modeling is important to inspire interests in simulating future trends of surface dynamics under a climate change scenario.

5.2.8 REFERENCES

- Aalto, J., & Luoto, M. (2014). Integrating climate and local factors for geomorphological distribution models. Earth Surface Processes and Landforms, 39(13), 1729-1740.
- Aiken, L. S., West, S. G., & Reno, R. R. (1991). Multiple regression: Testing and interpreting interactions. Sage.
- Arenson, L. U., Kääb, A., & O'Sullivan, A. (2016). Detection and Analysis of Ground Deformation in Permafrost Environments. Permafrost and Periglacial Processes, 27(4), 339-351.
- Baas, A.C.W., 2013. Quantitative Modeling of Geomorphology. In: Treatise on Geomorphology, Chapter: Quantitative Modeling of Geomorphology, Publisher: Academic Press, pp.1-5
- Bai, S. B., Wang, J., Lü, G. N., Zhou, P. G., Hou, S. S., & Xu, S. N. (2010). GIS-based logistic regression for landslide susceptibility mapping of the Zhongxian segment in the Three Gorges area, China. Geomorphology, 115(1), 23-31.
- Ballantyne, C. K. (1985). Nivation landforms and snowpatch erosion on two massifs in the Northern Highlands of Scotland. Scottish Geographical Magazine, 101(1), 40-49.
- Ballantyne, C. K. (2013). A 35-Year Record of Solifluction in a Maritime Periglacial Environment. Permafrost and Periglacial Processes, 24(1), 56-66.
- BECKER A. & BUGMANN H. (eds.) (1997) - Predicting Global Change Impacts on Mountain Hydrology and Ecology: Integrated Catchment Hydrology/Altitudinal Gradient Studies, IGBP Report 43, Stockholm.
- Benedict, J. B. (1970). Downslope soil movement in a Colorado alpine region: rates, processes, and climatic significance. Arctic and Alpine Research, 165-226.
- Berrisford, M.S., 1991. Evidence for enhanced mechanical weathering associated with seasonally late-lying and perennial snow patches, Jotunheimen, Norway. Permafrost and Periglacial Processes 2(4), 331–40.
- Boeckli, L., Brenning, A., Gruber, S. & Noetzli J. (2012b): A statistical approach to modelling permafrost distribution in the European Alps or similar mountain ranges, The Cryosphere, 6,125-140. doi:10.5194/tc-6-125-2012.
- Boeckli, L., Brenning, A., Gruber, S., & Noetzli, J. (2012a). Permafrost distribution in the European Alps: calculation and evaluation of an index map and summary statistics. The Cryosphere, 6(4), 807.
- Braun-Blanquet, J. (1951). Pflanzensoziologie, grundzuge der vegetations kunde (No. 581.5 B73).
- Brenning, A. (2005). Spatial prediction models for landslide hazards: review, comparison and evaluation. Natural Hazards and Earth System Science, 5(6), 853-862.
- Brunori, F., Casagli, N., Fiaschi, S., Garzonio, C. A., & Moretti, S. (1996). Landslide hazard mapping in Tuscany, Italy: an example of automatic evaluation. Geomorphic Hazards, Wiley, New York, 55-67.
- Burga, C. A., Frauenfelder, R., Ruffet, J., Hoelzle, M., & KääB, A. (2004). Vegetation on Alpine rock glacier surfaces: a contribution to abundance and dynamics on extreme plant habitats. Flora-Morphology, Distribution, Functional Ecology of Plants, 199(6), 505-515.

- Cai, Q. G., Zhu, Y. D., & Wang, S. Y. (2004). Research on processes and factors of rill erosion. Advances in Water Science, 15(1), 18-22.
- Cannone, N. 1997. Vegetazione periglaciale e crionivale: caratteristiche, modelli di aggregazione e rapporti con forme e processi periglaciali. PhD Thesis, X Cycle, University of Pavia.
- Cannone, N., & Gerdol, R. (2003). Vegetation as an ecological indicator of surface instability in rock glaciers. Arctic, Antarctic, and Alpine Research, 35(3), 384-390.
- Cannone, N., & Pignatti, S. (2014). Ecological responses of plant species and communities to climate warming: upward shift or range filling processes? Climatic change, 123(2), 201-214.
- Cannone, N., Sgorbati, S., & Guglielmin, M. (2007). Unexpected impacts of climate change on alpine vegetation. Frontiers in Ecology and the Environment, 5(7), 360-364.
- Carrara, A. (1983). Multivariate models for landslide hazard evaluation. Mathematical geology, 15(3), 403-426.
- Carrara, A., Cardinali, M., Detti, R., Guzzetti, F., Pasqui, V., & Reichenbach, P. (1991). GIS techniques and statistical models in evaluating landslide hazard. Earth surface processes and landforms, 16(5), 427-445.
- Carrara, A., Crosta, G., & Frattini, P. (2008). Comparing models of debris-flow susceptibility in the alpine environment. Geomorphology, 94(3), 353-378.
- Carter TR, Porter JH, Parry ML. 1991. Climatic warming and crop potential in Europe: prospects and uncertainties. Global Environmental Change 1: 291–312.
- Chapin, F. S., Randerson, J. T., McGuire, A. D., Foley, J. A., & Field, C. B. (2008). Changing feedbacks in the climate–biosphere system. Frontiers in Ecology and the Environment, 6(6), 313-320.
- Chung, C. J. F., & Fabbri, A. G. (2003). Validation of spatial prediction models for landslide hazard mapping. Natural Hazards, 30(3), 451-472.
- Coulthard, T. J. (2001), Landscape evolution models: a software review. Hydrol. Process., 15: 165–173. doi:10.1002/hyp.426
- Das, I., Sahoo, S., van Westen, C., Stein, A., & Hack, R. (2010). Landslide susceptibility assessment using logistic regression and its comparison with a rock mass classification system, along a road section in the northern Himalayas (India). Geomorphology, 114(4), 627-637.
- De Lannoy, G. J., Reichle, R. H., Houser, P. R., Arsenault, K. R., Verhoest, N. E., & Pauwels, V. R. (2010). Satellite-scale snow water equivalent assimilation into a high-resolution land surface model. Journal of Hydrometeorology, 11(2), 352-369.
- Diolaiuti, G. A., Maragno, D., D'Agata, C., Smiraglia, C., & Bocchiola, D. (2011). Glacier retreat and climate change: Documenting the last 50 years of Alpine glacier history from area and geometry changes of Dosde Piazzi glaciers (Lombardy Alps, Italy). Progress in Physical Geography, 35(2), 161-182.
- Dymond, J. R., Ausseil, A. G., Shepherd, J. D., & Buettner, L. (2006). Validation of a region-wide model of landslide susceptibility in the Manawatu–Wanganui region of New Zealand. Geomorphology, 74(1), 70-79.
- ESRI 2011. ArcGIS Desktop: Release 10. Redlands, CA: Environmental Systems Research Institute.

- Etzelmüller, B., Hoelzle, M., Flo Heggem, E. S., Isaksen, K., Mittaz, C., Mühll, D. V., ... & Sollid, J. L. (2001). Mapping and modelling the occurrence and distribution of mountain permafrost. Norsk Geografisk Tidsskrift-Norwegian Journal of Geography, 55(4), 186-194.
- Frattini, P., Crosta, G., Carrara, A., & Agliardi, F. (2008). Assessment of rockfall susceptibility by integrating statistical and physically-based approaches. Geomorphology, 94(3), 419-437.
- French, H. M. (2007). The periglacial environment. John Wiley & Sons.
- Fronzek, S., Luoto, M., & Carter, T. R. (2006). Potential effect of climate change on the distribution of palsa mires in subarctic Fennoscandia. Climate Research, 32(1), 1-12.
- Giacomini, V., & Pignatti, S. (1955). Flora e vegetazione dell'alta valle del Braulio con speciale riferimento ai pascoli di altitudine. Fondazione per i Problemi Montani dell'Arco Alpino.
- Gisnås, K., Westermann, S., Schuler, T. V., Melvold, K., & Etzelmüller, B. (2016). Small-scale variation of snow in a regional permafrost model. The Cryosphere, 10(3), 1201-1215.
- Gobiet, A., Kotlarski, S., Beniston, M., Heinrich, G., Rajczak, J., & Stoffel, M. (2014). 21st century climate change in the European Alps—a review. Science of the Total Environment, 493, 1138-1151.
- Goodfellow BW, Boelhouwers J. 2013. Hillslope processes in cold environments: an illustration of high-latitude mountain and hillslope processes and forms. In Treatise on Geomorphology, Shroder J, Jr (ed). Academic Press: San Diego; 320–336.
- Gottfried, M., Pauli, H., Futschik, A., Akhalkatsi, M., Barancok, P., Alonso, J. L. B., ... & Krajci, J. (2012). Continent-wide response of mountain vegetation to climate change. Nature climate change, 2(2), 111.
- Gottfried, M., Pauli, H., Reiter, K., & Grabherr, G. (1999). A fine-scaled predictive model for changes in species distribution patterns of high mountain plants induced by climate warming. Diversity and Distributions, 5(6), 241-251.
- Govers, G. (1992). Relationship between discharge, velocity and flow area for rills eroding loose, non-layered materials. Earth surface processes and landforms, 17(5), 515-528.
- Grab, S. (2001). Needle ice observations from the high Drakensberg, Lesotho. Permafrost and Periglacial Processes, 12(2), 227-231.
- Guglielmin, M, (2004). Observations on permafrost ground thermal regimes from Antarctica and the Italian Alps, and their relevance to global climate change. Global and Planetary Change, 40(1), 159-167.
- Guglielmin, M., & Siletto, G. B. (2000). Carta della criosfera. Regione Lombardia. Edilizia Residenziale, Firenze.
- Guglielmin, M., & Tellini, C. (1992). Contributo alla conoscenza dei rock glaciers delle Alpi Italiane. I rock glaciers del Livignasco.(Alta Valtellina, Sondrio). Riv. Geogr. It, 99, 395-414.
- Guglielmin, M., Aldighieri, B., & Testa, B. (2003). PERMACLIM: a model for the distribution of mountain permafrost, based on climatic observations. Geomorphology, 51(4), 245-257.
- Guglielmin, M., Cannone, N., & Dramis, F. (2001). Permafrost–glacial evolution during the Holocene in the Italian Central Alps. Permafrost and Periglacial Processes, 12(1), 111-124.
- Guglielmin, M., Dalle Fratte, M., & Cannone, N. (2014). Permafrost warming and vegetation changes in continental Antarctica. Environmental Research Letters, 9(4), 045001.
- Guglielmin, M., Donatelli, M., Semplice, M. and Serra Capizzano, S., 2017. Ground surface temperature reconstruction for the last 500 years obtained from permafrost temperatures observed in the Stelvio Share borehole, Italian Alps. Climate of the Past Discussions.

- Guglielmin, M., Evans, C. J. E., & Cannone, N. (2008). Active layer thermal regime under different vegetation conditions in permafrost areas. A case study at Signy Island (Maritime Antarctica). Geoderma, 144(1), 73-85.
- Guisan, A., & Thuiller, W. (2005). Predicting species distribution: offering more than simple habitat models. Ecology letters, 8(9), 993-1009.
- Guisan, A., Lehmann, A., Ferrier, S., Austin, M., OVERTON, J., Aspinall, R., & Hastie, T. (2006). Making better biogeographical predictions of species' distributions. Journal of Applied Ecology, 43(3), 386-392.
- Guisan, A., Tingley, R., Baumgartner, J. B., Naujokaitis-Lewis, I., Sutcliffe, P. R., Tulloch, A. I., ... & Martin, T. G. (2013). Predicting species distributions for conservation decisions. Ecology letters, 16(12), 1424-1435.
- Haeberli, W. (1978). Special aspects of high mountain permafrost methodology and zonation in the Alps. Third International Conference on Permafrost, NRC Ottawa, Proceedings, vol. 1, pp. 378-384.
- Haeberli, W., Hallet, B., Arenson, L., Elconin, R., Humlum, O., Kääb, A., ... & Mühll, D. V. (2006). Permafrost creep and rock glacier dynamics. Permafrost and periglacial processes, 17(3), 189-214.
- Harris, C., & Smith, J. S. (2003). Modelling gelifluction processes: the significance of frost heave and slope gradient. In Proceedings 8th International Conference on Permafrost, Zurich. Swets and Zeitlinger, Lisse (pp. 355-360).
- Harris, C., Arenson, L. U., Christiansen, H. H., Etzelmüller, B., Frauenfelder, R., Gruber, S., ... & Isaksen, K. (2009). Permafrost and climate in Europe: Monitoring and modelling thermal, geomorphological and geotechnical responses. Earth-Science Reviews, 92(3), 117-171.
- Harris, C., Rea, B., & Davies, M. (2001). Scaled physical modelling of mass movement processes on thawing slopes. Permafrost and Periglacial Processes, 12(1), 125-135.
- Harris, S. A., Cheng, G., Zhao, X., & Yongqin, D. (1998). Nature and dynamics of an active block stream, Kunlun Pass, Qinghai Province, People's Republic of China. Geografiska Annaler: Series A, Physical Geography, 80(2), 123-133.
- Hjort, J. (2006). Environmental factors affecting the occurrence of periglacial landforms in Finnish Lapland: a numerical approach.
- Hjort, J. (2014). Which environmental factors determine recent cryoturbation and solifluction activity in a subarctic landscape? A comparison between active and inactive features. Permafrost and periglacial processes, 25(2), 136-143.
- Hjort, J., & Luoto, M. (2013). 2.6 Statistical Methods for Geomorphic Distribution Modeling. Treatise on Geomorphology, Academic Press, San Diego, 59-73.
- Hjort, J., Luoto, M., & Seppälä, M. (2007). Landscape scale determinants of periglacial features in subarctic Finland: a grid-based modelling approach. Permafrost and Periglacial Processes, 18(2), 115-127.
- IPCC (2013) Summary for policymakers. In: Stocker TF et al (eds) Climate change 2013: the physical science basis. Contribution of working group I to the fifth assessment report of the intergovernmental panel on climate change. Cambridge University Press, Cambridge, United Kingdom and New York, NY, USA.

- James, M. R., Robson, S., d'Oleire-Oltmanns, S., & Niethammer, U. (2017). Optimising UAV topographic surveys processed with structure-from-motion: Ground control quality, quantity and bundle adjustment. Geomorphology, 280, 51-66.
- Kääb, A., Haeberli, W., and Gudmundsson, G. H., 1997: Analysing the creep of mountain permafrost using high precision aerial photogrammetry: 25 years of monitoring Gruben rock glacier, Swiss Alps. Permafrost and Periglacial Processes, 8: 409–426.
- Kääb, A., Kaufmann, V., Ladstädter, R., & Eiken, T. (2003). Rock glacier dynamics: implications from high-resolution measurements of surface velocity fields. In Eighth International Conference on Permafrost (Vol. 1, pp. 501-506).
- Karlsson JM, Bring A., Peterson GD, Gordon LJ, Destouni G (2011) Opportunities and limitations to detect climate-related regime shifts in inland Arctic ecosystems through eco-hydrological monitoring. Environ Res Lett 6:014015.
- Keller F, Goyette S, Beniston M (2005) Sensitivity analysis of snow cover to climate change scenarios and their impact on plant habitats in alpine terrain. Clim Chang 72:299–319.
- Keller, F., & Hoelzle, M. (1996). PERMAKART und PERMAMAP. Haeberli, W., Hölzle, M., Dousse, JP, Gardaz, JM, Imhof, M., Keller, F., Kunz P., Lugon. R., Reynard, E., Simulation der Permafrostverbreitung in den Alpen mit geographischen Informationssystemen, Arbeitsbericht FP, 31, 35-46.
- Keller, F., Kienast, F., & Beniston, M. (2000). Evidence of response of vegetation to environmental change on high-elevation sites in the Swiss Alps. Regional Environmental Change, 1(2), 70-77.
- Komac, M. (2006). A landslide susceptibility model using the analytical hierarchy process method and multivariate statistics in perialpine Slovenia. Geomorphology, 74(1), 17-28.
- Lee, S. (2005). Application of logistic regression model and its validation for landslide susceptibility mapping using GIS and remote sensing data. International Journal of Remote Sensing, 26(7), 1477-1491.
- Lehning, M., Völksch, I., Gustafsson, D., Nguyen, T. A., Stähli, M., & Zappa, M. (2006). ALPINE3D: a detailed model of mountain surface processes and its application to snow hydrology. Hydrological processes, 20(10), 2111-2128.
- Luckman, B. H. (1976). Rockfalls and rockfall inventory data: some observations from Surprise Valley, Jasper National Park, Canada. Earth Surface Processes and Landforms, 1(3), 287-298.
- Luckman, B. H. (1977). The geomorphic activity of snow avalanches. Geografiska Annaler. Series A. Physical Geography, 31-48.
- Luoto, M., & Hjort, J. (2004). Generalized linear modelling in periglacial studies: terrain parameters and patterned ground. Permafrost and Periglacial Processes, 15(4), 327-338.
- Marmion, M., Hjort, J., Thuiller, W., & Luoto, M. (2008). A comparison of predictive methods in modelling the distribution of periglacial landforms in Finnish Lapland. Earth surface processes and landforms, 33(14), 2241-2254.
- Matsuoka, N. (1998). Modelling frost creep rates in an alpine environment. Permafrost and Periglacial Processes, 9(4), 397-409.
- Matsuoka, N. (1998). Modelling frost creep rates in an alpine environment. Permafrost and Periglacial Processes, 9(4), 397-409.
- Matsuoka, N. (2001)a. Solifluction rates, processes and landforms: a global review. Earth-Science Reviews, 55(1), 107-134.

- Matsuoka, N. (2001)b. Direct observation of frost wedging in alpine bedrock. Earth Surface Processes and Landforms, 26(6), 601-614.
- Matsuoka, N. (2006). Monitoring periglacial processes: Towards construction of a global network. Geomorphology, 80(1), 20-31.
- Mazhitova, G., Chestnykh, O., & Zamolodchikov, D. (2004). Active-layer spatial and temporal variability at European Russian Circumpolar-Active-Layer-Monitoring (CALM) sites. Permafrost and Periglacial processes, 15(2), 123-139.
- Messenzehl, K., Meyer, H., Otto, J. C., Hoffmann, T., & Dikau, R. (2017). Regional-scale controls on the spatial activity of rockfalls (Turtmann valley, Swiss Alps)—a multivariate modeling approach. Geomorphology, 287, 29-45.
- Micheletti, N., Lambiel, C., & Lane, S. N. (2015). Investigating decadal-scale geomorphic dynamics in an alpine mountain setting. Journal of Geophysical Research: Earth Surface, 120(10), 2155-2175.
- Miska, L., & Jan, H. (2005). Evaluation of current statistical approaches for predictive geomorphological mapping. Geomorphology, 67(3), 299-315.
- Mod, H. K., Scherrer, D., Luoto, M., & Guisan, A. (2016). What we use is not what we know: environmental predictors in plant distribution models. Journal of Vegetation Science, 27(6), 1308-1322.
- Montrasio, A., Berra, F., Cariboni, M., Ceriani, M., Deichmann, N., Ferliga, C., ... & Longhin, M. (2008). Note illustrative della Carta Geologica d'Italia: foglio 024. Bormio, ISPRA, Servizio Geologico d'Italia, Roma.
- Necsoiu, M., Onaca, A., Wigginton, S., & Urdea, P. (2016). Rock glacier dynamics in Southern Carpathian Mountains from high-resolution optical and multi-temporal SAR satellite imagery. Remote Sensing of Environment, 177, 21-36.
- Nel, W., & Boelhouwers, J. (2014). First observations on needle ice formation in the sub-Antarctic. Antarctic Science, 26(3), 327.
- Notarnicola, C., Duguay, M., Moelg, N., Schellenberger, T., Tetzlaff, A., Monsorno, R., ... & Zebisch, M. (2013)a. Snow cover maps from MODIS images at 250 m resolution, Part 1: Algorithm description. Remote Sensing, 5(1), 110-126.
- Notarnicola, C., Duguay, M., Moelg, N., Schellenberger, T., Tetzlaff, A., Monsorno, R., ... & Zebisch, M. (2013)b. Snow cover maps from MODIS images at 250 m resolution, part 2: Validation. Remote Sensing, 5(4), 1568-1587.
- Oerlemans, J. (2005). Extracting a climate signal from 169 glacier records. science, 308(5722), 675-677.
- Paul, F., Kääb, A., & Haeberli, W. (2007). Recent glacier changes in the Alps observed by satellite: Consequences for future monitoring strategies. Global and Planetary Change, 56(1-2), 111-122.
- Pearson, R. G., Phillips, S. J., Loranty, M. M., Beck, P. S., Damoulas, T., Knight, S. J., & Goetz, S. J. (2013). Shifts in Arctic vegetation and associated feedbacks under climate change. Nature climate change, 3(7), 673.
- Pelfini, M. 1992. Le fluttuazioni glaciali oloceniche nel gruppo Ortles-Cevedale (settore lombardo). Tesi di Dottorato, IV ciclo, 1998–91, Università degli Studi di Milano.
- Pelletier, J. D., & Pelletier, J. D. (2008). Quantitative modeling of earth surface processes (Vol. 304). Cambridge: Cambridge University Press.

- Pérez, F. L. (1993). Talus movement in the high equatorial Andes: a synthesis of ten years of data. Permafrost and Periglacial Processes, 4(3), 199-215.
- Pfeffer, K., Pebesma, E. J., & Burrough, P. A. (2003). Mapping alpine vegetation using vegetation observations and topographic attributes. Landscape ecology, 18(8), 759-776.
- Pradhan, B. (2010). Remote sensing and GIS-based landslide hazard analysis and cross-validation using multivariate logistic regression model on three test areas in Malaysia. Advances in space research, 45(10), 1244-1256.
- Randin, C. F., Vuissoz, G., Liston, G. E., Vittoz, P., & Guisan, A. (2009). Introduction of snow and geomorphic disturbance variables into predictive models of alpine plant distribution in the Western Swiss Alps. Arctic, Antarctic, and Alpine Research, 41(3), 347-361.
- Räsänen, A., Kuitunen, M., Hjort, J., Vaso, A., Kuitunen, T., & Lensu, A. (2016). The role of landscape, topography, and geodiversity in explaining vascular plant species richness in a fragmented landscape. Boreal environment research, 21.
- Ridefelt, H., Etzelmüller, B., & Boelhouwers, J. (2010). Spatial analysis of solifluction landforms and process rates in the Abisko Mountains, northern Sweden. Permafrost and periglacial processes, 21(3), 241-255.
- Rixhon, G., & Demoulin, A. (2013). Evolution of slopes in a cold climate. Glacial and Periglacial Geomorphology, 392-415.
- Saito, H., Nakayama, D., & Matsuyama, H. (2009). Comparison of landslide susceptibility based on a decision-tree model and actual landslide occurrence: the Akaishi Mountains, Japan. Geomorphology, 109(3), 108-121.
- Salm, B. (1993). Flow, flow transition and runout distances of flowing avalanches. Annals of Glaciology, 18(1), 221-226.
- Statham, I. (1976). A scree slope rockfall model. Earth Surface Processes and Landforms, 1(1), 43-62.
- Tharp, T. M. (1987). Conditions for crack propagation by frost wedging. Geological Society of America Bulletin, 99(1), 94-102.
- Theurillat, J. P., & Guisan, A. (2001). Potential impact of climate change on vegetation in the European Alps: a review. Climatic change, 50(1-2), 77-109.
- Thorn, C. E., & Hall, K. (2002). Nivation and cryoplanation: the case for scrutiny and integration. Progress in Physical Geography, 26(4), 533-550.
- Tucker, G. E., & Hancock, G. R. (2010). Modelling landscape evolutio
- van Steijn, H., Boelhouwers, J., Harris, S., & Hétu, B. (2002). Recent research on the nature, origin and climatic relations of blocky and stratified slope deposits. Progress in Physical Geography, 26(4), 551-575.
- Virtanen, R., Luoto, M., Rämä, T., Mikkola, K., Hjort, J., Grytnes, J. A., & Birks, H. J. B. (2010). Recent vegetation changes at the high-latitude tree line ecotone are controlled by geomorphological disturbance, productivity and diversity. Global Ecology and Biogeography, 19(6), 810-821.
- Walther, G. R., Beißner, S., & Burga, C. A. (2005). Trends in the upward shift of alpine plants. Journal of Vegetation Science, 16(5), 541-548.
- Westermann, S., Duguay, C. R., Grosse, G., & Kääb, A. (2015). Remote sensing of permafrost and frozen ground. Remote Sensing of the Cryosphere, 307-344.

- Zemp, M., Paul, F., Hoelze, M., & Haeberli, W. (2008). Glacier fluctuations in the European Alps, 1850–2000. Darkening Peaks Glacier Retreat Sci. Soc.
- Zimmermann, N. E., & Kienast, F. (1999). Predictive mapping of alpine grasslands in Switzerland: species versus community approach. Journal of vegetation science, 10(4), 469-482.
- Zinko, U., Seibert, J., Dynesius, M., & Nilsson, C. (2005). Plant species numbers predicted by a topography-based groundwater flow index. Ecosystems, 8(4), 430-441.

5.2.9 SUPPLEMENTARY MATERIAL

Table 5.2.6. Values of the variable used in the multiple regression model. Landforms are divided into block streams (BS), debris flow (DF), scree slopes (SS) and solifluction lobes (SL). Categorical variables (age of the deposit, vegetation coverage and deposit type) have already been described in Fig. 5.2.3.

Set Type	Landform	Observed Surficial Displacement (cm)	Predicted Surficial Displacement (cm)	Age of the deposit	Vegetation Coverage	Deposit Type	DEM (m a.s.l.)	Slope (°)	Snow Days	Solar radiation (Wh m^2)	GHI (°C day^2)	GCI (°C day^2)	GSTI for SFT (°C day)	GSTI for FT (°C day)	GSTI for MT (°C day)
Training Set	BS	0	252.6	3	2	2	2652.8	15.8	249	9.05E+05	1.58E+06	-7.72E+04	307.1	11.2	16.6
		0	129.1	3	2	2	2649.5	2.8	249	1.00E+06	1.58E+06	-7.72E+04	307.6	11.2	16.6
		0	156.3	2	1	1	2688.3	15.5	245	1.07E+06	1.56E+06	-9.14E+04	301.1	23.6	8.4
		0	171.5	2	1	1	2683.5	15.2	245	1.05E+06	1.56E+06	-9.14E+04	301.9	23.6	8.4
		0	188.1	2	1	1	2686.0	16.0	245	1.07E+06	1.56E+06	-9.14E+04	301.5	23.6	8.4
		0	170.4	2	1	1	2683.5	16.8	245	1.07E+06	1.56E+06	-9.14E+04	301.9	23.6	8.4
		0	249.0	3	3	2	2657.3	11.5	246	9.54E+05	1.56E+06	-5.92E+04	306.3	11.2	24.4
		0	250.8	3	3	2	2658.0	11.9	246	9.49E+05	1.56E+06	-5.92E+04	306.2	11.2	24.4
		0	254.4	3	3	2	2656.7	11.8	241	9.51E+05	1.56E+06	-5.92E+04	306.4	11.2	24.4
		0	260.2	3	3	2	2655.9	12.1	241	9.48E+05	1.56E+06	-5.92E+04	306.5	11.2	24.4
	DF	500	705.7	3	1	2	2689.2	43.1	209	1.08E+06	1.43E+06	-1.74E+05	301.0	47.5	23.4
		123	252.4	3	1	2	2671.1	38.8	209	1.10E+06	1.67E+06	-1.01E+05	304.0	26.5	28.0
		70	242.7	3	1	2	2661.0	35.9	209	1.10E+06	1.67E+06	-1.01E+05	305.7	26.5	28.0
		9	241.3	3	1	2	2659.6	33.6	209	1.11E+06	1.67E+06	-1.01E+05	305.9	26.5	28.0
	SS	90	363.3	3	1	2	2668.1	33.8	226	1.12E+06	1.59E+06	-1.19E+05	304.5	29.8	24.9
		150	368.6	3	3	2	2666.3	33.6	226	1.11E+06	1.59E+06	-1.19E+05	304.8	29.8	24.9
		70	260.9	3	1	2	2637.0	28.2	226	1.09E+06	1.67E+06	-1.01E+05	309.7	26.5	28.0
		10	242.4	3	1	2	2637.0	25.5	226	1.10E+06	1.67E+06	-1.01E+05	309.7	26.5	28.0
		160	287.1	3	1	2	2636.9	29.7	226	1.09E+06	1.67E+06	-1.01E+05	309.7	26.5	28.0
		33	226.9	3	1	2	2632.2	22.3	226	1.11E+06	1.67E+06	-1.01E+05	310.5	26.5	28.0
		15	222.7	3	1	2	2628.9	20.7	226	1.10E+06	1.67E+06	-1.01E+05	311.1	26.5	28.0
		1000	698.2	3	3	2	2722.5	35.5	236	7.02E+05	1.33E+06	-1.10E+05	295.4	13.1	5.3
		60	237.7	3	3	2	2724.4	34.8	246	6.83E+05	1.56E+06	-5.92E+04	295.1	11.2	24.4
		50	239.2	3	3	2	2722.9	34.4	246	6.83E+05	1.56E+06	-5.92E+04	295.3	11.2	24.4
		250	695.1	3	3	2	2720.6	34.5	236	7.21E+05	1.33E+06	-1.10E+05	295.7	13.1	5.3
		20	295.5	3	3	2	2698.8	31.0	236	7.48E+05	1.56E+06	-5.92E+04	299.4	11.2	24.4
		20	304.9	3	3	2	2697.8	31.5	236	7.33E+05	1.56E+06	-5.92E+04	299.5	11.2	24.4
		30	301.3	3	3	2	2698.2	31.3	236	7.31E+05	1.56E+06	-5.92E+04	299.5	11.2	24.4
		0	282.7	3	3	2	2701.0	30.6	236	7.32E+05	1.56E+06	-5.92E+04	299.0	11.2	24.4
		60	283.8	3	3	2	2697.6	29.4	236	7.59E+05	1.56E+06	-5.92E+04	299.6	11.2	24.4
		15	336.5	3	3	2	2690.9	32.0	236	7.28E+05	1.56E+06	-5.92E+04	300.7	11.2	24.4
		5	326.1	3	3	2	2691.4	31.2	236	7.33E+05	1.56E+06	-5.92E+04	300.6	11.2	24.4
		60	321.8	3	3	2	2692.9	31.3	236	7.29E+05	1.56E+06	-5.92E+04	300.4	11.2	24.4
		110	327.4	3	3	2	2691.1	31.2	236	7.26E+05	1.56E+06	-5.92E+04	300.7	11.2	24.4
		0	314.0	3	3	2	2676.8	24.8	236	8.17E+05	1.56E+06	-5.92E+04	303.0	11.2	24.4
		10	305.6	3	3	2	2677.5	24.2	236	8.34E+05	1.56E+06	-5.92E+04	302.9	11.2	24.4
		0	316.3	3	3	2	2680.2	26.2	236	8.02E+05	1.56E+06	-5.92E+04	302.5	11.2	24.4
		0	319.9	3	3	2	2675.6	24.9	236	8.07E+05	1.56E+06	-5.92E+04	303.3	11.2	24.4
		6	268.8	3	2	2	2651.4	29.1	230	7.54E+05	1.65E+06	-8.36E+04	307.3	19.4	27.6
		10	280.5	3	2	2	2635.7	24.5	230	7.97E+05	1.65E+06	-8.36E+04	309.9	19.4	27.6
		20	257.3	3	2	2	2638.0	23.1	230	8.06E+05	1.65E+06	-8.36E+04	309.6	19.4	27.6
		15	217.2	3	2	2	2624.6	14.5	230	9.22E+05	1.65E+06	-8.36E+04	311.8	19.4	27.6
	SL	50	271.0	3	1	2	2676.1	29.2	206	7.33E+05	1.62E+06	-1.49E+05	303.2	48.0	32.6
		30	234.8	3	1	2	2675.7	29.1	206	7.34E+05	1.62E+06	-1.49E+05	303.2	48.0	32.6
		12	234.2	3	1	2	2673.6	29.1	206	7.36E+05	1.62E+06	-1.49E+05	303.6	48.0	32.6
		5	239.1	3	1	2	2674.4	29.0	206	7.39E+05	1.62E+06	-1.49E+05	303.4	48.0	32.6
	RG	8.5	239.1	2	1	1	2661.4	30.5	206	7.21E+05	1.61E+06	-1.79E+05	290.2	5.8	7.5
		6	236.6	2	1	1	2662.4	32.4	206	6.92E+05	1.61E+06	-1.79E+05	290.2	5.8	7.5
		5	205.2	2	3	1	2647.9	27.7	206	7.55E+05	1.61E+06	-1.79E+05	290.2	5.8	7.5
		19	225.1	2	1	1	2647.4	30.0	206	7.22E+05	1.61E+06	-1.79E+05	289.8	5.8	7.5
		4	249.5	2	3	1	2647.9	26.2	206	7.78E+05	1.62E+06	-1.49E+05	294.5	5.8	7.5
		3	266.1	3	1	4	2753.2	30.4	262	7.19E+05	1.48E+06	-5.59E+04	294.3	5.8	7.5
		3.5	254.2	3	1	4	2753.7	30.3	262	7.22E+05	1.48E+06	-5.59E+04	294.2	5.8	7.5
		0.5	273.5	3	1	4	2753.4	27.2	262	7.73E+05	1.48E+06	-5.59E+04	294.6	5.8	7.5
		23	225.8	3	1	4	2756.0	30.1	262	7.25E+05	1.48E+06	-5.59E+04	294.7	5.8	7.5
		0	225.6	3	1	4	2728.9	23.0	262	8.26E+05	1.48E+06	-5.59E+04	294.6	5.8	7.5
		2	255.2	3	1	4	2728.7	21.5	262	8.46E+05	1.48E+06	-5.59E+04	298.7	5.8	7.5
		10	236.5	3	1	4	2727.0	24.2	262	8.12E+05	1.48E+06	-5.59E+04	298.6	5.8	7.5
		15	338.6	3	1	4	2726.9	19.9	262	8.58E+05	1.48E+06	-5.59E+04	305.5	57.9	31.5
		50	297.1	3	1	4	2727.5	19.8	262	8.62E+05	1.48E+06	-5.59E+04	305.8	48.0	32.6
		10	345.2	3	1	4	2702.7	12.6	237	9.48E+05	1.48E+06	-5.59E+04	307.9	57.9	31.5
		0	370.7	3	1	4	2702.7	13.6	237	9.36E+05	1.48E+06	-5.59E+04	308.0	57.9	31.5
Validation Set	BS	0	132.0	3	2	2	2649.6	3.1	249	1.01E+06	1.58E+06	-7.72E+04	307.6	11.2	16.6
		0	252.0	3	2	2	2653.4	15.9	249	8.95E+05	1.58E+06	-7.72E+04	307.0	11.2	16.6
		0	167.6	2	1	1	2683.2	14.7	245	1.03E+06	1.56E+06	-9.14E+04	302.0	23.6	8.4
		0	169.0	2	2	1	2678.4	13.0	245	1.04E+06	1.56E+06	-9.14E+04	302.8	23.6	8.4
		0	243.9	3	3	2	2658.6	11.4	246	9.53E+05	1.56E+06	-5.92E+04	306.1	11.2	24.4
		0	262.4	3	3	2	2654.7	11.8	241	9.51E+05	1.56E+06	-5.92E+04	306.8	11.2	24.4
	DF	500	704.1	3	1	2	2683.7	40.9	209	1.09E+06	1.43E+06	-1.74E+05	301.9	47.5	23.4
		60	291.4	3	3	2	2660.0	38.4	209	1.08E+06	1.67E+06	-1.01E+05	305.9	26.5	28.0
	SS	90	358.6	3	1	2	2666.0	32.5	226	1.12E+06	1.59E+06	-1.19E+05	304.9	29.8	24.9
		15	209.2	3	1	2	2630.4	19.9	226	1.06E+06	1.67E+06	-1.01E+05	310.8	26.5	28.0
		200	244.8	3	3	2	2723.8	35.2	236	6.90E+05	1.56E+06	-5.92E+04	295.2	11.2	24.4
		0	345.3	3	3	2	2690.2	32.6	236	7.24E+05	1.56E+06	-5.92E+04	300.8	11.2	24.4
		3	316.3	3	3	2	2677.9	25.3	236	8.24E+05	1.56E+06	-5.92E+04	302.9	11.2	24.4
		20	231.8	3	2	2	2646.3	23.7	230	8.07E+05	1.65E+06	-8.36E+04	308.2	19.4	27.6
		0	189.9	3	2	2	2626.7	12.6	230	9.35E+05	1.65E+06	-8.36E+04	311.4	19.4	27.6
	SL	25	228.0	3	1	2	2676.7	28.8	206	7.40E+05	1.62E+06	-1.49E+05	303.1	48.0	32.6
		75	245.5	3	1	2	2673.3	29.2	206	7.34E+05	1.62E+06	-1.49E+05	303.6	48.0	32.6
	RG	50	297.5	2	1	1	2660.1	29.4	206	7.39E+05	1.62E+06	-1.49E+05	290.0	5.8	7.5
		6	221.8	3	1	4	2754.6	29.2	262	7.41E+05	1.48E+06	-5.59E+04	294.4	5.8	7.5
		4	266.5	3	1	4	2727.7	23.7	262	8.18E+05	1.48E+06	-5.59E+04	294.6	5.8	7.5
		3.5	249.9	3	1	4	2729.5	22.8	262	8.29E+05	1.48E+06	-5.59E+04	298.7	5.8	7.5
		23	226.2	3	1	4	2726.3	19.4	262	8.66E+05	1.48E+06	-5.59E+04	305.6	57.9	31.5
		10	236.9	3	1	4	2703.3	12.0	237	9.58E+05	1.48E+06	-5.59E+04	307.9	48.0	32.6